# Galactic Archaeology using the stellar vertical structure of galactic discs

Joaquín García de la Cruz

A thesis submitted in partial fulfilment of the requirements of
Liverpool John Moores University
for the degree of
Doctor of Philosophy.
December 2021

# Declaration

The work presented in this thesis was carried out at the Astrophysics Research Institute, Liverpool John Moores University. Unless otherwise stated, it is the original work of the author.

While registered as a candidate for the degree of Doctor of Philosophy, for which submission is now made, the author has not been registered as a candidate for any other award. This thesis has not been submitted in whole, or in part, for any other degree.

Joaquín García de la Cruz
Astrophysics Research Institute
Liverpool John Moores University
IC2, Liverpool Science Park
146 Brownlow Hill
Liverpool
L3 5RF
UK

April 22, 2022

# Abstract

The vertical distribution of stars within galactic discs is intrinsically connected to the evolution of the host galaxy: from the creation of galactic components such as the thin and thick disc to many disc features, like flaring, age gradients, or warps. Therefore, by understanding how the stellar vertical structure shapes these features, and how it is affected by different evolutionary processes, we can recover information from the past of galaxies: we can perform galactic archaeology. In this thesis, I use simulated galaxies in their cosmological context to study the connection between different disc features and galactic evolutionary paths with the shape of the stellar vertical density structure within galactic discs.

First, I analyse how the flaring of mono-age populations (MAPs) influences the flaring and the age structure of geometrically-defined thick discs. I also explore under which circumstances the geometric thin and thick discs are meaningfully distinct components, or are part of a single continuous structure as in the Milky Way. I find that flat thick discs are created when MAPs barely flare or have low surface density at the radius where they start flaring. When looking at the vertical distribution of MAPs, these galaxies show a continuous thin/thick structure. They also have radial age gradients and tend to have quiescent merger histories. Those characteristics are consistent with what is observed in the Milky Way. Flared thick discs, on the other hand, are created when the MAPs that flare have a high surface density at the radius where they start flaring. The thick discs' scale-heights can either be dominated by multiple MAPs or just a few, depending on the mass and scale-height distribution of the MAPs. In a large fraction of these galaxies, thin and thick discs are clearly distinct structures. Finally, flared thick

discs have diverse radial age gradients and merger histories, with galaxies that are more massive or that have undergone massive mergers showing flatter age radial gradients in their thick disc.

Second, I study the connection between disc warping and disc heating. I analyse the vertical stellar density structure within warped stellar discs, and monitor the evolution of the scale-heights of the MAPs and the geometrical thin and thick disc during the warp's lifetime. In addition, I compare the overall thickness and the vertical velocity dispersion in the disc before and after the warp. I find that for warps made of pre-existing stellar particles shifted off-plane, the scale-heights do not change within the disc's warped region: discs bend rigidly. For warps made of off-plane new stellar material (either born in-situ or accreted), the warped region of the disc is not well described by a double $\text{sech}^2$ density profile. Yet, once the warp is gone, the thin and thick disc structure is recovered, with their scale-heights following the same trends as in the region that was never warped. Finally, I find that the overall thickness and vertical velocity dispersion do not increase during a warp, regardless of the warp's origin. This holds even for warps triggered by interactions with satellites, which cause disc heating but before the warp forms. These findings suggest that the vertical structure of galaxies does not hold any memory of past warps.

I finish this thesis by proposing how the findings explained in this document can be applied to the study of the Milky Way's disc. On the one hand, exploring the stellar vertical structure of Milky Way's disc can constrain its evolutionary past. On the other hand, by comparing and supporting observations of the Milky Way's disc with samples of simulated galaxies, we can better understand the Milky Way in the context of its neighbouring disc galaxies.

# Publications

In the course of completing the work presented in this thesis, the following papers have been submitted for publication in a refereed journal:

**García de la Cruz, J.**, Martig, M., Minchev, I., James, P., "On the Flaring of Thick Discs of Galaxies: Insights from Simulations", 2021, MNRAS 501, 4, 5105-5120

**García de la Cruz, J.**, Martig, M., Minchev, I., "No memory of past warps in the vertical density structure of galaxies", 2021, eprint arXiv:2111.01522

JOAQUÍN GARCÍA DE LA CRUZ APRIL 22, 2022

# Acknowledgements

There is no better way to start this than to express my infinite gratitude to my first PhD supervisor, Marie Martig. Marie, you took me in blindly when I was about to quit the PhD despite not knowing whether I was actually a good PhD student. Your generosity in that moment changed my life, and I cannot express how profoundly grateful I feel. I have not ever regretted doing a PhD with you since that day, and if I have to mention what has been one of the bigger pressures I have felt during these years, it would be to try my best to live up to it and that you would not regret that blind decision. Thank you for your excellent scientific guidance, thank you for your endless patience, and thank you for all your emotional support. You have been the best PhD advisor I could have asked for.

I would like to thank my second PhD supervisor, Phil James, for his advice and contagious cheerful spirit. Together with your patience with my poor English, you have helped me when I needed it the most. A very special thanks goes to Ivan Minchev, who has been like another PhD advisor rather than just a collaborator. Thank you for your scientific knowledge, motivation, and great help along this thesis.

I would like to thank all the people I have met at the ARI and LIV.DAT program, including PhD students, postdocs, professors, and admin. Thanks for all the conversations, the laughs and the good moments, the tea breaks and the beers at the pub. It has been a real pleasure to meet all of you. I would like to mention some people from the ARI who have earned a especial place during these years. First, I would like to thank my PhD sister, Charlotte, for sharing the journey of learning about galactic astrophysics with me. To Simon, for letting me stay at your place for over a month when I did not

have accommodation. It has been so much fun to sit next to your desk, and I feel that at least half of my codes are written because of you. Same goes for the wild laughs. You have been a true friend. To Joe and Danny, my Spanish family at the ARI and also my partners in crime. You guys have taken care of me so much, and I cannot wait to meet the three of us together and party again. Danny, even though you were on the opposite side of the planet, you have managed to consistently check on me. Thank you for being an inspiration for me so many levels. To Sarah, for being and excellent flatmate and the best band manager ever. And last but definitely not least, to Tom. It has been such a joy to live with you and to play music with you, you are such a talented musician. Sharing our musical experience surpassed all the expectations I had when I arrived to Liverpool. It is with no doubt one of the best things that has happened to me during these years. I am so lucky to have met you the very first day I walked through Liverpool's city centre. Thank you, my friend.

I would also like to thank all the people I met in eDreams during my placement. To José Luis, Nicky, and especially Croqueta, for making the necessary arrangements for it to happen. To mis chamitos Gaby and JC, for being the best managers ever. Finally, to all the data science team, for making me feel welcomed since the first day and for creating such a healthy working environment that I enjoyed so much.

The last and biggest thanks go to my parents, who have been believing and supporting me in every single step of the way unconditionally. Both of you never hesitated to encourage me to pursue this journey, even though it meant being further away from you, and seeing each other only a few times a year. Since I was a child, you have fueled my curiosity and love for knowledge, and exposed me to as many experiences as possible so I could find my passions. I feel truly blessed for having you as my parents. Gracias por todo. Os quiero mucho.

*"Sólo el misterio nos hace vivir. Sólo el misterio."*

– Federico García Lorca

*"La verdadera ciencia enseña, por encima de todo, a dudar y a ser ignorante."*

– Miguel de Unamuno

*"I must not fear. Fear is the mind-killer. Fear is the little-death that brings total obliteration. I will face my fear. I will permit it to pass over me and through me. And when it has gone past I will turn the inner eye to see its path. Where the fear has gone there will be nothing. Only I will remain."*

– Frank Herbert, Dune

# Contents

# List of Tables

# List of Figures

# Chapter 1

# Introduction

*"A journey of a thousand miles begins with a single step."*
– Chinese proverb

Galaxies are a central component in the study of the universe, therefore in astrophysics. On a small scale, galaxies are home of almost all the stars in the universe, providing the conditions for the latter to form and evolve. On a large scale, galaxies are the building block of the large scale structure, and cosmologists use galaxies to understand the structure and the evolution of the universe as a whole.

Galaxies have a wide range of different characteristics, e.g. mass, luminosity, age. The morphological shape is usually used to classify galaxies, being the main categories elliptical, spiral, and 'dwarf' galaxies. The morphology type as well as many other characteristics such as their internal structure come from different evolutionary scenarios. Understanding how galaxies form and evolve in their cosmological context is crucial to understand the diversity in the properties shown by galaxies, and ultimately provides a better understanding of the universe we live in.

## 1.1 Disc galaxies

### 1.1.1 Hubble's Diagram

Edwin Hubble proposed the first scheme to classify galaxies based on their morphological appearance (Hubble, 1926). This scheme has survived since its creation and has been expanded by other authors like Allan Sandage and Gerard de Vaucouleurs (see figure 1.1). This is scheme is commonly called the Hubble Tuning Fork Diagram and it is not an evolutionary scheme, but rather a way to connect the different morphologies and their characteristics.

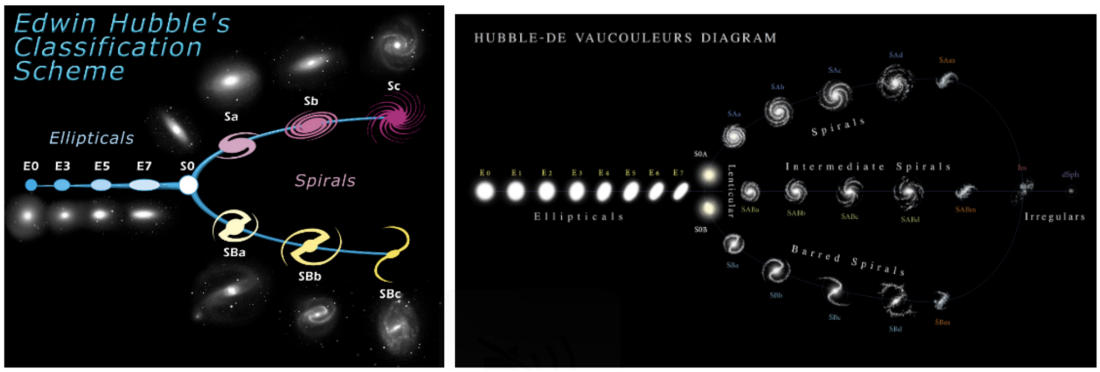


Figure 1.1: *On the left:* The Hubble's classification diagram. *On the right:* de Vaucouleurs' classification diagram.

In this diagram, elliptical galaxies are differentiated only by their ellipticity: from a circular E0 to a very flattened ellipse E7. The number is given by $10 \times (1 - (\frac{b}{a}))$, where $b$ is the measured minor axis and $a$ the major axis at some isophote. Then, the tuning fork diverges into two or three (depending on whether we are using Hubble's or de Vaucouleurs's scheme) parallel tracks. All of them fall into the category of disc galaxies, and each track groups galaxies based on how strong the presence of the bar in the galaxy is. They all range from more lenticular 'S0' galaxies to more disc-dominated systems with higher cold gas content and more open spiral arms. In the de Vaucouleurs's scheme (the most presently used) the 'SA' types have no bar, 'SAB' have a bar without a strong presence, and 'SB' are strongly bar dominated. Our own Milky Way (MW) would probably fall into this category (Gerhard, 2002). Galaxies with no bulge live in the right-hand extreme of the three tracks. Finally, 'Sm' galaxies

on the very right part of the scheme, are the more irregular galaxies.

Among these three main categories of galaxies (elliptical, disc, irregular), this thesis is focused on disc dominated galaxies regardless of the presence of a bar. As will be described in further sections, however, other parameters will define better the type of galaxies this work studies.

### 1.1.2 Structure of Disc Galaxies

As previously said, disc galaxies are located on the right-hand side of the tuning fork of the Hubble/de Vaucouleurs scheme. The main stellar components of such galaxies are: a disc, often divided into two components (thin and thick discs), a stellar halo (with various shapes and mass fractions), and depending on the galaxy also a bulge.

**The bulge:** There are two kinds of bulges normally found in the literature: the "classical" bulge and the pseudo-bulge (the latter will be discussed in Sec. 1.2.6). A classical bulge usually has a spheroidal shape and is located in the geometrical and dynamical centre of the galaxy. Bulges are thought to be formed in the early stages of the galaxy's life, hence they contain mainly old stars and not much interstellar dust or molecular clouds (Ortolani et al., 1995; Clarkson et al., 2008). Stars living in the bulge have orbits with up to large eccentricities and overall higher velocity dispersion compared to stars living in the disc. Because of their steeper density profile and the hot kinematics of the stars living within them, bulges are often compared with elliptical galaxies (Bender et al., 1993; Fisher et al., 1996). A large fraction of bulges usually host bars (a longer discussion on bars can be found in Sec. 1.2.6), up to 50% when considering galaxies observed in the optical regime (Marinova & Jogee, 2007) or 70% when considering the infrared (Knapen et al., 2000).

**The discs:** Discs, on the other hand, contain more cold molecular gas compared to bulges. This gas fuels star formation. Thus, the stellar populations within discs may present a wide range of ages. Stars living in the disc have more circular orbits and are in colder configurations compared to those living in the bulge. Typically, the disc is

decomposed into two components: the thin disc, brighter, with smaller scale-heights, and typically younger stellar populations; and the thick disc, dimmer, with larger scale-heights, and typically older stellar populations. Many discs have spiral arms (Toomre, 1977), although the fraction of galaxies with spiral arms is still debated (see Hart et al., 2016 for fraction estimations using *Galaxy Zoo*, and Sellwood, 2021 for a review).

**The halo:** It is the more extended and dim part of galaxies, containing only about ∼1% of the total stellar mass. It is thought to be made of both accreted stars from other galaxies and heated-up stars from the disc component described above. Therefore, haloes usually have older stars with high velocity dispersion. Because stars from thick discs and haloes (especially the inner halo) are made of heated up stars, they used to unravel the formation and evolution history of galaxies (e.g., Cook et al., 2016).

### 1.1.3 Disc general properties

#### Exponential profiles

Discs have exponential radial profiles (e.g., van der Kruit & Freeman, 2011), i.e. their luminosity decreases exponentially with galactocentric radius. One of the main parameters for characterising discs of galaxies is the scale-length, which can be written as:

$$I(r) = I(0)e^{-r/h_r}, \tag{1.1}$$

where $h_r$ is the scale-length, and I(0) is the central surface brightness. Fathi et al. (2010) found that the average scale-length is independent of the morphological type and is very similar in the optical bands (g, r, i, and z). Less massive galaxies ($10^9$ to $10^{10}$ $M_\odot$) have smaller scale-lengths (1.5 ± 0.7 kpc) than intermediate ($10^{10}$ to $10^{11}$ $M_\odot$) mass galaxies (1.65 ± 0.65 kpc) and massive ($10^{11}$ to $10^{12}$ $M_\odot$) galaxies (5.7 ± 1.9 kpc). For MW-mass galaxies, then the expected scale-length of the Galactic disc is 4.4 kpc with a one-sigma range between 3.6 and 6.6 kpc (van der Kruit & Freeman,

2011 and references therein). Courteau et al. (2007) confirmed the non-dependency of both central surface brightness and scale-length with wavelength band, but found that these two parameters correlate weakly with Hubble morphological type: earlier types have fainter surface brightness and larger scale-lengths, although it is a small effect.

Scale-heights are the equivalent of scale-lengths for the vertical direction. The vertical density profile can be described by an exponential function:

$$I(z) = I(0)e^{-z/h}, \tag{1.2}$$

where $h$ is the scale-height. However, if the disc is in vertical isothermal equilibrium (i.e. the vertical velocity dispersion does not change with height) the mathematical solution is a $sech^2$ function:

$$I(z) = I(0)sech^2(-z/h), \tag{1.3}$$

For many cases, a single exponential or $sech^2$ function does not describe well the behaviour of the light profile in the vertical direction. Instead, two $sech^2$ functions are used, and therefore the disc is subsequently divided into two components: the thin and thick disc. A more detailed discussion about this topic is in Sec. 1.3. On average, discs' scale-heights range from about 0.3 kpc in SC and SBc galaxies to 1 kpc in S0 galaxies, so when compared with typical values of scale-lengths, discs are flattened by factors of about 5–10 (e.g. Freeman & Bland-Hawthorn (2002) and references therein).

### 1.1.4 The Milky Way

The Milky Way (MW) is a barred spiral galaxy with a disc diameter of around 52 kpc (López-Corredoira et al., 2018). The median mass enclosed within 100 kpc is $M(< 100\text{kpc})$ is $0.69 \times 10^{12} M_\odot$ (Shen et al., 2021), of which the total stellar mass is around $M_\star = 6 \pm 1 \times 10^{10} M_\odot$ (Bland-Hawthorn & Gerhard, 2016a). Yet, more high precision estimates need to be made (see a discussion in, for example, Patel et al., 2018

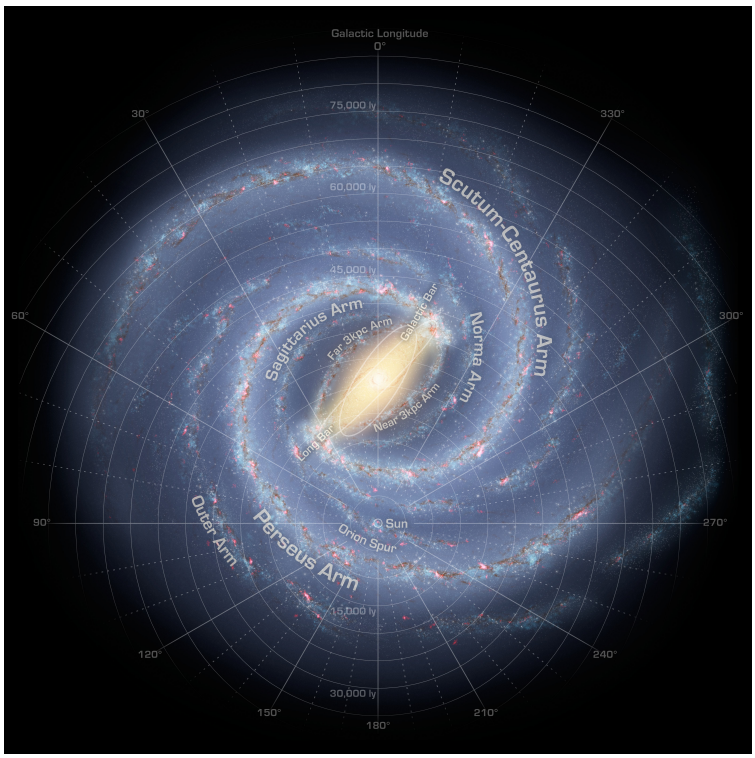


Figure 1.2: Artist's conception of the Milky Way. The Sun, as well as the spiral arms and the bar, are represented. Credits: R. Hurt (SSC/Caltech)

for estimating the total mass of the MW).

The MW is, in many regards, a very peculiar galaxy. It is in transition between the 'red sequence' and the 'blue cloud' of galaxies (Kormendy et al., 2010), something unusual for large disc galaxies in low-density environments as ours (see fig 1.3). On top of that, the MW has not experienced a major merger (mass ratio of 4:1 or higher) for the past 10 Gyr despite being a luminous galaxy (Stewart et al., 2008), and has two luminous dwarf galaxies (the Magellanic Clouds) that are both forming stars (Robotham et al., 2012). This puts the probability of finding a galaxy like the MW on less than 1% (Bland-Hawthorn & Gerhard, 2016a).

The bulge constitutes the central part of the MW. A large fraction of the bulge stars follows a rotating, barred, box/peanut-shaped bulge with an exponential density distribution. This provides evidence of the existence of a Galactic bar (Binney et al., 1991). This box/peanut component is embedded in a more extended thin bar component called the long bar. A super massive black hole resides at the dynamical center of the MW

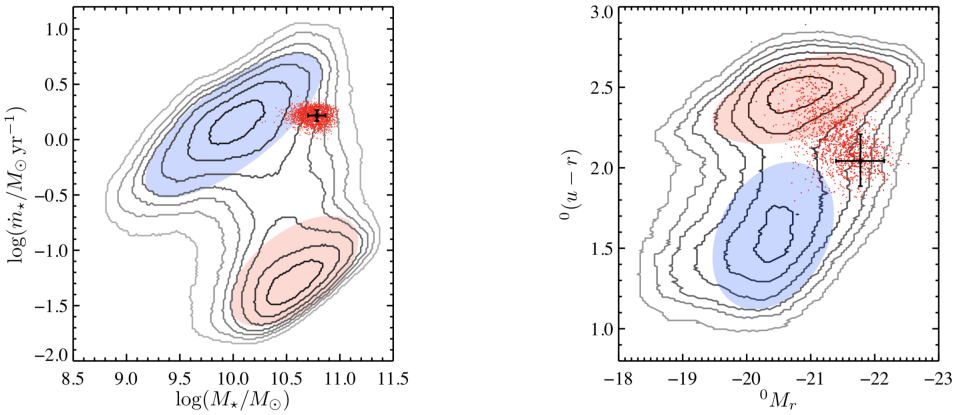


Figure 1.3: Figure 3 from Bland-Hawthorn & Gerhard (2016a). Sample of 3500 Milky Way analogues (red dots) drawn from the SDSS survey with the same stellar mass $M_\star$ and star formation rate $\dot{m}_{star}$, given the measurement uncertainties. The Galaxy indicated by a cross resides in the 'green valley' just below the 'blue cloud' on the left panel, and right to both the 'red' and 'blue cloud' on the right panel.

with a mass of $M_\bullet = 4.2 \pm 0.2 \times 10^6 M_\odot$ (Gillessen et al., 2017). All stars orbiting under the strong influence of this super massive black hole form the so-called nuclear star cluster. Although mainly formed by old stars (Pfuhl et al., 2011), a surprisingly high number of massive stars were found (Bartko et al., 2009).

The Solar System resides between two spiral arms of the MW in the Galactic disc, around an estimated galactocentric distance of $R_\odot = 8.2 \pm 0.1$ kpc (Bland-Hawthorn & Gerhard, 2016a). The Sun is very close to the Galactic plane, with an offset only of about $z_\odot = 25 \pm 5$ pc. Due to the thinness of the disc, this position allows for a good view of the halo and the outer bulge but, on the other hand, cosmic dust makes it hard to observe through other areas of the disc. For instance, Jurić et al. (2008) estimated scale-heights of 300 and 900 pc for the thin and thick disc components respectively around the solar position. While scale-heights can be studied using the optical and IR bands, this is not true for scale-lengths. Only measurements using the IR band can provide strong constrains on the scale-length of the disc. Zheng et al. (2001) measured a scale-length of $2.8 \pm 0.3$ kpc using M dwarfs.

The MW's stellar Halo contains around 1% of the total stellar mass, yet it is of crucial importance for the study of the MW's formation history. In the beginning, it was identified as an old, high-velocity, metal-poor population, with no rotation, and a

spheroidal spatial distribution. Modern data from large stellar surveys show that the stellar halo possesses an internal structure with multiple components. Firstly, the halo can be splitted into the inner and the outer halo (Carollo et al., 2008; De Jong et al., 2010). The inner halo component reaches from 10 kpc to 15 kpc from the Galactic centre, while the outer halo reaches from 15 kpc to 20 kpc. Stars belonging to each component differ in metallicity. The mean metallicity of the inner halo ranges from [Fe/H] 1.2 to 1.7, while the outer halo is from [Fe/H] 1.9 to 2.3 (e.g., An et al., 2013).

Regarding their chemical composition, Halo stars can be also split into two components, an older, high-$\alpha$ and a younger, low-$\alpha$ population (e.g., Nissen & Schuster, 2010). This suggested a dual origin for halo stars, being high-$\alpha$ stars born ex-situ and accreted, and low-$\alpha$ stars born in-situ and heated-up from the disc. This confirmed predictions of hierarchical galaxy formation models (see a discussion in Belokurov, 2013). In fact, cosmological simulations predict that the MW accreted around 100 satellite galaxies (most of them $\sim$ 10 Gyr ago) (Bland-Hawthorn & Gerhard, 2016a). It was confirmed later on that high-$\alpha$ are debris from ancient mergers like Gaia-Enceladus galaxy (Helmi et al., 2018a) the most dominant, the Sequoia galaxy (Myeong et al., 2019), or the Heracles galaxy (Horta et al., 2020); being the former the most dominant. Other large stellar structures of the halo are the Sagittarius Stream, the Galactic Anti-Center Stellar Structure, the Virgo Overdensity, and the Hercules-Aquila Cloud, each of them containing $\sim 10^7 - 10^8 M_\odot$ (Bland-Hawthorn & Gerhard, 2016a). As will be discussed in Section 1.3, the Gaia-Enceladus galaxy has also been proposed to be connected to the high-$\alpha$ thick disc. Indeed, massive accretion events may heat up stars from the thick disc. Supporting evidence has been very recently found with the discovery of metal-rich halo stars (Bonaca et al., 2017).

Together with the stellar halo, the MW also contains a hot plasma (corona) halo, and a dark matter halo. The MW's mass of the dark matter halo has been estimated through different methods such as the kinematics of bright satellites (Barber et al., 2013; Busha et al., 2011), stellar streams (Newberg et al., 2010), or escape velocity measurements of high-velocity stars using the RAVE survey (Smith et al., 2007; Piffl et al., 2014). A distribution function is used to fit the observed distances and velocities of these

dynamical tracers. The mass of the dark matter halo is estimated to be the order of $10^{12} M_{\odot}$ (e.g., Kafle et al., 2014; Wang et al., 2015; Callingham et al., 2019; Posti & Helmi, 2019; Eadie & Jurić, 2019).

## 1.2 Galaxy Formation and Evolution in a ΛCDM model

### 1.2.1 The standard cosmological model

The current picture of the universe establishes that it was formed 13.7 billion years ago with the Big Bang, and it is composed of baryonic matter in 4.5%, cold dark matter in 22%, and dark energy in 73.5% (Cole et al., 2005; Percival et al., 2007; Kowalski et al., 2008; Dunkley et al., 2009; Vikhlinin et al., 2009; Rozo et al., 2010). Surveys of Type Ia supernovae proved the existence of dark energy and show that the universe is expanding at an accelerated rate (Riess et al., 1998). This expansion is produced by the negative pressure made by dark energy. The so-called Lambda Cold Dark Matter (ΛCDM) model is the framework that best reproduces the observations such as the Cosmic Microwave Background and the large scale structure of the Universe so far (Peebles, 1982; Blumenthal et al., 1984; Davis et al., 1985; Springel et al., 2006; Percival et al., 2007; Sánchez et al., 2009). It is thought that after the Big Bang, small quantum density fluctuations that grew during the inflation led to the formation of galaxies (Liddle & Lyth, 1993). The primordial fluctuations were amplified through gravity, becoming high-density regions that started to accrete dark matter (DM) and gas. Similarly, those under-dense regions became emptier and emptier. The result of this process is the cosmic web, seen in the observations and cosmological simulations (Press & Schechter, 1974; Lacey & Cole, 1993; Frenk & White, 2012).

In the early times, dark and baryonic matter accreted similarly (Rees & Ostriker, 1977; White & Frenk, 1991; Somerville & Davé, 2014). Throughout this accretion process, haloes acquired angular momentum from mergers and tidal interactions (further explanation below) and settled at virial equilibrium (White, 1984; Maller et al., 2002; Vitvitska et al., 2002). However, as gas can cool radiatively (White & Rees, 1978a),

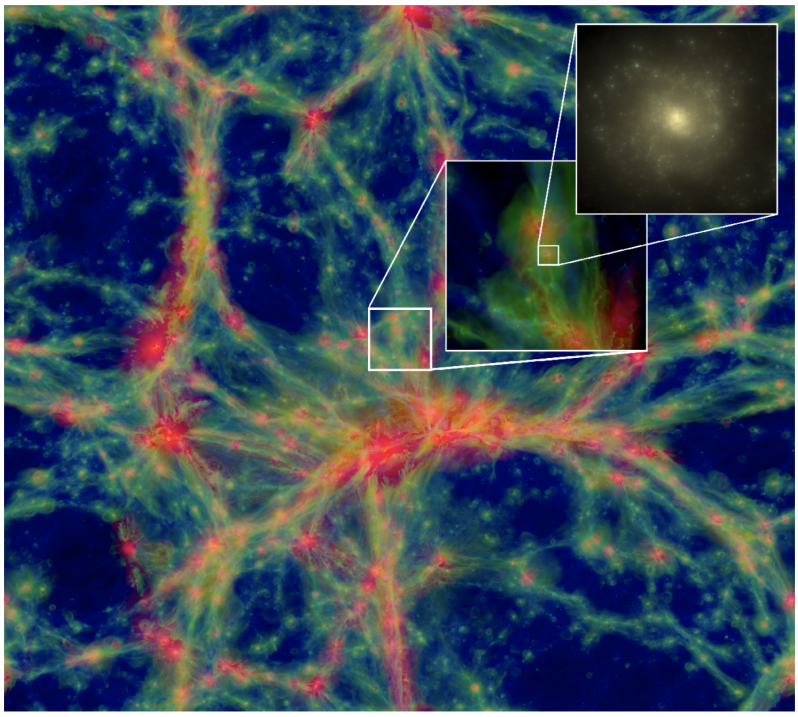

Figure 1.4: Figure 1 from Schaye et al. (2015) representing the cosmic web, extracted from the EAGLE simulations.

it fell into the center of dark matter haloes and settled in a rotationally supported disc with similar specific angular momentum as the dark matter counterpart.

It is within this supported gas disc that most first-generation stars were born (Bromm & Loeb, 2003; Yoshida et al., 2008). These stars (often referred to as Population III) were mainly composed of hydrogen, they were very massive (likely more massive than 100 $M_{\odot}$) and short-lived. At the end of their lives, the supernova explosions enriched the interstellar medium with heavy metals, allowing more efficient cooling mechanisms to take place and the formation of the second generation of stars.

### 1.2.2 Disc galaxies at high redshift

After having a description of how the universe may have started as a whole and how the first generations of stars were born, it is necessary to understand how disc galaxies like the MW have evolved through time. Observations of galaxies at high redshift can provide constraints on the conditions disc galaxies formed and grew under. The

Hubble Space Telescope (the Hubble Deep Field, HDF, and the Hubble Ultra Deep Field, UDF) provided crucial constraints on the size of galaxies at $z \sim 2$–3. On average, they seem to be less massive (Ferguson et al., 2000) than present-day galaxies. For instance, elliptical galaxies are a factor 2–3 smaller at $z > 1.5$ than $z = 0$ (Daddi et al., 2005). Spiral galaxies are a factor 2 smaller for $z \geq 1.5$ (Ferguson et al., 2004; Trujillo et al., 2006), but they do not seem to change much size-wise between $z = 1$ and 0 (Ravindranath et al., 2004; Barden et al., 2005; Trujillo & Pohlen, 2005). The ratio of different morphologies of galaxies at $z \sim 2$–3 is not the same as at $z = 1$. Irregular galaxies are more common, forming 40% of the total population (Abraham et al., 1999) as opposed to only 3% in the Local Universe. Spiral and elliptical galaxies only sum up to 31% and 13% respectively. Among the irregular galaxies, and following the morphology classification described in Elmegreen et al. (2008), relatively common morphologies are chains (12%), tadpoles (11%), clumps (19%) or doubles (13%) (see Fig. 1.5).

Therefore, there must be some mechanisms that explain the transformation of irregular galaxies into elliptical and spiral galaxies in numbers as we see at $z = 0$.

### 1.2.3 Hierarchical growth: mergers

Hierarchical growth describes the formation and evolution of structures within the ΛCDM paradigm (White & Rees, 1978b; Baugh et al., 1999; Fakhouri & Ma, 2008). In a bottom-up fashion, small low mass structures are the first to form, and they merge to become increasingly bigger, more massive, and more complex (Baugh et al., 1996; Cole et al., 2000; Baugh, 2006). The main process governing hierarchical growth is galaxy merging.

As previously explained, baryonic matter can form denser and less extended structures compared to their DM counterparts due to radiative cooling of gas. When two haloes fly by, their more extended DM haloes will go through each other (sometimes even the baryonic content of one halo goes through the DM halo of the other). The gravitation interaction between the two systems produces an accumulation of mass in the galactic

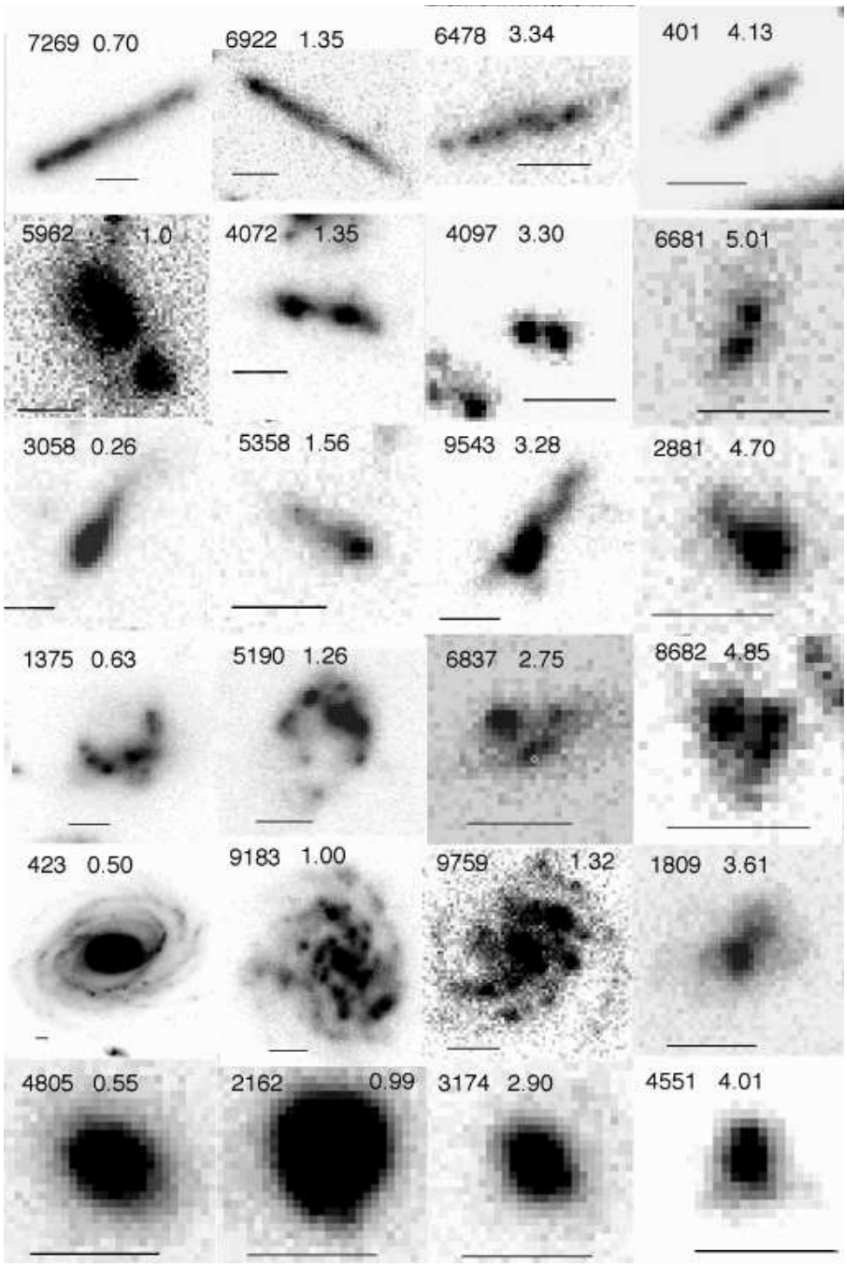


Figure 1.5: Figure from Elmegreen et al. (2008), where different galaxy morphologies from the Hubble Ultra Deep Field are shown. From top to bottom, the rows show chains, doubles, tadpoles, clump clusters, spirals, and ellipticals. The number on the top centre of each image indicates the redshift.

wake, which works as a break reducing the orbital energy of the haloes. This process, known as dynamical friction, results in the smaller halo spiraling down towards the bigger halo, eventually merging (Binney, 1977). Dynamical friction is then a key driver behind galaxy mergers, and allows several small systems to combine into a single, more massive object.

Mergers can induce drastic changes in galaxies: from morphological changes to their kinematics or their star formation rate. There are two types of mergers regarding the relative mass of the merging halos. Major mergers happen when the two galaxies have relatively equal mass, e.g. the mass ratio ranges from 1:1 to 4:1; while the rest are considered minor mergers (e.g., Bournaud et al., 2007; Lotz et al., 2011; Martig et al., 2012). There are also two categories of mergers regarding their gas content. Wet mergers are those with high gas content, and they can alter the morphology of the main galaxy significantly. Dry mergers are those with low gas content and are collisionless. Although at smaller scale, they can also alter the main galaxy's morphology. The lack of gas will then induce different changes in the host galaxy compared to wet mergers. Hence, not only the number of mergers, but their mass fraction and their gas content will be determinant for the morphological changes mergers induce.

One of the most changing effects mergers can induce is the transformation of the host galaxy from a disc galaxy into an elliptical galaxy. This is typically possible only for major mergers through a process called violent relaxation. Major mergers induce changes in the shape of the gravitational potential that are shorter in time than the average dynamical timescale (completing an orbit around the galaxy center) of disc stars. If the mass distribution/gravitational potential changes rapidly due to a major merger, the orbital energy of stars living in the disc after and before the merger is quite different. Some stars will gain energy increasing their orbital semi-major axis (some may even escape), while some others will loose energy and sink into the center of the galaxy. The central part of the galaxy becomes denser while the outer part becomes more extended (Lynden-Bell, 1967).

In the ΛCDM model, major mergers, however, are rare events compared to minor mergers. Minor mergers have been observed (Lin et al., 2004; Jogee et al., 2009;

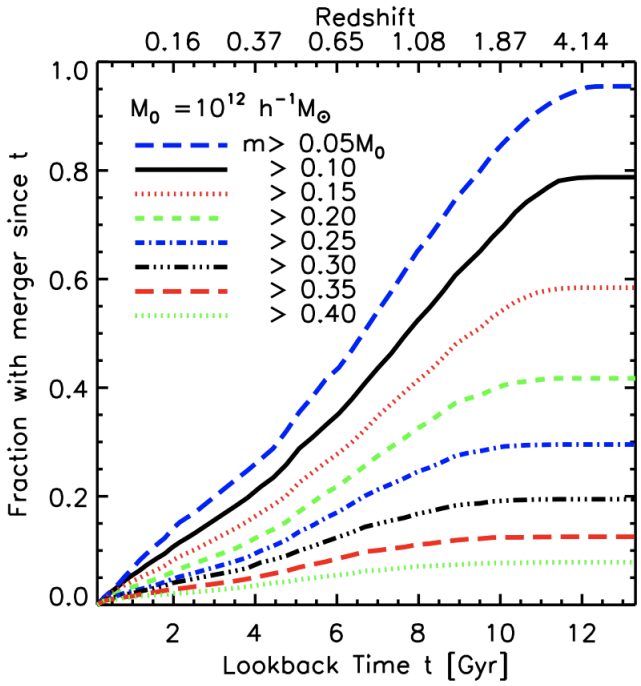


Figure 1.6: The fraction of MW size halos, $M_0 \simeq 10^{12} M_\odot$, that have experienced at least one merger larger than a given mass threshold since a look-back time (Stewart et al., 2008).

López-Sanjuan et al., 2010) and predicted in simulations (Maller et al., 2006; Stewart et al., 2008; Fakhouri & Ma, 2008; Kaviraj et al., 2009) to be 3-4 times more frequent than major mergers (see also Fig. 1.6). Mergers create asymmetries specially visible in the outskirts of discs that last for about 1.5 to 2 Gyr. During the merging process, tidal interactions between merging galaxies deposit part of their energy into stellar motions in the disc of the primary galaxy, thus causing the disc to become kinematically hotter and to spread out both radially and vertically, changing its morphology as well as its kinematics. Therefore, the main effects of minor mergers on discs are heating and tilting, not destroying them. For instance, numerical simulations have been carried out to study the effect of mergers on the creation of thick discs. Indeed, Qu et al. (2011) found that minor mergers heat the thin disc and create a stellar excess that requires a double sech$^2$ profile to be fitted. Villalobos & Helmi (2008) found that mergers with masses 10 to 20 per cent of the main galaxy lead to the formation of thick discs with similar characteristics to those of the MW's thick disc. The scale-lengths of the final thick discs are more extended after the merger and the thick discs are flared in the outskirts.

Hence, while minor mergers induce less dramatic changes to galaxies, they are still a crucial contribution to galaxy evolution. This is more so because the effect of minor mergers has been proposed to be accumulative (Bournaud et al., 2007). However, after a consecutive number of mergers, their impact may saturate.

Although there has been significant progress on the study of mergers from a theoretical point of view, mergers are difficult to study from the observational point of view since the signatures of mergers are in many cases weak or hard to detect, especially sometime after the event (Le Fèvre et al., 2000).

### 1.2.4 Gas accretion

As previously discussed, on a large scale in the universe, matter is structured in filaments or sheets leaving vast extensions of void between them. These filaments and nodes of dark matter then accrete gas to form galaxies in clusters. Simulations predict that these filaments are also associated with a diffuse gas component (Cen et al., 1994) that creates the so-called Lyman $\alpha$ forest, which has been used to infer the structure of dark matter filaments (e.g., Croft et al., 2002; Lee et al., 2014; Iršič et al., 2016). Gas follows the filaments to the nodes, where it feeds galaxies and fuels star formation (e.g. Blanton et al. (2005)). Gas accretion from gas filaments provide a smoother and less disruptive enrichment mechanism than mergers, and several evidence over the last decade support this scenario (e.g., Ocvirk et al., 2008). Without gas accretion, galaxies would deplete their gas in a matter of a few Gyr and subsequently quench (Bigiel et al., 2008; Leroy et al., 2008, 2013; Rahman et al., 2012).

In high-resolution cosmological simulations, gas is considered to exist in typically two regimes: hot and cold. Gas gets heated as it infalls into the galactic halo (Rees & Ostriker, 1977; Silk et al., 1977; Binney, 1977; White & Rees, 1978b). If the gas cooling time is larger than the dynamical timescale, it will not be able to cool down and therefore will remain in the hot regime. Instead, gas will form a hot hydrostatic halo whose pressure will prevent it from collapsing gravitationally (Birnboim & Dekel, 2003; Dekel & Birnboim, 2006). The temperature of this gas is considered as the temperature

of the halo. One of the most important gas heating mechanisms is feedback, whose bigger sources are stellar winds and supernovae on a local scale (Heckman et al., 1990; Hopkins et al., 2012), and active galactic nuclei on a more global scale (Silk & Rees, 1998; Bower et al., 2006; McNamara & Nulsen, 2007). Feedback heats the gas pushing it into the halo (Heckman et al., 1990; Shapley et al., 2003; Martin et al., 2005; Weiner et al., 2009; Rubin et al., 2014). Sometimes, gas will completely escape the galaxy, whereas sometimes it will cool down and fall back into the galaxy sometime after. The latter is a key cycle to provide the galaxy with fuel for star formation whilst not consuming all the gas at once.

In the cold regime, gas is not heated up and thus manages to fall into the central parts of the galaxy (Kereš et al., 2005, 2009). This mode is more dominant at higher redshifts when a hot gas halo has not grown yet, potentially shocking and heating infalling gas (Kereš et al., 2005; Benson & Bower, 2011). Therefore, cold gas filaments from the cosmic web directly feed galaxies at the cosmic nodes. The high density of these filaments allows for fast cooling. Later on, when hot gas haloes are in place, cold gas accretion happens mainly through wet mergers and gas filaments which are sufficiently dense and therefore cool down more efficiently (Dekel et al., 2009).

### 1.2.5 Early growth of disc galaxies

Having reviewed the two most important mechanisms for mass growth in galaxies, it is possible to reconcile the smaller and more morphologically varied galaxies at high redshift previously explained with the amount and sizes of disc galaxies seen at $z = 0$ (Park et al., 2007; Kelvin et al., 2014).

One of the main consequences of mergers is the transformation of disc galaxies into elliptical galaxies as described above. This is true especially for major mergers or successive minor mergers, and it is supported by simulations (Toth & Ostriker, 1992; Stewart et al., 2008). Even if major mergers are rare events, especially at lower redshifts, it is very unlikely that all the observed disc galaxies grew up in isolation. Simulations of galaxy mergers whose results were the inevitably production of elliptical galaxies did

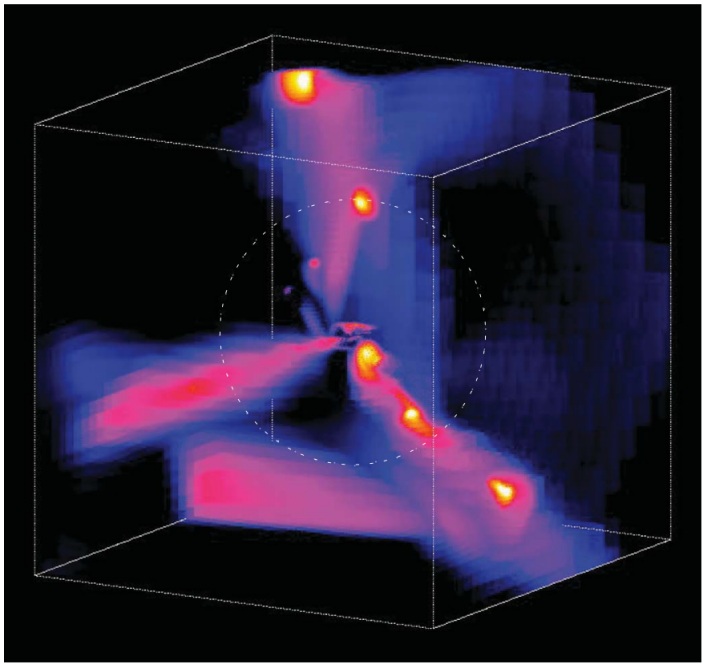

Figure 1.7: Figure 2 from Dekel et al., 2009. It shows the gas radial flux of a box 320 kpc wide. The colours indicate the inflow rate per solid angle.

not include gas (Toomre & Toomre, 1972; Toomre, 1977; Hammer et al., 2009; Taranu et al., 2013; Deeley et al., 2017). The inclusion of gas changed this (Athanassoula et al., 2016; Rodionov et al., 2017; Peschken et al., 2017; Sparre & Springel, 2017). By allowing each galaxy to have a gas halo, the collisionless interaction of the stellar haloes that results in the formation of a classical bulge is followed by cold gas accretion. The gas heated up during the merger can cool down and get accreted onto the main galaxy together with gas from filaments forming a disc. Thus, disc-dominated galaxies can form even when undergoing a major merger, especially if it happens at high redshift and there is time for cold gas accretion afterwards.

As for minor mergers, they can also transform a galaxy into an elliptical. However, most of the time, they will make the disc grow both radially and vertically as discussed above. This does not mean that minor mergers do not contribute to bulge growth. The instabilities created by minor mergers can result in stars falling to the galaxy centre due to angular momentum exchange. Gas brought by mergers can also fall into the centre and form stars there, growing the stellar mass of the bulge.

As already discussed, cold gas accretion also plays a crucial role in galaxy growth and

disc growth, especially at high redshift. This is because cold gas streams can penetrate deeper into the host halo (Ocvirk et al., 2008; Dekel et al., 2009). Intense gas mass inflows can create turbulence in the disc. The gravitational instabilities created by a gas dense region in the disc creates gas clumps which grow larger and larger in mass (Bournaud et al., 2008; Van Starkenburg et al., 2008). When the density is high enough, there is a burst of star formation and a massive star formation region is created, which later on will spiral down towards the bulge. These massive star formation regions can explain the chain and clump morphologies mentioned in Sec 1.2.2 (Bournaud et al., 2007, 2009; Dekel et al., 2009; Ceverino et al., 2010, 2012; Inoue et al., 2016). This whole process is usually referred to as violent disc instability. Likewise, because clumps scatter stars as they sink towards the centre, violent instabilities have been proposed as one possible mechanism for thick disc creation (Bournaud et al., 2009) (also discussed on in Sec. 1.3), and is thought to be an additional possible channel for bulge formation and growth (e.g., Bournaud, 2015 and references therein).

In summary, cold gas accretion (with violent instabilities) and wet mergers are two ways for rapid galaxy growth (Kereš et al., 2005; van de Voort et al., 2011), especially at early times peaking at around $z \approx 2$ (Dekel et al., 2009). Also, they can explain the transition from a large number of galaxies with irregular shapes at high redshift into the fraction of discs galaxies we see at $z \approx 0$, since both wet mergers and cold gas accretion bring gas that can form stars in disc-like configurations.

### 1.2.6 Secular evolution

For $z \leq 2$, mergers and violent disc instabilities become less dominant processes of galaxy evolution, and internal or secular processes start being more important. For instance, most disc galaxies possess bars and spiral arms. These two features are of great importance for the evolution of galaxies, especially in isolation. They change the radial gravitational potential of the galaxy and couple non-linearly with each other, inducing different kinds of perturbations, and dynamically affecting disc stars.

### Giant Molecular Clouds

The gravitational perturbation of stellar orbits by Giant Molecular Clouds (GMCs) has been proposed as a source of disc heating (Spitzer et al., 1951). GMCs typically range $\approx 10^4 - 10^6 M_\odot$ in mass, and have sizes of a few tens of parsecs, with average densities of the order of 100 $cm^{-3}$. Recent N-body simulations (Aumer et al., 2017) have shown that GMCs can heat the disc both horizontally and vertically. However, their influence has decreased over time. This could be due to both the decrease in GMCs' mass fraction over disc mass as a result of disc growing, and the decline of the star formation rate in disc galaxies which would have reduced numbers and/or densities of GMCs.

### Resonances

Galactic discs such as the MW rotate differentially with roughly constant circular velocity as a function of radius. Non-axisymmetric structures like bars or spiral density waves rotate like solid bodies, exerting a force upon stars. Due to the different circular velocities of stars and the perturbing non-axisymmetric structures, this force will vary depending on galactocentric radii. In particular, there are special places within the disc where the motion of the stars and the non-axisymmetric structures resonate. The corotation resonance (CR) is where the angular rotation of stars matches that of the perturber. The Lindblad resonance (LR) is where the star's epicyclic frequency matches the frequency of that star receiving a force by the perturber. This happens at two points in the disc, one inwards the CR and another outwards the CR, and are therefore called the inner Lindblad resonance (ILR) and the outer Lindblad (OLR) respectively.

### Galactic bars

Galactic bars are present in most spiral galaxies. Depending on the study, the fraction may go from 50% (Marinova & Jogee, 2007; Reese et al., 2007; Barazza et al., 2008) in the optical, to 70% in the infrared (Knapen et al., 2000; Eskridge et al., 2000; Menendez-Delmestre et al., 2007). With radii typically ranging between 2.5 to 5 kpc

long (Marinova & Jogee, 2007; Barazza et al., 2008; Durbala et al., 2008; Aguerri et al., 2009; Gadotti, 2011), they are one of the most identifiable features of spiral galaxies. How long bars can live is still an open question, and many efforts have been carried out in order to date bars (see a full discussion on bar age determination in Donohoe-Keyes et al., 2019).

Bars influence the secular evolution of galaxies in many ways. One of them is angular momentum redistribution. Bars experience dynamical friction as they rotate within the galaxy's dark matter halo. Bars will then slow down and grow in radius trapping more disc material. Angular momentum will be transferred everywhere through the disc in order to be conserved, making parts of the disc change into more elongated configurations (Athanassoula, 2003).

As some stellar material slows down due to the bar's action, it will sink into the galactic centre. This material will form a pseudobulge. The main differences between bulges and pseudobulges are that pseudobulges have Sersic profiles with a lower coefficients (Courteau et al., 1995; Carollo et al., 1999; Seigar et al., 2002; Fisher & Drory, 2008), they have star formation and hence young stellar populations (Peletier et al., 2007), and they have lower velocity dispersion and therefore are more rotationally dominated (Kormendy & J., 1993; Falcón-Barroso et al., 2006; Kormendy & Fisher, 2008). Gas is also accreted towards the center (Sakamoto et al., 1999; Sheth et al., 2005), which can cause episodes of enhanced star formation (Ellison et al., 2011; Catalán-Torrecilla et al., 2017). Also, this gas can potentially feed super massive black holes and therefore fueling Active Galactic Nuclei (AGN), although other works suggest otherwise (see a discussion in Knapen, 2005).

Therefore, bars are important angular momentum regulators and are important for the evolution of different parts of disc galaxies.

### Spiral arms

Spiral arms are also able to redistribute angular momentum in the disc. Lynden-Bell & Kalnajs (1972) showed that outside of resonances, spiral perturbations that grow

and decay adiabatically (i.e. on longer time scales than orbital and epicycle periods) leave stars unperturbed, only phase-space oscillatory ripples remain (Carlberg et al., 1985). At resonances, however, spiral waves can induce long lasting changes in the motions of stars. At the inner Lindblad resonance (ILR), for instance, stars will loose angular momentum, while they will gain it at the outer Lindblad resonance (OLR). These changes in angular momentum occur only during the spiral's growth and decay (Carlberg et al., 1985; Jenkins, 1992; De Simone et al., 2004). Changes in angular momentum of stars can happen without an increase of the velocity dispersion in the radial direction, i.e. if the orbit remains circular. This process is called churning.

However, Minchev & Quillen (2006) found an increase in the radial velocity dispersion after the spiral wave stops growing, and pointed out that this is an additional heating mechanism caused by spiral arms. Hence, spiral arms serve as radial heating mechanisms, but not as vertical heating ones because the coupling of the spiral perturbation with the vertical motion of stars is very weak (Sellwood, 2013).

#### Radial migration

The processes described above cause the redistribution of angular momentum in the disc and therefore stars change the guiding centre of their orbits. Sellwood & Binney (2002) showed that migration can have long-term effects on the entire disc. For example, transient spiral arms (which disappear and reappear on the time-scale of a galactic rotation) is one of the main consequences of migration. This has been seen in many simulations (e.g., Roškar et al., 2008; Minchev & Famaey, 2010; Solway et al., 2012). Radial migration can change the distribution of metals within the disc. Some works have claimed that whereas the metallicity gradient does not change much, the metallicity distribution broadens with time at any given radius because of radial migration (e.g., Grand et al., 2014). Other works have highlighted that the metallicity gradient might indeed change (e.g., Chiappini et al., 2003; Minchev et al., 2013, 2014).

Another important effect of radial migration is disc thickening. Schönrich & Binney (2009) used radial migration to explain the MW's thin and thick disc characteristics

found in observations, i.e. stars from the inner regions of the disc and the bulge, which usually have higher velocity dispersion, migrate outward thickening the disc. This has been also supported by other works (Roškar et al., 2008; Loebman et al., 2011). Minchev et al. (2012a) found this, but also found that this effect can be cancelled out by migration from outer and colder stars into inner regions of the disc, keeping the overall disc thickness intact (this was confirmed by later works e.g., Martig et al., 2014a; Grand et al., 2016; Aumer et al., 2017). Only at the very outer and inner regions of the disc, where only one of the two types of migration (inward, outward) exists, radial migration has a significant effect. For instance, radial migration can produce disc flaring in the outskirts of the galaxy.

### 1.2.7 The Age-Velocity-Relation

Most of the processes described above contribute to the vertical heating of the disc over time –either by themselves or in combination with others. Therefore, it is expected that for stars within the disc, there is a relation between stellar age and vertical velocity dispersion $\sigma_z$. Such relation is the Age-Velocity-Relation (AVR). Determining the shape of this relationship is a difficult task from an observational point of view since it is difficult to obtain stellar ages with low uncertainties (Soderblom, 2010) and because of selection function effects when choosing the sample (Haywood et al., 2013). A couple of examples of different AVR shapes for the MW are shown in Fig. 1.8.

The AVR is therefore a reflection of the galaxy's evolution history, particularly vertical disc heating. However, part of the high vertical velocity dispersion present in older stars may be determined already by the conditions these stellar populations were born in rather than the posterior evolution of the galaxy. In other words, old stellar populations may have been born with a high velocity dispersion already. Observations of turbulent gas discs at high redshift (e.g., **?**) support this, but it is not clear yet that galaxies with very turbulent gas discs at high redshift are progenitors of MW-like galaxies (Van Dokkum et al., 2013; Inoue et al., 2014).

On the simulation side, works like Martig et al. (2014b) find that regardless of the

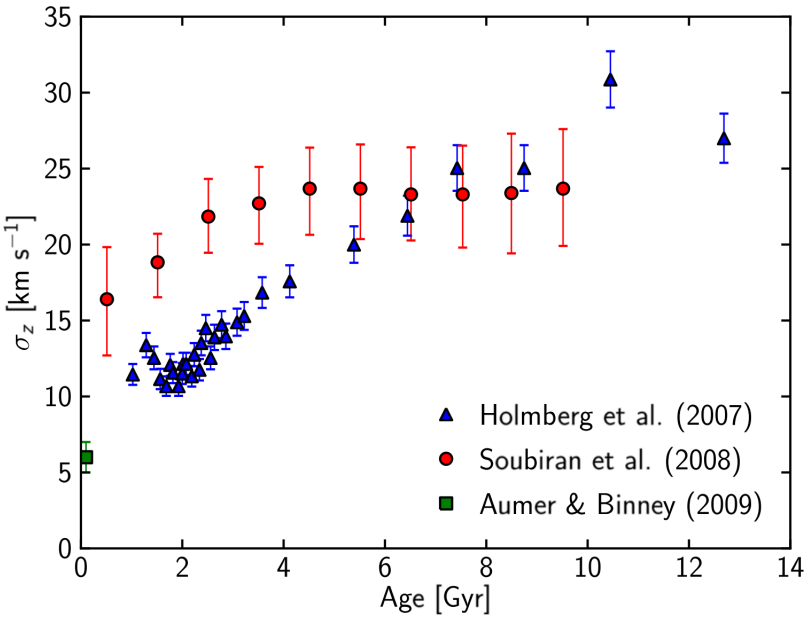


Figure 1.8: Figure 1 from Martig et al. (2014b). It shows that depending on the sample, the AVR looks very different in the Solar neighbourhood. Blue triangles are from Holmberg et al. (2007), red circles from Soubiran et al. (2008), and green triangles from Aumer & Binney (2009)

galaxy evolution at later times, galaxies undergo a period of mergers and turbulent star formation at high redshift, therefore stars with ages higher than 8-9 Gyr old (some cases even 7 Gyr) are born already hot. It is at later times where the shape of the AVR depends on disc heating agents, especially mergers (also found in other works like Quinn et al., 1993; Velázquez & White, 1999; Kazantzidis et al., 2008). Even 1:10 or 1:15 mergers can heat up the disc creating a gap between $\sigma_z$ of stars born prior and after the merger. In the case of galaxies with quiescent merger histories, $\sigma_z$ increases with age more smoothly.

Therefore, the AVR can be very effective at probing the merger history of galaxies. The large uncertainties when determining ages are still a challenge since they can blur signatures of past mergers (Martig et al., 2014b). However, it is clear that important events in the history of galaxies such as mergers cause disc heating, and it is through quantifying the heating and understanding its sources that we can attempt to unveil the past of galaxies.

## 1.3 Thick discs

Thick discs were first discovered in external galaxies by Tsikoudi (1979) and Burstein (1979), and later on, in the Milky Way by Gilmore & Reid (1983). Since then, they have been shown to be present in the majority of disc galaxies (Dalcanton & Bernstein, 2002; Yoachim & Dalcanton, 2006; Comerón et al., 2018). However, the origin of such components is still a matter of debate. A question that still remains open is whether thin and thick discs are two distinct components or not, which is addressed in this thesis. Thin and thick discs may or not be two different galactic components depending on what their definitions are based on.

### 1.3.1 Definition(s) of thick disc

As mentioned, the division between thick and thin disc has been a debate for a very long time. A part of the controversy comes from the very definitions of thin and thick disc themselves. There are many ways to define thin and thick discs. This is due to the different information astronomers can access depending on whether they study the MW or external galaxies. Different parameters set different definitions for the thin and thick disc, hence different thin and thick disc components. The definitions are:

- A definition is based on the morphology of the galaxy. The vertical light profile of galactic discs can be fit by two exponential-like functions (e.g., Tsikoudi, 1979). Therefore, each exponential can be attributed to a different component of the disc: the thin and the thick disc. This has been observed in many different nearby galaxies (e.g., Comerón et al., 2011, 2012, 2014). This definition is equivalent to the one based on the vertical stellar density, which has been characterised for the MW (Jurić et al., 2008). Hence, this definition is often labeled the geometrical definition, and can be used both for external galaxies and the MW.

- Based on the proper motions of the stars in the solar neighbourhood, the stellar population in the solar vicinity can be divided into the kinematic thin and thick disc (Prochaska et al., 2000; Bensby et al., 2003, 2005; Reddy et al., 2003).

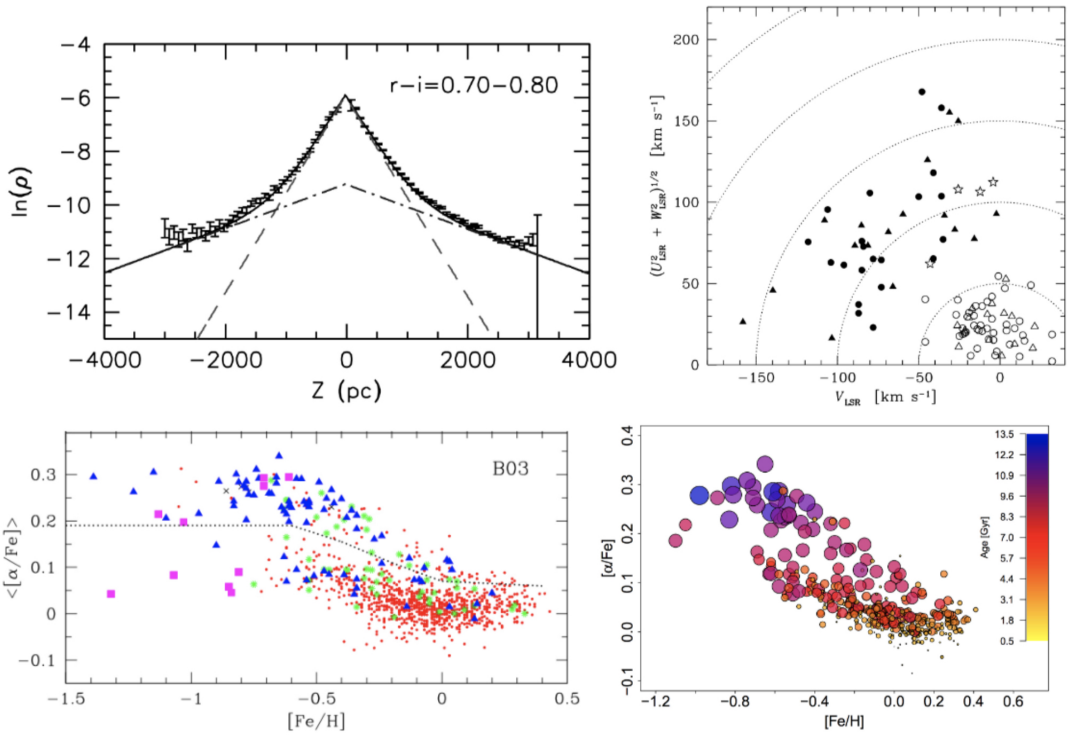


Figure 1.9: Four plots representing each of the thick disc definitions for the MW. *Top left:* Definition based on morphology: vertical density profile with the fit of the two exponential-like functions. Extracted from Jurić et al. (2008). *Top right:* Definition based on kinematics: Toomre diagram extracted from Bensby et al. (2005). *Bottom left:* definition based on chemistry. Distribution of $[\alpha/Fe] - [Fe/H]$ of disc stars extracted from Adibekyan et al. (2012). *Bottom right:* Definition based on age: distribution of $[\alpha/Fe] - [Fe/H]$ associated with age extracted from Haywood et al. (2013)

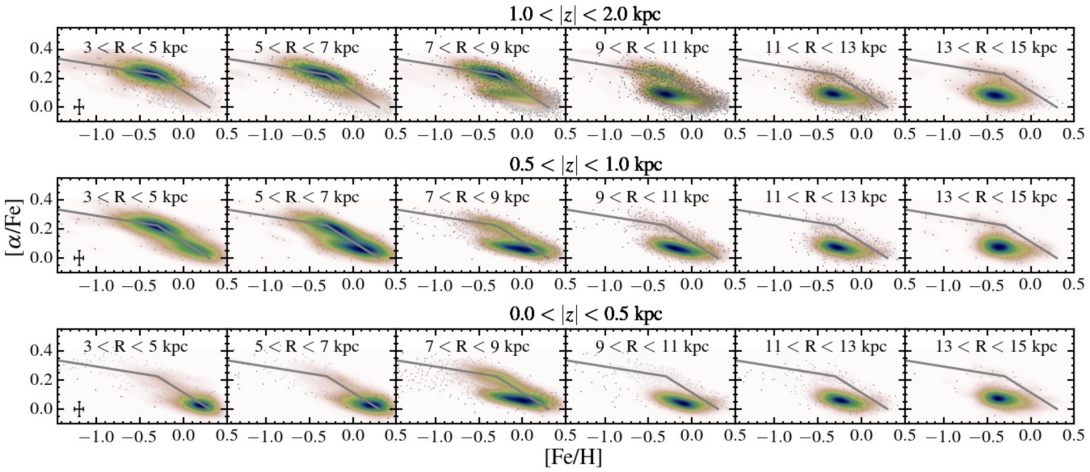


Figure 1.10: extracted from Hayden et al. (2015), where they show the two distinct chemical populations of the MW and their radial extension. As it can be seen, the $\alpha$-rich disc component of the MW disc only has a significant presence up to 11 kpc from the galactic centre at $1.0 < |z| < 2.0$ kpc.

- Works on chemical analysis of the MW disc (e.g., Fuhrmann, 1998; Navarro et al., 2011; Adibekyan et al., 2012; Hayden et al., 2015; Mackereth et al., 2018) reveal two components: one made of stars with enhanced $\alpha$-elements chemistry, or $\alpha$-rich component; and one made of stars without such enhancement, or $\alpha$-poor component. $\alpha$-rich stars also possess overall greater vertical velocities, indicating that they belong to the thick disc. Therefore, $\alpha$-rich and $\alpha$-poor stars correspond to the chemical thick and thin discs respectively.

- Traditionally, the thin disc was considered as a star-forming region, therefore made by young stars; whereas the thick disc was made by old stars. This was confirmed when the stellar age of stars in the solar vicinity was measured (Haywood et al., 2013; Bensby et al., 2014; Kubryk et al., 2015). Two components were found: the old and the young disc, which correspond to the age thick and thin disc respectively.

To see visually these different definitions and thin/thick disc components, please see figure 1.9. The are two main problems with these different definitions. The first one is that the different thick and thin components do not correspond to each other depending on the definitions. The second problem is that parameters of individual stars like proper motion, chemical composition, and age, are only possible to be measured in the MW,

so there is no way to compare the subsequent thin and thick disc components with those of nearby galaxies. For instance, it has been observed that for the MW, the $\alpha$-rich disc (chemical thick disc) has a short radial extension compared to the $\alpha$-poor disc (see figure 1.10), but it is still unclear if this is the case for the geometrical definition in the MW case. On the other hand, observations of nearby galaxies, for instance Comerón et al. (2011), reveal an extended geometrical thick disc (see in figure 1.11).

Everything described so far leads to a set of questions: why the different definitions of thin and thick disc separate galactic discs into different components? Are there really two different populations? Since the kinematic, chemical, and age definition can be only applied to the MW as of today due to lack of data, how similar is the MW to nearby galaxies? Are nearby galaxies diverse as well in their chemical and dynamic thick components?

Ultimately, all these different definitions reflect that there are two different populations that potentially have different evolutionary histories. Among these definitions, this thesis uses the geometrical definition because is the best for comparing the MW with other nearby galaxies.

### 1.3.2 Mass and structure of geometrical thick discs

The stellar masses of such geometrically thick discs range from $10^{8.5}$ to $10^{10.5}$ $M_\odot$ (e.g., Comerón et al., 2011), and seem to correlate with their host galaxy's masses, or circular velocities (Comerón et al., 2018). By contrast, the thick-to-thin disc mass ratio, which spans values from 0.3 to 3, is anticorrelated with galaxy mass (Yoachim & Dalcanton, 2006; Comerón et al., 2011, 2014; Elmegreen et al., 2017; Martínez-Lombilla & Knapen, 2019). For instance, the ratio of thick disc stars to thin disc stars depends on the luminosity or circular velocity of the galaxy: it is about 10% for large spirals like the Milky Way, and rises to about 50% for the smallest disc systems.

Scale-heights range from 0.07 to 0.46 kpc for thin discs, and 0.33 to 2.4 kpc for thick discs (Comerón et al., 2011). In the Milky Way, Jurić et al. (2008) find the scale-

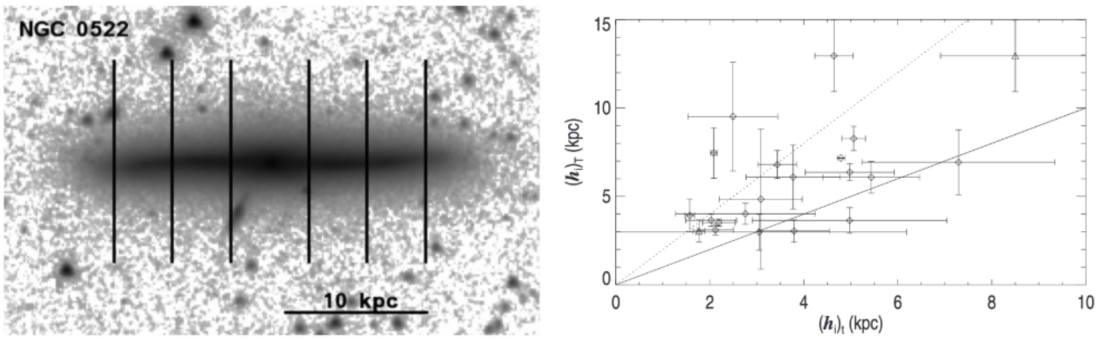


Figure 1.11: *On the left:* figure from Comerón et al. (2011) in which it can be seen that the thick disc component is extended. *On the right:* figure from Comerón et al. (2012) where the thin disc scale-lengths are represented against thick disc scale-lengths. Nearby galaxies show larger thick disc scale-lengths than thin disc scale-lengths

heights for the thin and thick discs to be $\sim$ 0.3 and $\sim$ 0.9 kpc respectively, but more recent estimations of the thick disc scale height are around $\sim$ 0.5-0.7 kpc (Robin et al., 2014; Mateu & Katherina Vivas, 2018, see also Bland-Hawthorn & Gerhard, 2016b and references therein).

Among other thick disc properties, one this work focuses on is the global shape of the disc, i.e. the possible variations of scale-height with radius. Studies on large samples of galaxies (e.g., Yoachim & Dalcanton, 2006; Comerón et al., 2011, 2012, 2014, 2018) concluded that the vast majority of thick discs in external galaxies have a constant scale-height with radius, even though other works had suggested that flat thick discs should belong to late-type galaxies only (De Grijs & Peletier, 1997; Bizyaev et al., 2014). The studies which found only flat thick discs, however, either show one averaged scale-height for the whole thick disc (Yoachim & Dalcanton, 2006), or describe the disc with only a few radial bins (Comerón et al., 2011, 2012, 2014, 2018), making it difficult to observe variations in the scale-heights with galactic radius. This does not mean that thick discs are never flat: this has been clearly shown in some cases, for instance by Ibata et al. (2009) and Streich et al. (2016). However, other works have also found thick discs with a significant amount of flaring (Narayan & Jog, 2002; Kasparova et al., 2016; Sarkar & Jog, 2019; Kasparova et al., 2020), and Rich et al. (2019) found boxy shaped isophotes in the outer disc of some edge-on galaxies, which indicate strong disc flaring (Mosenkov et al., 2020).

In the Milky Way, although flaring in the inner disc (∼11 kpc) is highly disfavoured (Mateu & Katherina Vivas, 2018), the existence of thick disc flaring in the outskirts (Robin et al., 2014; Mateu & Katherina Vivas, 2018; López-Corredoira et al., 2018; Thomas et al., 2018), and the amplitude of the effect (Reylé et al., 2009; Polido et al., 2013; Kalberla et al., 2014; López-Corredoira & Molgó, 2014; Amôres et al., 2017) are still a matter of debate. In any case, there is increasing evidence that thick discs might be more diverse than previously thought in terms of global shape and flaring.

### 1.3.3 Age structure of thick discs

Similarly, the age structures created by the stellar populations in thick discs are also showing more diversity in recent studies than previously thought. Some works using broadband photometry (e.g., Dalcanton & Bernstein, 2002; Seth et al., 2005; Mould, 2005) and spectroscopy (Yoachim & Dalcanton, 2008; Comerón et al., 2015, 2016) helped establish the classical view of thick discs as red, old, and metal poor components. However, on the one hand, colour cannot account for the age-metallicity degeneracy, especially for old ages (> 6 Gyr). On the other hand, spectroscopy is limited by the low surface brightness of the outer regions of the thick disc (see a more detailed discussion in section 4.2 in Martig et al., 2016). Despite these limitations, more recent works suggest that thick discs are diverse and have complex age structures. Kasparova et al. (2016) analysed spectroscopically three edge-on galaxies, and found that while one has a very old thick disc (∼10 Gyr), the other two have intermediate age (∼5 Gyr) stars in their thick discs. In the Fornax cluster, Pinna et al. (2019a,b) found that in FCC 170 (NGC 1381), FCC153 and FCC 177, the thick discs are very old but host complex populations. In the Milky Way, the geometrically thick disc is made of old stars in the solar neighbourhood and the inner disc, but shows a strong radial age gradient: Martig et al. (2016) performed an analysis on red giants selected from the APOGEEE Data Release 12 (Holtzman et al., 2015) using the APOGEE Stellar Parameter and Chemical Abundances Pipeline (ASPCAP, García Pérez et al., 2016). Using a training sample of ≈ 1,500 stars from APOKASC survey (Pinsonneault et al., 2015) (which is a combination of APOGEE with the Kepler Asteroseismic Science Consortium (KASC)), a good

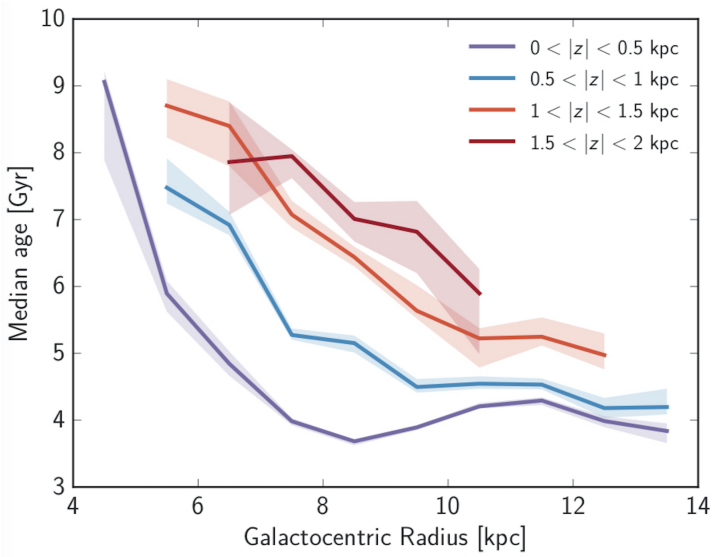


Figure 1.12: Figure 1 from Martig et al. (2016) in which the radial age gradient of the geometrically thick disc of the MW was measured

determination of stellar masses, hence ages, was obtained. The results can be seen in figure 1.12. Indeed, the median age of the stellar population decreases with increasing galactocentric radius at all heights above the mid-plane. Between galactocentric radii of 6 and 12 kpc, the mean age of red clump stars in the thick disc drops from $\sim 9$ to $\sim 5$ Gyr (for other works on the same topic, see also Ness et al., 2016; Xiang et al., 2017; Feuillet et al., 2019).

Such a radial age gradient has not been found yet in any other galaxy, either because the few galaxies that have been observed do not have the same structure as the Milky Way, or because the observations were not able to probe the very outer regions of the thick disc. In any case, a picture is emerging where thick discs can host complex stellar populations and have different age structures.

### 1.3.4 Thin/Thick disc distinction

The age structure of thick discs is also connected to the important question of their relationship to thin discs: are thin and thick discs clearly distinct components, and is the separation meaningful? In the MW, it has been suggested for a long time that the thin and thick discs could just be part of the same continuous structure (Nemec &

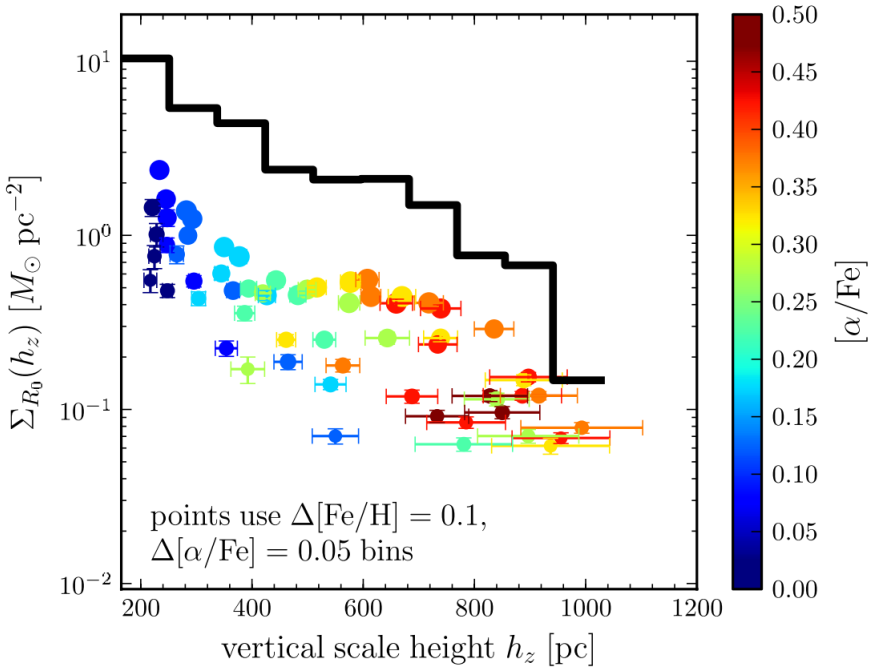


Figure 1.13: Figure 2 from Bovy et al. (2012b). Stellar surface density as a function of scale-height for different stellar populations colour-coded by [$\alpha$/Fe]. The thick black histogram shows the total stellar surface-mass density.

Nemec, 1991, 1993; Norris, 1999). Bovy et al. (2012a) and Mackereth et al. (2017) have shown that the transition from thin to thick disc corresponds to a continuum of stellar populations, and that the Milky Way's thick disc is not a distinct component (see Fig. 1.13). Rix & Bovy (2013) further argued that while the vertical density profile can be very well fitted by a sum of two exponentials, these do not correspond to a meaningful physical decomposition (see also Park et al., 2020 for a discussion of this issue using numerical simulations). Whether the Milky Way is a unique case or not is still unknown, but what is most likely is that there exists a variety of disc structures.

Streich et al. (2016) do not find a separate thick disc structure for three external galaxies, while MUSE observations by Guérou et al. (2016) or Pinna et al. (2019a) find thick discs that seem distinct from the thin disc. Yet, these results cannot be compared straightforwardly with the MW.

Ultimately, the age structure of thick discs and the thin/thick disc dichotomy must be linked to the formation process of galactic discs.

### 1.3.5 Thick disc formation

Thick discs have been proposed to be a natural consequence of ΛCDM (Read et al., 2008). The question of how thick discs form has been tackled abundantly in the literature. Yet, their exact origin is still a matter of debate as of today.

One mechanism for thick disc formation is radial migration, proposed by Schönrich & Binney (2009); Loebman et al. (2011); Roškar et al. (2013), and discussed in Sec. 1.2.6. According to this theory, stars with high velocity dispersion from the bulge and the inner disc migrate outwards, thickening the disc. However, later on, works like Minchev et al. (2012b); Martig et al. (2014a); Vera-Ciro et al. (2014) found that radial migration does not contribute much to disc thickening and, on the contrary, it suppresses flaring when external perturbations are included (Minchev et al., 2014; Grand et al., 2016).

Another possibility is that thick disc stars are in turn thin disc stars that have been heated up by minor mergers (Quinn et al., 1993; Read et al., 2008; Villalobos & Helmi, 2008; Di Matteo et al., 2011). Other mechanisms include thick discs originating from stars born out of accreted gas from gas-rich mergers (Brook et al., 2004, 2005), or stars accreted from galaxy mergers (Abadi et al., 2003; Meza et al., 2005). In the latter case, thick discs would have an extragalactic origin. Finally, Bournaud et al. (2009) proposed that flat thick discs could form through a clumpy and turbulent phase in the evolution of galaxies at early times, explained in Sec. 1.2.5.

### 1.3.6 Flaring mono-age populations vs. flat thick discs

Observations of flat thick discs (e.g., Yoachim & Dalcanton, 2006; Comerón et al., 2011, 2012, 2014, 2018) favoured the formation scenario proposed by Bournaud et al. (2009), but it remained unknown why mergers (an inevitable consequence of ΛCDM) did not produce disc flaring as seen in the simulations (Kazantzidis et al., 2008, 2009; Qu et al., 2011; Moetazedian & Just, 2016). This remained a conundrum until Minchev et al. (2015) proposed a thick disc formation mechanism by which the superposition of coeval flaring disc populations would form a flat thick disc. The key to understanding

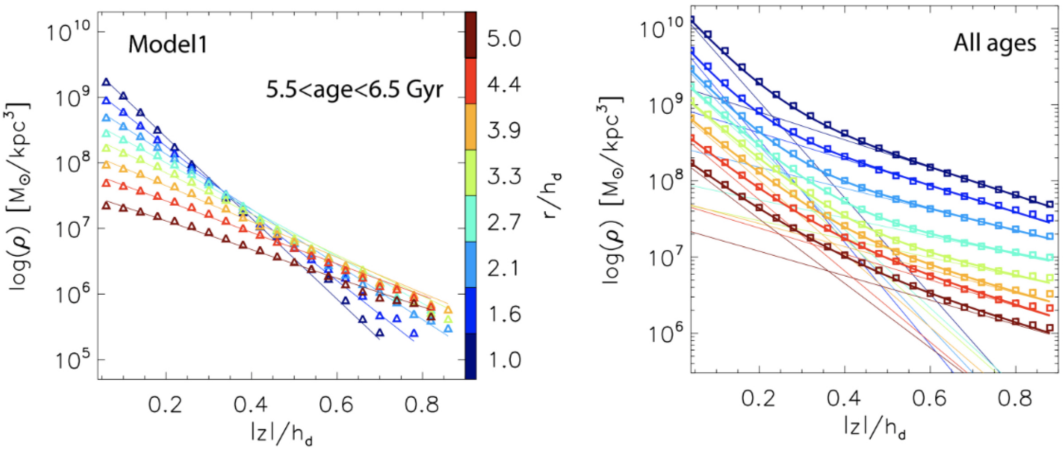


Figure 1.14: Figure 1 of Minchev et al. (2015). *On the left*: vertical density profiles of a single mono-age population at different radii. These vertical density profiles can be fitted with a single exponential function, and reveal that the population is more flared with increasing radius. *On the right*: vertical density profiles of all the mono-age populations together. It shows that when all the mono-age populations within these radii are included, the vertical density profiles change to a double-exponential distribution, in agreement with observations. All physical distances are normalized to the galaxy scale-length.

the apparent discrepancy between natural flaring predicted by simulations and the flat thick discs scale-height observed in nearby galaxies is to study mono-age populations within the disc. Minchev et al. (2015) used zoom-in cosmological simulations from Martig et al. (2009, 2012) and Springel et al. (2008); Scannapieco et al. (2009) to study the distribution of mono-age populations throughout the disc (for more details on the simulations by Martig et al. (2009), please see Chapter 2 of this thesis). After decomposing the stellar disc into bins of $\Delta$age = 1 Gyr, it was possible to fit the column density of each mono-age population in the vertical direction with a single exponential, as shown in the left panel of Fig. 1.14. These exponential fits flare with increasing radius. However, when all ages are taken into account, two exponentials are needed to fit the vertical density columns at every radius (see right panel of Fig. 1.14).

To reconcile the flaring of mono-age populations with the constant scale-height of galactic discs, Minchev et al. (2015) studied the variation of scale-height, surface density, and mean age with galactocentric radius (see Fig. 1.15). Simultaneously, they overplotted the values of the overall thin and thick disc components of the two models studied. In contrast to the flaring found for all mono-age populations, the thin and thick disc decomposition of the total stellar population including all ages, results in no

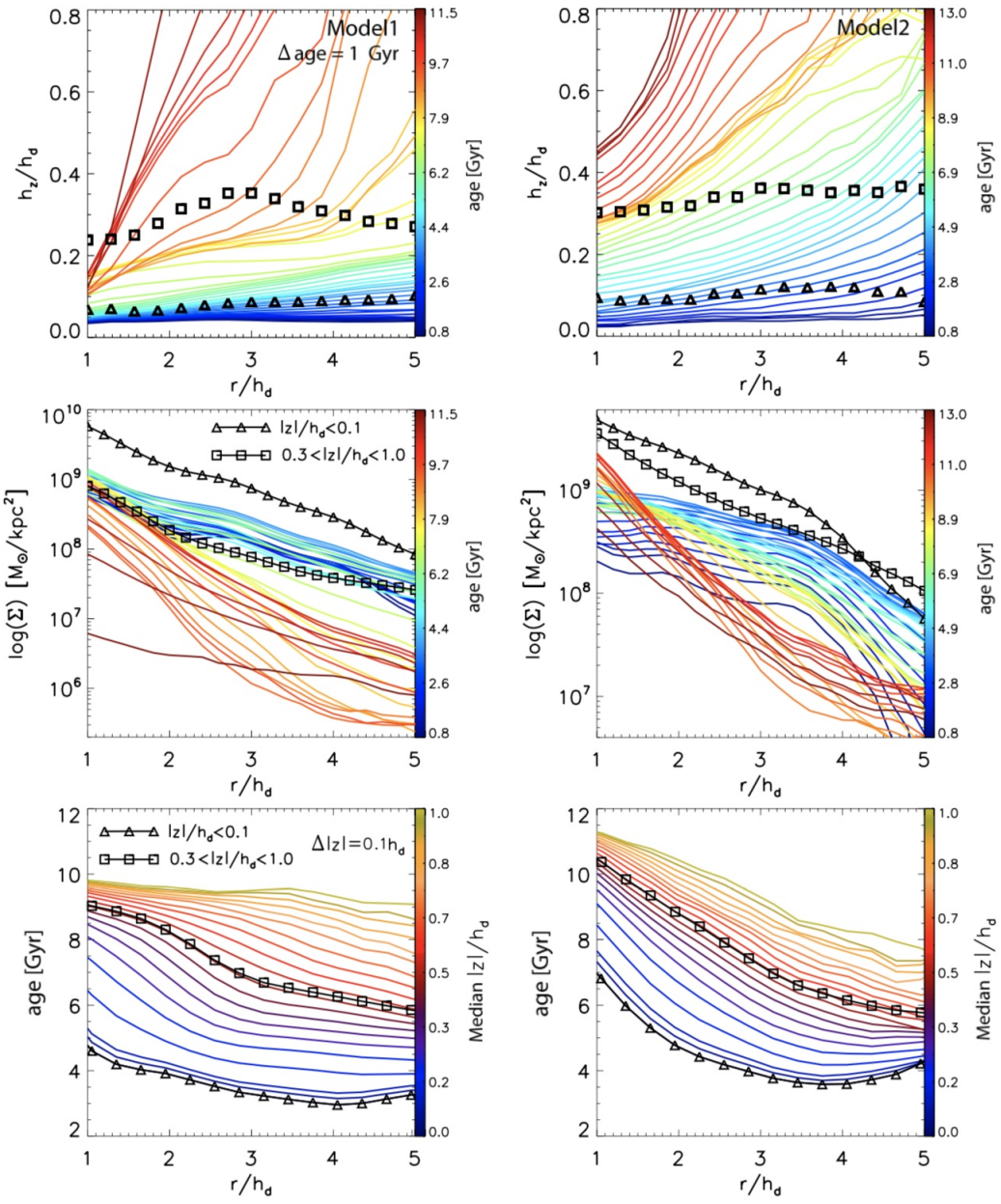


Figure 1.15: Figure 2 of Minchev et al. (2015). *On the top:* variation of scale-height, $h_z$, with galactocentric radius. Triangles and squares correspond to the thick and thin disc components respectively. *On the middle:* Disc surface density radial profiles of mono-age populations. Triangles and squares correspond to the surface density profiles of stars close to and high above the disc midplane respectively. *On the bottom:* Variation of mean age with radius for samples at different distance from the disc midplane, indicated by the color bars. Triangles and squares correspond to the age radial profiles of stars close to and high above the disc midplane respectively. All physical distances are normalized to the galaxy scale-length.

apparent flaring. In other words, the constant scale-height of the thick disc is the result of the superposition of flaring mono-age populations.

This scenario can be explained with an inside-out galaxy formation history, in which mono-age populations form at progressively larger radii and then flare due to interactions of the galaxy with satellites, mergers, and other processes described above. Since mergers and masses of satellites decrease with time, the younger the stellar population, the further out it dominates in terms of stellar mass.

In summary, old stellar populations tend to have shorter scale-lengths and more flaring, while the scale-length of younger populations is larger and their flaring smaller. When combined, the resulting global thick disc has a constant scale-height as a function of radius. The power of this mechanism is that it reconciles the geometrical thin and thick disc with other thick disc definitions such the $\alpha$-rich/poor thick/thin discs. This is not to say that the $\alpha$-rich thick disc and the geometrical thick disc are the same. Rather, it shows that, at least for the MW, different definitions can be linked to different evolutionary processes or time periods.

In conclusion, it is clear that thick discs are more diverse and complex than previously thought. As new instruments such as MUSE are providing a wealth of data of external thick discs, it will be possible to better compare the MW's thick disc with other galaxies' in new ways. Yet, neighbouring galaxies have different evolutionary histories, and subsequently might not necessarily fit into the picture Minchev et al. (2015) describes. Therefore, theoretical work is needed to support future observations. Chapter 3 of this thesis addresses this issue by analysing a sample of 27 MW-like simulated galaxies and expands on the work by Minchev et al. (2015).

## 1.4 Warps

Warps in the stellar disc of galaxies were first discovered by van der Kruit & Searle (1981). Large surveys of galaxies have since then shown that stellar warps are present in 40 to 75% of galaxies, depending on the nature of the sample (Reshetnikov & Combes,

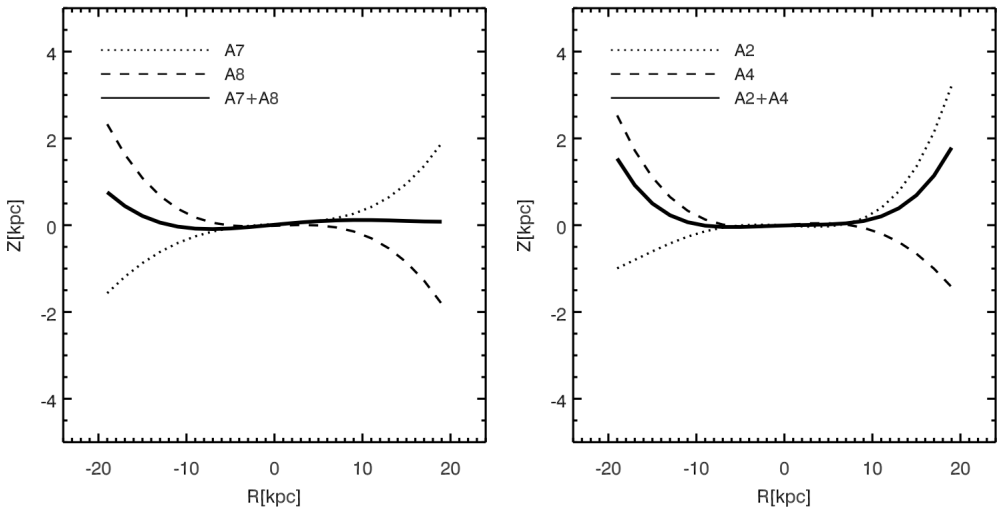


Figure 1.16: Figure 13 from Kim et al. (2014), where modelled L- and U-shaped warps are shown. These shapes could be the result of many S-shaped patterns superposed.

1998; Ann & Park, 2006). Schwarzkopf & Dettmar (2001) even found that 93% of interacting/merging galaxies present warps (vs. 45% of the non-interacting galaxies). Warps are also commonly observed in the HI disc of galaxies (Sancisi, 1976; Bosma, 1981; Heald et al., 2011). Stellar warps reach amplitudes up to 25° (Sánchez-Saavedra et al., 2003), and gas warps amplitudes up to 33° (García-Ruiz et al., 2002). The duration of warps is difficult to establish from observations, but simulations have found that warps can last from several Myr (Semczuk et al., 2020) to several Gyr (Shen & Sellwood, 2006), depending on their formation mechanism. Different formation processes can also explain many of the warps' morphological properties (Saha & Jog, 2006), for instance, whether warps are L-shaped (one sided), S-shaped (one side of the disc rises, the other declines), or U-shaped (both sides of the disc rise/decline) (see Fig. 1.16 from Kim et al., 2014).

In the Milky Way (MW), an HI warp has been detected at galactocentric radii larger than R∼10 kpc, reaching a height ∼4 kpc above the midplane in the North (l ∼ 90°) and curving to the South (l ∼ 270°) below 1 kpc (Levine et al., 2006). A warp in the stellar Galactic disc has also been detected (see Fig. 1.17) at galactocentric radii larger than R∼9 kpc, reaching heights above the mid plane up to R∼5 kpc (e.g., López-Corredoira & Molgó, 2014; Liu et al., 2016; Poggio et al., 2018; Romero-Gómez et al., 2019; Cheng et al., 2020; Antoja et al., 2021). Simulations suggest that the warp in the

Galactic disc is probably due to the gravitational influence of the infall of the Large Magellanic Cloud (Laporte et al., 2018, 2019; Poggio et al., 2020).

While Van Der Kruit (2007), using the SDSS survey, suggested that stellar and gaseous warps are different components with different evolution scenarios, Gómez et al. (2017) found in simulations that gas and stars in warps follow the same pattern and that they remain coincident for at least 1 Gyr. This seems to agree with what Chen et al. (2019) found in the MW, where the morphology of the warp for the gas and the youngest stellar populations trace each other up to at least 20 kpc, suggesting that the two components are closely linked to each other.

Many mechanisms have been proposed for warp formation, including misalignment between the disc and the halo (Debattista & Sellwood, 1999; Ideta et al., 2000), misalignment between the inner stellar disc and the gas disc (Roškar et al., 2010; Aumer & White, 2013), interactions between magnetic fields and HI gas (Battaner et al., 1990; Battaner & Jiménez-Vicente, 1998), accretion of intergalactic matter onto the disc (López-Corredoira et al., 2002; Semczuk et al., 2020), bending modes or waves embedded in the disc (e.g. Sparke & Casertano, 1988; Revaz & Pfenniger, 2004; Chequers & Widrow, 2017), and the gravitational interaction of an in-falling satellite (Ostriker & Binney, 1989; Weinberg, 1998; Jiang & Binney, 1999). In the latter scenario, new infalls can regenerate and maintain the warp for several Gyr (Shen & Sellwood, 2006).

Many of the warp forming mechanisms are often associated with disc heating and flaring (e.g., Gerssen & Shapiro Griffin, 2012; Minchev et al., 2015; Pinna et al., 2018). Therefore, disc heating and warping may happen simultaneously. However, works like Velázquez & White (1999) and Shen & Sellwood (2006) suggest that this may not be the case. This question is addressed in this thesis in Chapter 4, where I explore how much vertical disc heating happens during warps, and what happens to the vertical stellar density of discs depending on the warp's origin.

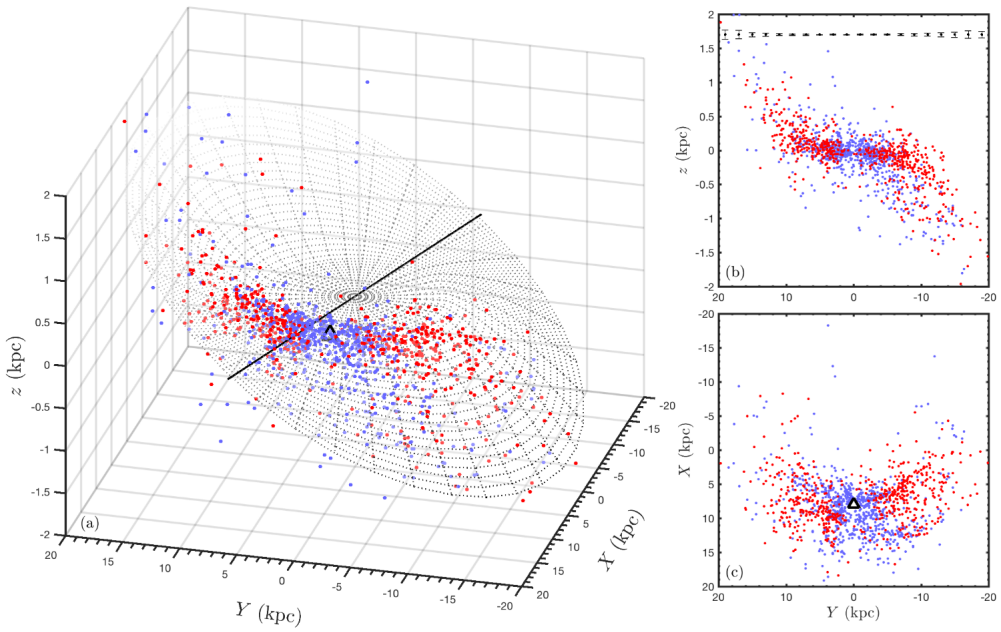


Figure 1.17: Figure 1 from Chen et al. (2019), showing a 3D map of the MW's warp traced by Cepheids. Red and blue dots represent respectively Cepheids discovered with infrared and optical passbands. The black upward-pointing triangle is the position of the Sun.

## 1.5 Scientific goals

In this thesis, I explore the vertical density structure of galactic disc using simulations. The aim is to understand how many features related to the vertical stellar density of disc galaxies are connected among them, and how they can be used for galactic archaeology. In Chapter 2, I explain the technique implemented in the simulations used for this work, as well as the computation of the scale-heights for the thin, thick discs, and mono-age populations, which play a crucial role in this study.

In Chapter 3, I study the connection between different aspects of the vertical density structure of galactic discs and bring them together into a coherent picture. These aspects are the connection between the morphology of the thin and thick disc and that of the mono-age populations inhabiting them, how these shape radial age gradients in the disc, and whether they define distinct thin and thick discs or not. Finally, I connect these aspects with the merger history of the galaxies, and put these findings within the context of the MW and its neighbouring galaxies.

In Chapter 4, I explore the vertical density structure within galactic warps. More specifically, I study the evolution of the stellar vertical density structure during warps depending on their origin, and the signatures they may leave on the disc's vertical density structure.

Finally, I present in Chapter 5 my final conclusions and propose possible directions in which this work could further expand.

# Chapter 2

# Methods

*"I was taught that the way of progress was neither swift nor easy."*

– Marie Curie

For this PhD project, I analyse zoom-in numerical simulations of galaxies in their cosmological context created by Dr. Marie Martig. The simulation technique is explained in Martig et al. (2009) and the whole sample of galaxies presented in Martig et al. (2012). In this chapter, I will summarise the content of these publications. In addition, I will explain the basic principles of Markov Chain Monte Carlo (MCMC) techniques, which are used in many occasions within this thesis and were a crucial tool for obtaining results.

## 2.1 Simulation technique

Galaxy simulations can be grouped into three main categories. One group is galaxies grown in isolation, like the AGORA high-resolution simulations (Kim et al., 2016). This type of simulation can implement many physical processes and reach very high

resolutions. However, the simulated galaxies lack the cosmological context real galaxies grow in. The second group, large-scale structure simulations, where a huge volume of the universe is simulated, successfully reproduce the cosmological context galaxies grow in. EAGLE simulations (Schaye et al., 2015) or TNG50 (Nelson et al., 2019) are perfect examples of this. The downsides of this kind of simulation are that are computationally expensive and do not have the same resolution as isolated simulations. The third group are zoom-in simulations, where a large cosmological volume is simulated at low resolution, but where the targeted haloes grow within that volume, the resolution is increased. ARTEMIS (Font et al., 2020) or Auriga simulations (Grand et al., 2017) are examples of this kind.

The simulations used in this thesis are zoom-in cosmological simulations. However, the technique employed for these simulations differs from the commonly used in other zoom-in simulations, being computationally cheaper. During the first phase, the cosmological simulation, only dark matter is simulated for a large cosmological volume. Then, dark matter haloes with similar characteristics to those of the Milky Way are selected from the final snapshot of the simulation (at $z$ =0) and traced back to higher redshift ($z \approx 5$), recording their merger and accretion history. During the second phase, the high resolution re-simulation, the history recorded for the target haloes in the cosmological simulation is re-run again at very high resolution for dark matter as well as baryonic matter, implementing gas dynamics and star formation. Since the parts of the cosmological volume without target galaxies are not run during the second phase, the computational cost is lower compared to other zoom-in simulations. Also, the baryonic content of the targeted areas is not simulated prior $z \approx 5$ (see appendix A from Martig et al., 2009 for additional information to what is explained in this section). In summary, this numerical technique allows for the implementation of processes like gas evolution and subsequent star formation while keeping the information of the cosmological context (all this with a significantly high spatial resolution). Yet, this technique is not exempted of downsides, the main being the large number of free parameters in the structure and baryonic content of galaxies interacting with the main galaxy. This is especially true of the galaxies at $z \approx 5$ where there is little observational data available

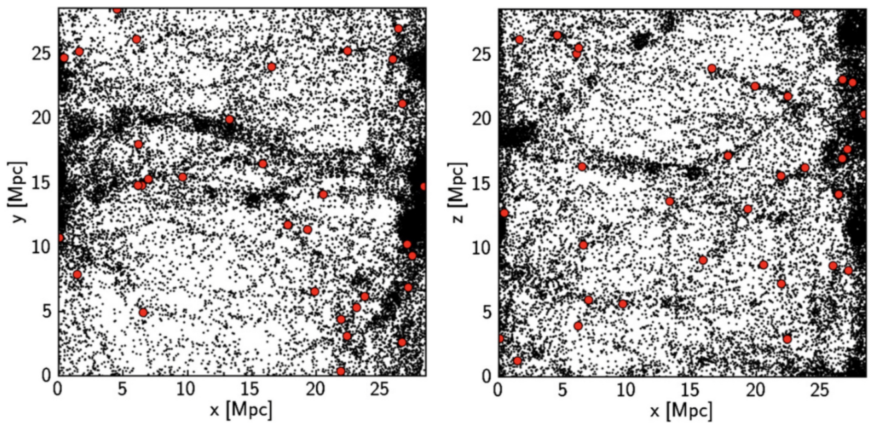


Figure 2.1: Figure 1 from Martig et al. (2012). The figures are a 2-D projection of the dark matter haloes' positions. Each black dot corresponds to a dark matter halo while each red dot corresponds to the selected galaxies chosen for the re-simulation.

for comparison.

**Analysis of the cosmological simulation**

In this first phase of the simulation only dark matter is taken into account, hence, gravity is the only physical process implemented. The cosmological simulation phase uses the massively parallel adaptive mesh refinement (AMR) code RAMSES (Teyssier, 2002) for $512^3$ dark matter particles in a cosmological box with a comoving length of $20h^{-1}$ Mpc, with a mass resolution of $6.9{\cdot}10^6 M_\odot$, around $10^5$ particles per MW-like halo, and using $\Omega_m = 0.3$, $\Omega_\Lambda = 0.7$, $\mathrm{H}_0 = 70\mathrm{km.s}^{-1}.\mathrm{Mpc}^{-1}$, and $\sigma_8 = 0.9$.

As mentioned above, once the simulation is finished, the merger and accretion history of MW-like dark matter haloes is recorded. To do that, dark matter haloes with a minimal number of particles of 10 (equivalent to $6.9 \times 10^7 M_\odot$) are detected using the HOP algorithm (Eisenstein & Hut, 1998) (see an example in Fig. 2.1). The selected haloes are those with a mass similar to the MW and without any other massive halo within 2 Mpc radius (see section 2.1.1). A sphere with radius equals to the virial radius of the galaxy halo at $z$ =0 is then set as boundary. The virial radius is defined as:

$$R_{vir} = \left( \frac{3M_{tot}}{4\pi \times 200\rho_c} \right)^{\frac{1}{3}}, \tag{2.1}$$

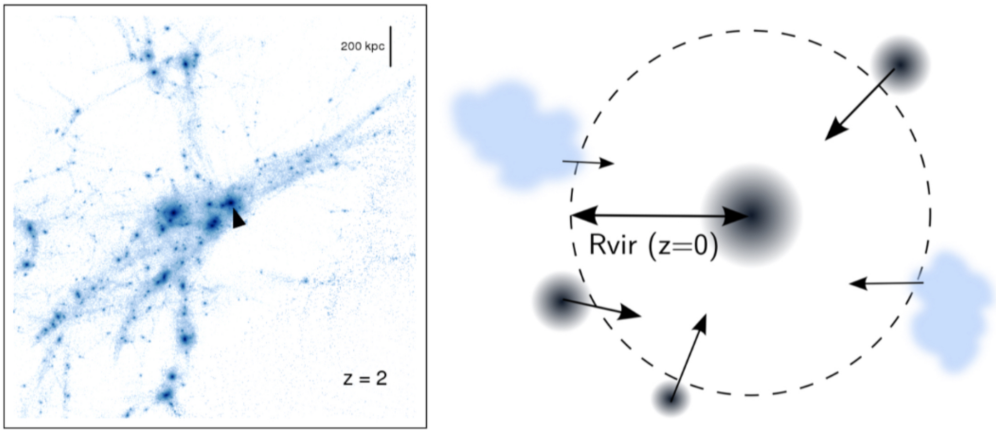


Figure 2.2: *On the left:* extracted from Figure 1 from Martig et al. (2009) showing the dark matter distribution at z=2 within the simulation. *On the right:* illustration of how the merger and accretion history of the target haloes is recorded. The area around the halo selected with the arrow on the left-hand figure is zoomed in to record the incoming satellites as well as the accretion of diffuse material along the filaments (image credit: Dr. Marie Martig).

where $M_{tot}$ is the mass of the main halo at $z$ =0. The positions, masses, velocities and spins of all satellites crossing this boundary are recorded from $z$ =0 to $z$ =5, building the merger history of the target halo. Finally, particles that do not belong to a gravitationally bounded halo but cross the boundary are taken into account as “diffuse" mass accretion.

The final products of this simulation are thus:

1. A list with all the haloes and particles in initial conditions (z = 5).

2. A catalog with all the particles that cross the boundary between z = 5 and z = 0, and all the interacting companion haloes.

### High resolution re-simulation

Once the cosmological simulation is done, haloes are replaced by gas, star, and dark matter particles, and the second phase of the simulation runs now implementing more physical processes. The total size of the simulation is an 800 kpc cubic box. To deal with the large number of particles, the simulations use a particle-mesh (PM) code described in Bournaud & Combes (2002, 2003). This PM code converts the particle distribution

into a density field projected on a grid with a Cloud-in-Cell (CIC) interpolation. The particles are modelled as constant density cubes whose mass is spread on the 8 closest cells. The potential is obtained by computing Fourier transforms of $\rho$ and $f$, multiplying them and performing an inverse Fourier transform. The equation used is the Poisson equation:

$$\Phi(r) = -G \int \frac{\rho(u)}{|r-u|} du, \tag{2.2}$$

which is simply a convolution of the density with $f(u) = 1/u$. The gravitational potential is solved from this density grid using the Poisson equation, and the gravitational force (the gradient) is computed and interpolated to the position of each particle. Time integration is made using a leapfrog algorithm with a time step of 1.5 Myr, with a maximum spatial resolution of 150 pc. The mass resolution is $3 \times 10^5 M_\odot$ for dark matter particles, $1.5 \times 10^4 M_\odot$ for stellar particles created after the beginning of the simulation, and $7.5 \times 10^4 M_\odot$ for the stellar particles placed at redshift z = 5. Finally, the mass resolution for gas particles is $2.1 \times 10^4 M_\odot$.

The code models gas dynamics using a sticky-particle scheme with restitution factors $\beta_r = 0.8$ and $\beta_t = 0.7$. The restitution factors represent how much the relative radial and tangential velocities of colliding gas particles decrease after a collision. Star formation is modelled following a Kennicutt law (Kennicutt, 1998) with an exponent equal to 1.5 and above a fixed threshold of 0.03 $M_\odot pc^{-3}$. Kinetic energy feedback from supernovae explosions is included: 20% of the explosion energy is distributed to neighboring gas (within 70 pc radius). Gas return from high-, intermediate-, and low-mass stars is included as well, following the scheme proposed by Jungwiert et al. (2001). The sticky-particle algorithm employed affects the accuracy of the simulations in the high mass regime due to the poor treatment of gas in a hot phase, including supernova ejecta. However, cold gas accretion is dominant in lower mass galaxies like the ones in this suite of simulations. Therefore, gas can still be modelled up to certain level of realism.

The substitution of haloes is made as follows: the total mass of the galaxy is divided in 17% of baryons and 83% of dark matter (the latter being the one from the cosmological

simulation). The gas content varies depending on both its halo mass and the redshift at which the halo is introduced (30% of the stellar disc at all redshifts for small galaxies, and 15% and 30% for massive galaxies at “low" redshift ($z < 0.8$) and “high" redshift respectively (Roberts & Haynes, 1994)). As for the shape, galaxies contain a disc (gas and stars) with a Toomre profile, a stellar bulge following a Plummer profile, and a dark matter halo with a Burkert profile (Burkert, 1995). In order to decrease computational time, a set of galaxies is created in the range of mass needed and then every time a new halo comes into the simulation, one of these galaxies is put in. More information about the specific galaxies can be found in table 2 in Martig et al. (2009). The accretion particles, described in the cosmological section above, are replaced by blobs containing 65 gas particles (17% of the mass) and 15 dark matter particles (83%). These particles are randomly distributed in a sphere of mean density 100 $\rho_c$ so that it can be tidally disrupted when approaching the main galaxy. The radii of these blobs are 2.5, 3.3, and 5 kpc for redshifts higher than 1, between 1 and 0.5, and smaller than 0.5 respectively. As a last remark, every galaxy is evolved during 500 Myr in isolation before being introduced in the simulation so that they acquire a realistic structure. The way the introduction of satellites onto the high resolution simulation is implemented could potentially introduce some bias since the satellites are extracted from a limited pool of models. However, the goal of these simulations is the study of interactions between galaxies themselves and not so much the products of non-axisymmetric structures derived from axisymmetric initial conditions. Also, given the amount of possibilities satellites can exist and grow, it is not realistic to systematically cover all these possibilities in these simulations. The results derived from these simulations, however, will be valid for satellites with characteristics as described above, which represent a large number of cases. Plus, when choosing the substitute halo with a mass-based criterion, it is noteworthy that the most massive companions are exactly reproduced. Therefore, interactions between the host galaxy and massive satellites (which are more dramatic) are quite realistic (see Appendix A from Martig et al. (2009) for a detailed discussion).

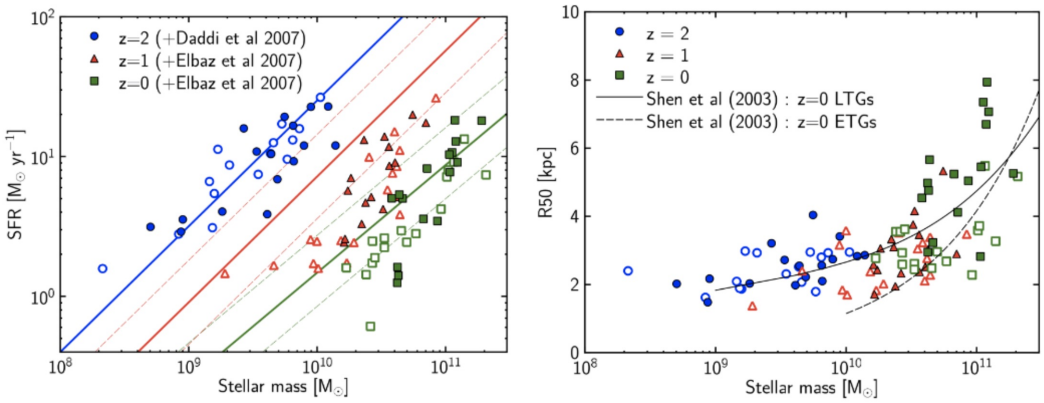


Figure 2.3: *On the left:* Figure 11 from Martig et al. (2012). Star formation rate as a function of stellar mass for the simulated galaxies at $z$ =2 (blue dots), 1 (red triangles), and 0 (green squares), compared to correlations observed for star-forming galaxies. *On the right:* Figure 13 from Martig et al. (2012). Half-mass radius as a function of stellar mass for the simulated galaxies at $z$ =2 and 0, compared to observations at z=0.

### 2.1.1 Sample

The sample includes 33 main haloes with a dark matter mass range selected from $2.7 \times 10^{11}$ to $2 \times 10^{12} M_{\odot}$ that are relatively isolated at z = 0: haloes more massive than half of the mass of the main haloes are more than 2 Mpc away, and the main haloes are at least 6 Mpc away from the most massive haloes of the simulation box. These 33 haloes represent 26% of the total number of haloes within this mass range, and 69% of the haloes that fulfill the mass and environment conditions. They share common mass growth histories: 20% of their final mass is reached at z = 2, between 30% and 60% at z = 1, and 50% and 80% at z = 0.5. When compared with observations, some differences as well as similarities are noted:

- At z = 0, the simulated galaxies cover a large range of bulge-to-total fractions –from 0.05 to 0.8. On average, these B/T tend to be too high in the simulations. In fact, there are not bulgeless disc galaxies in the sample, although this could be due to the limited number of selected haloes.

- There are no pure elliptical galaxies, although it can be expected from isolated environments.

- Contrary to Weinzirl et al. (2009), there is no correlation between stellar mass

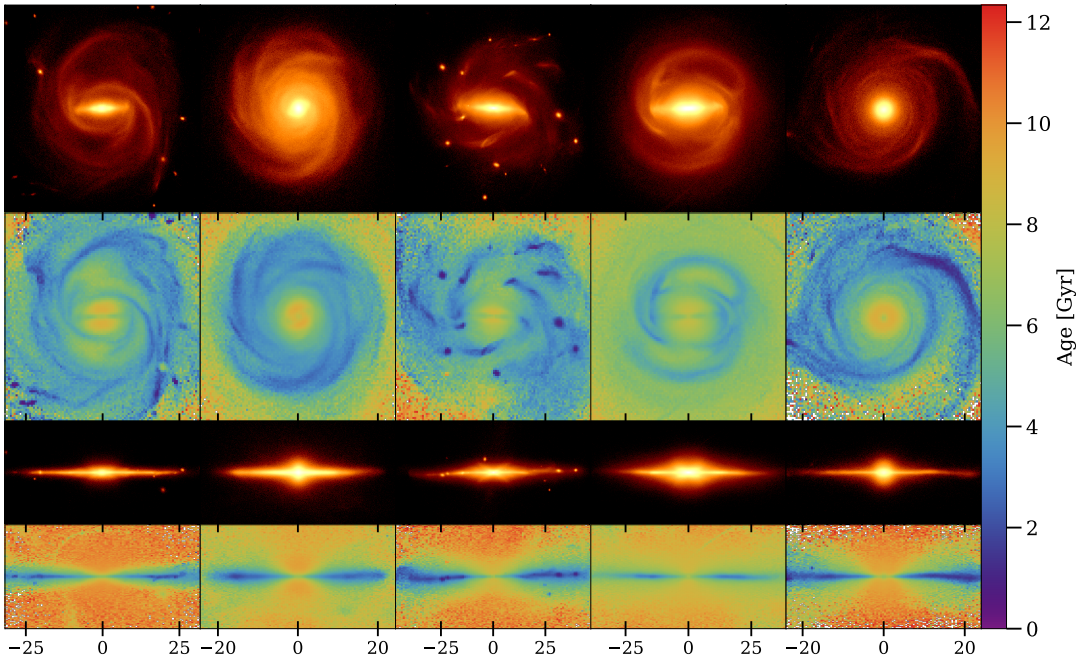


Figure 2.4: Density and age maps seen face-on and edge-on of five galaxies from our sample. From left to right: g92, g47, g36, g39, and g102. I choose these same galaxies as representatives of the scenarios discussed in Chapter 3.

and bulge content.

- The simulated galaxies show the similar Sérsic indexes as spiral galaxies in observations (Laurikainen et al., 2007).
- The bar fraction content of the simulated galaxies is roughly consistent with observations (Eskridge et al., 2000; Marinova & Jogee, 2007).
- As seen in Fig. 2.3, the simulations overall agree nicely with observations in terms of mass growth and star formation histories at higher redshifts (Daddi et al., 2007; Elbaz et al., 2007).

Some examples of simulated galaxies can be seen in Fig. 2.4.

## 2.2 Markov Chain Monte-Carlo techniques

The scale-heights of the geometrical thin and thick discs of the simulated galaxies introduced in the previous section are crucial information for the subject of this work. Therefore, I wanted to use a solid method that could both determine their values with high accuracy and provide information on the reliability of the computed parameters. Markov Chain Monte-Carlo (MCMC) techniques are an ideal tool for such aim. MCMC uses Bayesian statistics, which works with probability distributions. The advantage of MCMC is that it fully explores the parameter space to obtain the posterior probability distribution (e.g., Jaynes & Bretthorst, 2003; Gregory, 2010).

### 2.2.1 Bayes theorem

In general terms, Bayes' theorem describes the probability of an event to happen taking into account the information known about that event. The equation representing Bayes' theorem is:

$$P(A|B)P(B) = P(B|A)P(A), \tag{2.3}$$

where $A$ and $B$ are events, and $P(B)$ needs to be $\neq 0$. $P(A|B)$ represents the probability of $A$ given $B$. $P(B|A)$ represents the probability of $B$ given $A$. $P(A)$ and $P(B)$ are the probabilities of $A$ and $B$ respectively.

Bayes' theorem is often used for fitting data. Part of its power comes from the ability to incorporate all the prior knowledge of the target system when testing the goodness of the fitting model. There are four main probability distributions in a Bayesian approach: a prior, a likelihood, a posterior, and the evidence. Bayes' theorem establishes the relationship between the different probability distribution functions, so eq. 2.3 transforms into:

$$P(\Theta|D) = \frac{P(D|\Theta)P(\Theta)}{P(D)}, \tag{2.4}$$

where D is the data and $\Theta$ is the model parameters. The prior distribution $P(\Theta)$ contains all the information known of a parameter before seeing any data. The likelihood distribution $P(D|\Theta)$ describes the joint probability of the observed data as a function of the parameters of the chosen statistical model. Lastly, $P(D)$ the model evidence, which is invariant. The posterior distribution $P(\Theta|D)$ represents the probability of observing the data with the model parameters given the prior information of the parameters. Therefore, for a given model and prior, the set of parameters that maximises the posterior is the one that best reproduces the data.

### 2.2.2 Posterior sampling

MCMC methods are a great way to sample the posterior. Using randomly generated numbers, Monte Carlo simulations are a useful tool to approximate parameters where other methods fail because of the computational expense, or because of the impossibility to directly compute that parameter. Markov chains are sequences of events where the outcome of an event determines what happens next. For this to happen, each event's outcome must have all the required information to predict the next step, making storing previous steps' information unnecessary.

MCMC methods combine Monte Carlo simulations technique with Markov chains (Metropolis et al., 1953). Starting from a given guess of the parameter value, random numbers are generated (Monte Carlo). If the new values are more likely to describe well the data, the values are added to the chain and the next step is taken (Markov chain).

However, because the aim of MCMC is exploring the full parameter space to obtain the posterior probability distribution, sometimes a step is accepted despite the likelihood being worse than the previous step. A possible way to describe the probability of a step being accepted is described as:

$$P_{accepted} = \frac{P(D|\Theta)P(\Theta)}{P(D|\Theta_0)P(\Theta_0}, \tag{2.5}$$

where $\Theta_0$ is the current parameter and $\Theta$ is the proposed for the next step. The equation is, basically, the fraction of the two posteriors. The implication of this is that even if the probability of the current value is twice as large, there is a 0.5 chance of accepting the new value. With this, all the posterior probability region is sampled, although high probability regions are favored against low probability ones. Hence, even though the generated numbers are random, the Markov chain will tend to converge in the region of highest probability after a number of steps. The final result is samples from the posterior distribution of as many parameters as required (Sharma, 2017). Exploring the full parameter space has the advantage of avoiding convergence in local maxima, and identifying the true highest probability region.

Therefore, MCMC methods are well fitted for computing the scale-heights of thin and thick discs of the simulated galaxies. This process is explained in the next section.

## 2.3 Fitting the vertical density profiles

In this section, I explain how I computed the scale-heights of the thin and thick discs using MCMC techniques.

I first compute a global estimate of the overall disc thickness: I define $h_{\rm scale}$ as the standard deviation of the vertical position of stars located at half the optical radius of the galaxy, $R_{25}$. To compute the scale-heights of the global thin and thick disc, I bin the disc stellar particles in cylindrical shells with a width of 2 kpc and a height of 3 $h_{\rm scale}$. At each radius, I compute the vertical number density of particles using 20 bins, and fit the profile using a combination of two $\mathrm{sech}^2$ functions:

$$N(z) = N_0 \left( (1-\alpha)\mathrm{sech}^2\left(\frac{z}{h_{\rm thin}}\right) + \alpha\mathrm{sech}^2\left(\frac{z}{h_{\rm Thick}}\right)\right), \tag{2.6}$$

where $N_0$ is the stellar number density at the mid-plane, $h_{\rm thin}$ and $h_{\rm Thick}$ correspond to the scale-heights of the thin and thick disc respectively, and $\alpha$ is the number density fraction of the thick disc over the global disc. I find that a single $\mathrm{sech}^2$ could not describe well the vertical distribution of stars, especially for the thickest discs. To determine the vertical stellar distribution of stars, following Bennett & Bovy (2019), I use a Poisson distribution for the likelihood, which I write as follows:

$$\ln\mathcal{L}(N_c|N_p) = \sum -N_p + N_c \cdot \ln(N_p) - \ln(N_c!), \tag{2.7}$$

where $N_{\rm c}$ is the number of stellar particles counted in the bin, $N_{\rm p}$ is the number of stellar particles predicted by the model, and $N_{\rm c}!$ is independent of the models and thus ignored for the computation of the likelihood.

The fits for the scale-height were obtained using MCMC sampling with the `python` package `emcee` (Foreman-Mackey et al., 2013), with 200 walkers and 5000 steps. The walkers start from random positions around the best fit value obtained using the `ScyPy` routine `curve_fit` (Virtanen et al., 2019), and the first 1000 steps are discarded. For the priors, I let $h_{\rm thin}$ and $h_{\rm Thick}$ take any value from 0 to 15 kpc, $\alpha$ from 0 to 1, and I set $N_0$ to be positive. The final values I report for each parameter are the median and the $16^{\rm th}$ to $84^{\rm th}$ percentiles range of the posterior distribution. An example of the MCMC fits can be seen in Fig. 2.5.

In addition to fits to the thin and thick discs, I also determine the scale-heights of MAPs, for which I split the stellar particles into 0.5 Gyr age bins ranging from 0 to 13 Gyr old, and the same spatial bins as for the fits of the global thin and thick discs. Martig et al. (2014a) showed that a single exponential provides a good fit to the vertical density profile of MAPs, as was also found by Minchev et al. (2015). Therefore I used a squared hyperbolic secant to fit the MAPs. The fits for the MAPs' scale-heights are done in each radial bin, from the galactic centre to $R_{25}$ until either there are fewer than 10 stellar particles inside the bin or the scale-heights are greater than 10 kpc.

The study of the scale-heights of MAPs, thin, and thick discs as a function of radius is

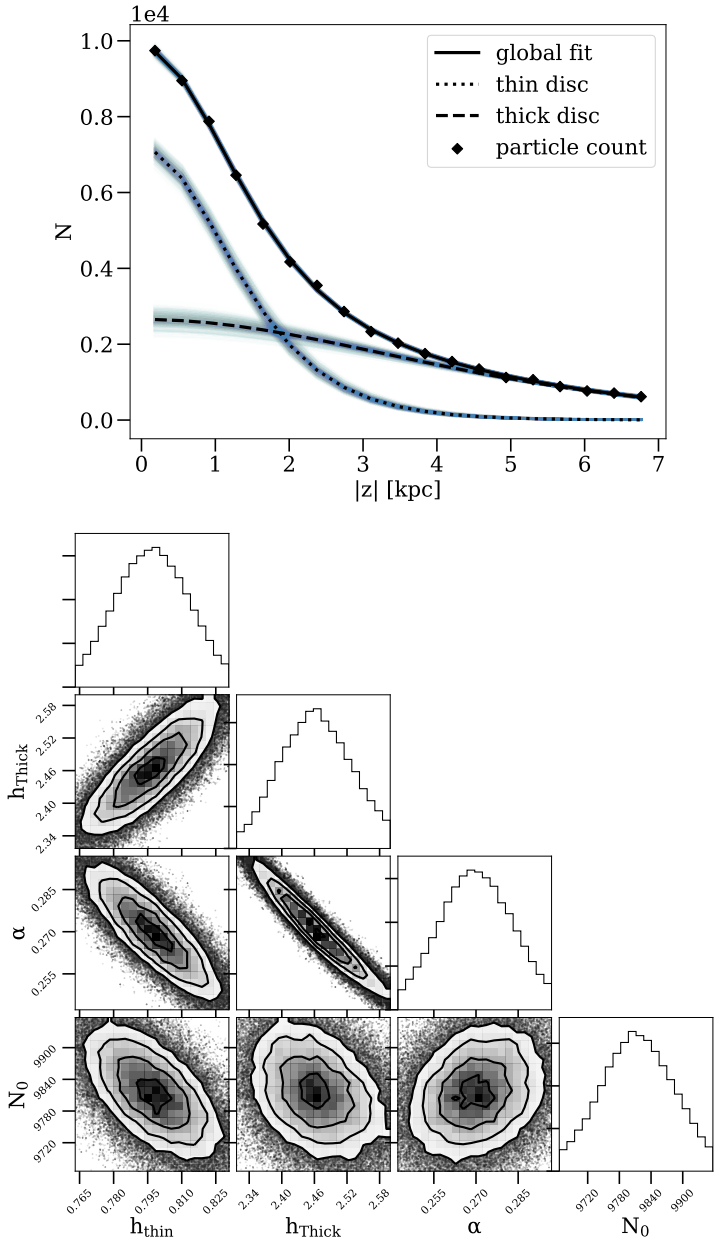


Figure 2.5: *On the top*: for galaxy g36 within the sample, vertical distribution of number density of stellar particles in black diamonds and the MCMC fit in solid black line. The dotted and dashed line represent the thin and thick disc contribution to the total particle count. The blue range indicates the $16^{th}$ to $84^{th}$ percentiles ranges of the posterior distribution. *On the bottom*: corner plot of the parameter values for the MCMC fit to the vertical number density profile presented in the upper panel.

a central part of this thesis.

# Chapter 3

# On the Flaring of Thick Discs of Galaxies

*"If you know you are on the right track, if you have this inner knowledge, then nobody can turn you off... no matter what they say."*

– Barbara McClintock

## 3.1 Introduction

As already mentioned in Chapter 1, Minchev et al. (2015) explained the conundrum between theoretical models showing thick disc flaring due to mergers, and observational studies finding flat thick discs. The two simulated galaxies chosen, one from (Martig et al., 2012), and the other from the Aquarius Project haloes (Springel et al., 2008; Scannapieco et al., 2009), successfully explained the case of galaxies with flat thick discs. This picture fitted well with other features seen in the MW, like the existence of a radial age gradient (Martig et al., 2016) or the flatness of the inner thick disc (Mateu &

Katherina Vivas, 2018). However, within the simulated galaxy sample of Martig et al. (2012), there are other MW-like galaxies with different merger histories, and likely different radial age gradients and thick disc morphologies. Hence, in this chapter, I expand on the work of Minchev et al. (2015) by studying the structure of discs in the full sample of simulated galaxies presented in Martig et al. (2012). All the galaxies are star-forming spiral galaxies with masses on the order of the MW's and grew in relatively isolated environments as described in Chapter 2. Nevertheless, the fact that they present a large diversity regarding some properties like the merger history can help compare MW analogs like the one use in Minchev et al. (2015) with others, potentially more similar to nearby galaxies for which data on the radial and vertical distribution of their stellar populations will be available in the future. Therefore, studies like this one constrain how unique the MW is in the context of its neighbouring galaxies.

I first present some general properties of the simulated galaxies and their discs, but the main focus of this chapter is to explore how much mono-age populations (MAPs) flare, and what kind of thick disc they create. I pay special attention to three aspects: a) how flaring MAPs can create either a flat or flared thick disc, b) whether those thick discs define a separate structure from the thin disc or not (in terms of their stellar populations), c) and the different kinds of age gradients MAPs create. Finally, I look into the merger histories of our galaxies, and show the connection between mergers and different thick disc properties.

The work presented in this chapter has been published in García de la Cruz et al. (2021b).

## 3.2 Method

The original sample from Martig et al. (2012) consists of 33 simulated galaxies. Some of the galaxies in the sample have structural features that would vastly complicate the analysis: these are galaxies either undergoing a massive merger at z=0, or having a polar ring, or presenting a dramatically warped and distorted disc. For that reason, in

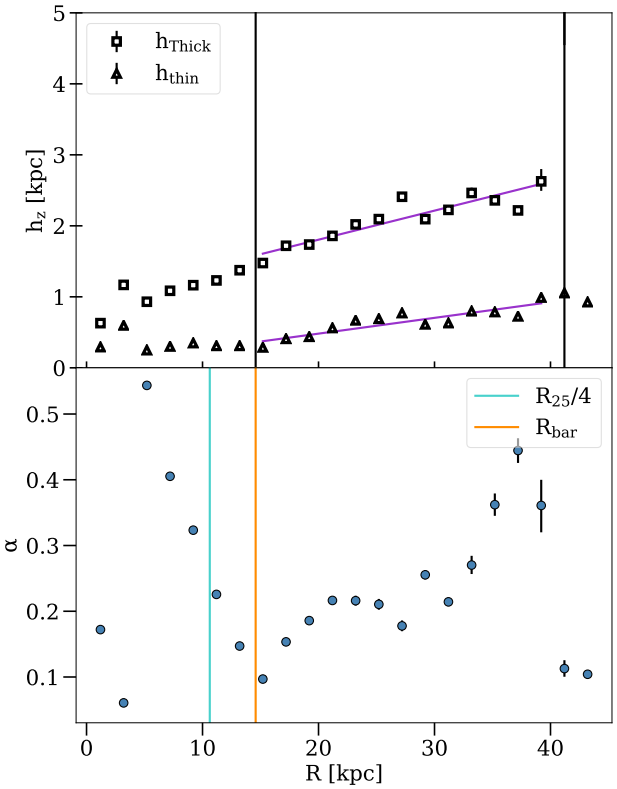


Figure 3.1: *Top*: radial profile of the thin and thick discs' scale-heights for galaxy g36. The two vertical black lines represent the inner $R_{\rm inner}$ and outer $R_{\rm outer}$ boundaries of the disc, whereas the purple lines represent the linear fits to the scale-heights of the two components of the disc. *Bottom*: Radial distribution of the thick disc fraction. I see a change in the behaviour of $\alpha$ in the inner disc, corresponding to the end of the bar (I use $R_{\rm bar}$ to define the inner boundary of the thick disc), and I also see a drop at the outer edge of the thick disc.

this chapter I exclude galaxies g35, g38, g60, g97, g125, and g146 from the original sample, leaving 27 galaxies.

### 3.2.1 Radial extent of thick discs

First, the scale-heights of MAPs, thin, and thick disc are computed following the methodology described in Chapter 2. Although the scale-height fits are initially done all the way from the centre to $R_{25}$, I am interested in the disc only. The fits in the very inner parts of the galaxy most likely represent the vertical density distribution of other components —e.g. the bulge and the bar if the galaxy has one— which are not within the scope of this thesis.

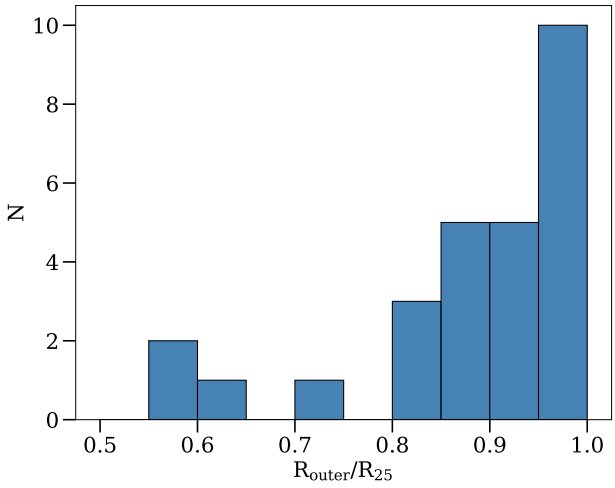


Figure 3.2: Histogram representing the radial extent of the thick disc over $R_{25}$ after applying our criteria. For 15 galaxies the thick disc extends beyond 90% of $R_{25}$.

In order to separate the central part of the galaxy from the disc, I study the density maps of the galaxies and see that the bulges end at around a quarter of $R_{25}$, e.g. the stellar density drops dramatically. I also noticed that the behaviour of the thick disc fraction, $\alpha$, changes at around the same radius. This can be explained if indeed the sech$^2$ are describing different galaxy components inside and outside of this radius. For some galaxies, the bar goes beyond $R_{25}/4$. In these cases, the changing in trend of $\alpha$ is not at $R_{25}/4$, but at the bar's end. Therefore, I consider the inner boundary of the disc, $R_{\rm inner}$ hereafter, to be at a quarter of $R_{25}$ for most galaxies, or at the bar's end if it extends beyond $R_{25}/4$.

For some galaxies, the MCMC fits in the outer part of the disc show either very large errors or values significantly higher than for the rest of the disc. When I look at the behaviour of $\alpha$ in the same region, it shows very low values, indicating that the thick disc component is marginal in terms of mass. The reasons behind this change of behaviour or poor fits at large radii can be multiple: a break in the thick disc, the vertical density follows a different distribution than a sech$^2$, a warp, etc. I define the outer limit of the thick disc, hereafter $R_{\rm outer}$, to be this radius at which the fit starts to perform poorly. An example of how these criteria were applied and their result is shown in Fig. 3.1. In Fig. 3.2 I present the distribution of $R_{\rm outer}/R_{25}$. In most cases, I find that thick discs have nearly the same extent as the overall disc: for 15 out of 27 galaxies, $R_{\rm outer}$ is greater

than 0.9 $R_{25}$.

The total mass of each disc component is the sum of the corresponding $\mathrm{sech}^2$ at every radial bin from $R_{\mathrm{inner}}$ to $R_{25}$ for the thin disc, and from $R_{\mathrm{inner}}$ to $R_{\mathrm{outer}}$ for the thick disc. The total mass of the disc, $M_{\mathrm{disc}}$, is the sum of the mass of the thin and thick discs. Hereafter, I denote the latter $M_{\mathrm{Thick}}$.

### 3.2.2 Fitting the disc flaring

To quantify the level of flaring for the thin and thick discs, I study how their scale-heights change with radius. I find that when taking into account the radial extent criteria explained in the previous subsection, the radial profiles of both scale-heights are well described by a single line (see Figure 3.1), and the slope of that line can be used to quantify the level of flaring. Therefore, I use the `least_squares` algorithm from `ScyPy` (Virtanen et al., 2019) to perform a linear fit to the radial profiles of both the thin and the thick discs' scale-heights. I use the Cauchy loss function in order to minimise the effect of outliers. The respective slopes $\nabla_{\mathrm{thin}}$ and $\nabla_{\mathrm{Thick}}$, will be hereafter the thin and thick disc scale-height gradients respectively.

## 3.3 General properties

In this section, I study the global properties of the discs, i.e. their mass, thickness, and degree of flaring. The upper left panel of Fig. 3.3 shows the thick disc stellar mass fraction $M_{\mathrm{Thick}}/M_{\mathrm{disc}}$ as a function of the total disc stellar mass $M_{\mathrm{disc}}$, colour-coded by the total stellar mass of the galaxy $M_{\mathrm{galaxy}}$ (the symbols represent the radial extent of the thick disc, as will be discussed later). The stellar mass ratio of the thick disc varies from cases like g82 and g83 where the mass fraction is below 25%, to cases like g72, g44, or g31, whose mass fraction is above 60% of the total disc stellar mass. The disc stellar mass correlates strongly with the stellar mass of the galaxy, but it does not correlate strongly with the thick disc stellar mass ratio. It seems that low mass discs

can have a wide range of thick disc stellar mass ratios, and that high mass discs tend to have slightly higher thick disc ratios on average, but the trend is quite weak and I do not have enough simulated galaxies to confirm this effect.

In addition to disc stellar mass, I also want to quantify the thickness of both the thin and thick discs, which can vary significantly with radius in flared discs. I define the thicknesses as the scale-height $h_{\rm Thick}$ value at half $R_{25}$, which I denote as $R_{1/2}$. In the upper right panel of Fig. 3.3, I compare the thicknesses of the thin and thick discs, colour-coded by the mass of the disc $M_{\rm disc}$. The respective thicknesses of the thin and thick discs are tightly correlated: thick discs are approximately 4 times thicker than thin discs. I also find that low mass discs tend to be relatively thinner, with some exceptions (which shows that mass is not the only factor controlling disc structure).

In the bottom left panel of Fig. 3.3, I plot the slope of the thick disc $\nabla_{\rm Thick}$ against the slope of the thin disc $\nabla_{\rm thin}$, colour-coded by the thickness of the disc. Overall, thick discs tend to be more flared than thin discs and the values of both slopes mildly correlate with each other. Also, in general trends, galaxies with a flatter thick disc tend to be thinner, and galaxies with a thinner thick disc have similar slopes for thin and thick discs.

Finally, the thick disc general properties studied in this section are summarised in the bottom right panel of Fig. 3.3. The flaring of the thick disc and its thickness are correlated, and are also correlated with the thick disc mass ratio. A final aspect that I investigate is whether the radial extent of thick discs is correlated with any of the properties I have mentioned so far. To this end, in all panels of Fig. 3.3, I represent with triangles galaxies where the thick disc extends out to more than 90% of $R_{25}$, and with circles galaxies with a less extended thick disc. I do not find any difference between the two populations, and for the rest of this work I do not separate galaxies into categories based on the extents of their thick discs.

The MW seems to be a bit different from the galaxy sample in terms of mass. For instance, estimates of the MW's total stellar mass are around $\mathrm{M_{galaxy}} \sim 6 \times 10^{10} \mathrm{M_{\odot}}$, which belongs to the lower half of the sample. Yet, in terms of disc mass, $\mathrm{M_{disc}} \leq$

$3.5 \times 10^{10} M_{\odot}$, the MW seems to posses a quite higher mass compared to the galaxy sample. The thick/total disc mass ratio is below 5%, which is way below the galaxy sample's values. It seems that, compared to the galaxies in the simulation, the MW has a more massive disc, of which the thin disc holds most of the mass budget, and a very little massive thick disc. All these numbers are extracted from the review on the MW Bland-Hawthorn & Gerhard (2016b), including those of the thick disc mass. On Chapter 1, I discuss the different definitions of thick disc, and therefore how comparing the MW with the simulations needs to be done with caution. Regarding the scale-heights at $R_{1/2}$, the MW seems to fall in the lower end of the sample's distribution with 0.3 kpc for the thin disc and 0.9 for the thick disc (Bland-Hawthorn & Gerhard, 2016b). Finally, in terms of disc flaring, it is hard to compare the MW with the sample, as the way the flaring level computed for the galaxies within the sample (see Sec. 2.1.1) has the advantage of knowing the real distribution of the vertical stellar density of the galactic discs at large radii. As explain in Chapter 1, the amount of flaring in the outer disc is still and unsettled matter. However, it is well known that the inner disc of the MW is quite flat (e.g., Mateu & Katherina Vivas, 2018), so preliminary, the MW could be placed on the lower half of the galaxy sample in terms of thick and thin disc flaring.

In summary, the sample of galaxies shows a large range of masses, thicknesses, and flarings of thin and thick discs. From galaxies whose thick discs are quite flat, to galaxies with very flared thick discs, I observe a continuum with no clear gaps or separated categories. Hereafter, although I will refer to flat and flared thick discs, the reader should keep in mind that there are intermediate cases and no clear threshold separates one category from the other.

## 3.4 Mono-Age Populations and thick disc connection

In this section, I will explain how this range of flaring for the thick discs is possible due to the connection between the flaring of the thick disc and the flaring of MAPs. As Minchev et al. (2015) explained, there are three main factors that come into play: 1) the level of flaring of the different MAPs, 2) their individual contribution to the total surface

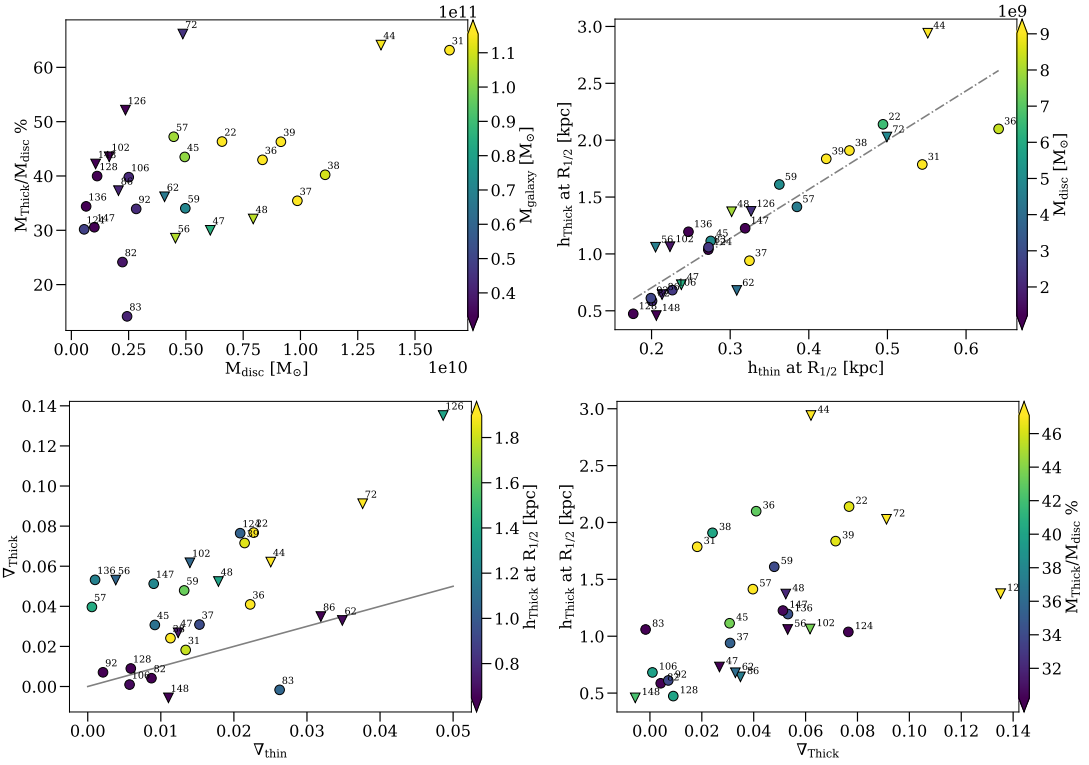


Figure 3.3: *Top left:* thick disc mass ratio against total disc mass, colour-coded by the stellar mass of the galaxy. *Top right:* scale-height of the thick disc at the middle of the disc against scale-height of the thin disc at the middle of the disc, colour-coded by the mass of the disc. The gray line represents a linear fit to the data. *Bottom left:* thick disc scale-height gradient against thin disc scale-height gradient, colour-coded by the scale-height of the thick disc at the middle of the disc. The gray line is a 1:1 line to show that thick discs are more flared than thin discs in most cases. *Bottom right:* scale-height of the thick disc at the middle of the disc against thick disc scale-height gradient, colour-coded by the thick disc mass ratio. The number on the top right of each data point is the galaxy number/label. Triangles indicate that the extent of the thick disc is above 0.9 of $R_{25}$, and circles otherwise. The arrow-shaped ends of the colourbar indicate that values range from the 16th to the 84th percentile of the variable.

density, and 3) how these two change with radius. The latter is strongly connected with the inside-out formation of the disc. Non-flaring MAPs will not contribute to the flaring of the thick disc anywhere, rather, they will tend to minimise the flaring of the thick disc especially at those radii where their contribution to the total disc's surface density is more significant. Likewise, flaring MAPs that have a low surface density at the radii they flare, will not contribute either to the flaring of the thick disc. On the contrary, flaring MAPs with a substantial contribution to the total surface density at the radii they flare will drive thick disc flaring. Since the surface density contribution changes with radius for every MAP, the global flaring will be driven by different MAPs at different parts of the disc.

### 3.4.1 General structure of MAPs

To illustrate the full range of possible configurations for MAPs and global thin and thick discs, I pick five representative galaxies from our sample and show them in Figs. 3.4 to 3.8. In the upper left panels of these figures, the scale-heights of the thin disc, thick disc, and every MAP, computed as explained in Chapter 2, are represented as a function of radius and colour-coded by age. Although I show only five examples, the reader can already see some general trends that hold in every galaxy within our sample. Older MAPs — especially older than 9 Gyr — tend to be concentrated in the inner part of the galaxy, i.e. within $R_{\rm inner}$ (the radius where the disc starts, see Section 3.2.1). They also flare strongly with radius, with already large scale-heights at the beginning of the disc and very low surface density values. This would imply that these MAPs' contribution to the global disc flaring should be negligible. In order to be sure, I re-computed the thick disc slopes $\nabla_{\rm Thick}$ excluding all stellar particles 9 Gyr old and older. I find extremely small changes for $\nabla_{\rm Thick}$ in the vast majority of the galaxies in our sample, which confirms the negligible influence of the oldest stars on the flaring of the thick disc. This does not mean that MAPs older than 9 Gyr do not have an influence over the global shape of the thick disc. When excluding all stellar particles older than 9 Gyr, I find that the scale-heights of the global thick disc have lower values by 25% on average. Within certain variability, this effect has the same intensity all over the disc.

This explains why the flaring level is unaffected by these MAPs. In other words, MAPs older than 9 Gyr thicken the disc and increase the scale-heights of the global thick disc uniformly but do not have an influence on the scale-heights' gradient.

The youngest MAPs — younger than 3 Gyr — generally dominate the surface density of the disc, especially towards the outskirts. They are normally quite flat, show very little flaring compared to older MAPs, and their scale-heights are too low to affect the shape of the thick disc. Therefore, generally speaking, MAPs younger than 3 Gyr old dictate the flaring of the thin disc. This can be seen in the upper left panels of Figs. 3.4 to 3.8, where the thin discs' scale-heights follow very tightly the flaring of these MAPs. Based on all this, I can say that MAPs older than 9 Gyr and younger than 3 Gyr old contribute little or nothing to thick disc flaring. Intermediate age MAPs — from 3 to 9 Gyr roughly — are the ones which exhibit the most varied behaviours, from flaring minimally to dramatically. In some galaxies, the scale-heights and flaring levels of MAPs increase gradually with age. In others, there are gaps between particular MAPs, or quite a few MAPs have roughly the same scale-heights. Martig et al. (2014a) found that these gaps are linked to the galaxy merger history. The different flaring scenarios showed by the intermediate age MAPs, together with their contribution to the total surface density of the disc at every radii, will dictate the flaring level of the thick disc.

### 3.4.2 Flaring of MAPs and flaring of the thick disc

Generally speaking, I establish two main scenarios based on whether the thick disc is flat or flared. I would like to stress that flat and flared thick discs are not two completely distinct categories, and the galaxies in our sample exhibit a continuous spectrum between the two. Based on visual criterion, I pick a value of $\nabla_{\mathrm{Thick}}$ around 0.03 to split galaxies into flat or flared, keeping in mind that this number is somewhat arbitrary. I also would like to remind the reader that flat does not mean an absolute absence of flaring but rather very small or minimal flaring. In this subsection, I first pick five galaxies which are representative of the different ways MAPs create thick discs and explain how the different mechanisms come into play. Afterwards, I analyse

the whole galaxy sample.

### The five cases

Out of the five representative galaxies I have chosen, cases **1a** and **1b** in Figs. 3.4 and 3.5 represent two possible ways to obtain a flat thick disc, whereas cases **2a**, **2b**, and **2c** in Figs. 3.6, 3.7, and 3.8 respectively, represent three possible ways to obtain a flared thick disc.

Galaxy g92 in Fig. 3.4 represents our **case 1a**, which is when all or most MAPs are flat or flare minimally. Galaxies in this category have MAPs with scale-heights that do not increase much in absolute value as a function of radius. This can still sometimes correspond to relatively large fractional increases in the level of flaring. For instance, in g92, MAPs between 5 and 8 Gyr almost double their scale-height values from $R_{\rm inner}$ to $R_{\rm outer}$, but in absolute values this represents an increase of less than 0.5 kpc over a 15 kpc disc radius.

The values of the global thick disc's scale-heights do not follow one particular MAP's scale-heights, but a combination of all MAPs' scale-heights following the mechanism proposed by Minchev et al. (2015). Still, there is no stellar population that could drive strong thick disc flaring as all of them are practically flat. In the upper right panel of Fig. 3.4, I show the stellar surface density against radius for every MAP (only including particles up to a height of three times $h_{\rm scale}$). I find that different MAPs contribute at different radii, in particular the inner disc is dominated by older populations and the outer disc by younger populations, reflecting the inside-out formation process of the disc. This combination of MAPs with different radial surface density profiles results in the scale-height values of the flat thick disc. Also, this succession of dominant MAPs in the radial direction creates an age gradient in the thick disc as will be described below in Section 3.5. In other words, there are no MAPs with significant flaring and significant surface density to drive thick disc flaring. Yet, the interplay between flaring, surface density, and radius determines the global thick disc's scale-height values and creates an age gradient. In our sample I find 6 galaxies in this category: g31, g82, g86,

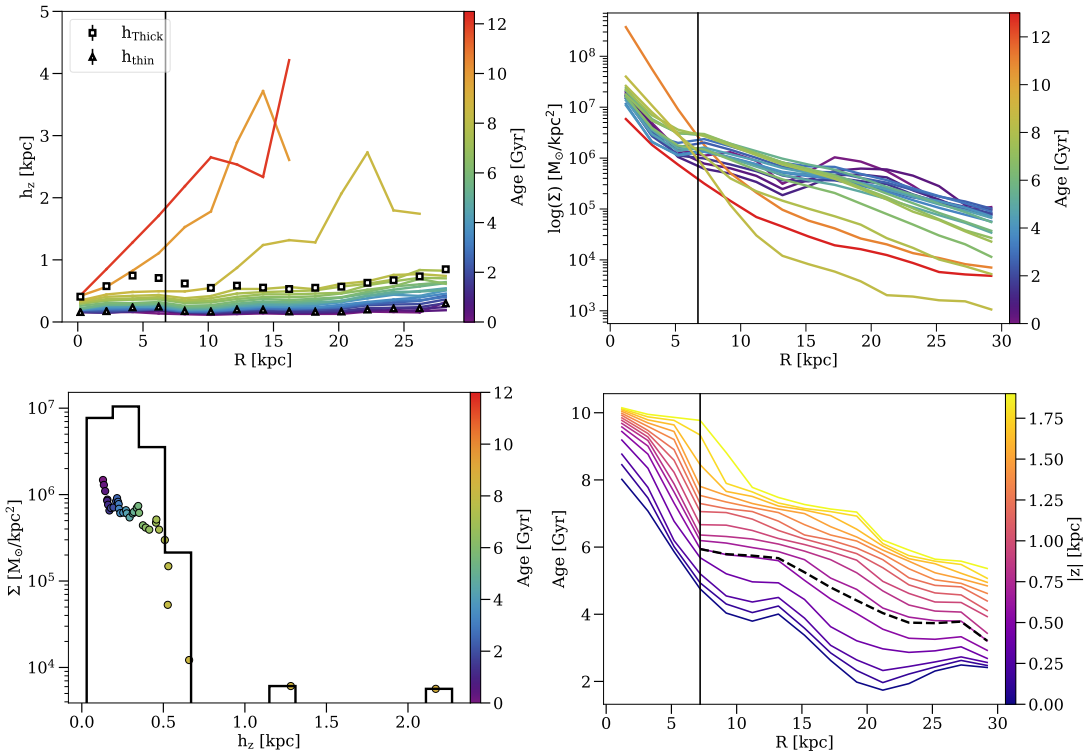


Figure 3.4: Case 1a, illustrated by g92: both MAPs and thick disc flare minimally. *Top left*: values of the scale-height against radius for the thin disc (triangles), thick disc (squares), and MAPs (solid lines) colour-coded by age. MAPs from 9 to 11 Gyr and from 11 to 13 Gyr are binned together, every other MAP spans 0.5 Gyr. The vertical black line on the left represents where I consider the galactic disc starts based on our criteria from Section 3.2.1. A second vertical black line represents the end of the thick disc extent for cases when it is below 100% of $R_{25}$. *Top right*: surface density against radius for every MAP, binned and colour-coded in the same way as the top left panel. The vertical black line represents the same as in the top left panel. *Bottom left*: surface density against scale-height for every MAP, colour-coded by age, at the middle of the disc. The black line is the histogram of the surface density, with 15 bins over the range of scale-heights. *Bottom right*: median stellar age against radius colour-coded by height above the mid-plane. The dashed black line represents the age profile following the scale-heights of the thick disc. The vertical black line represents the same as in the top left panel.

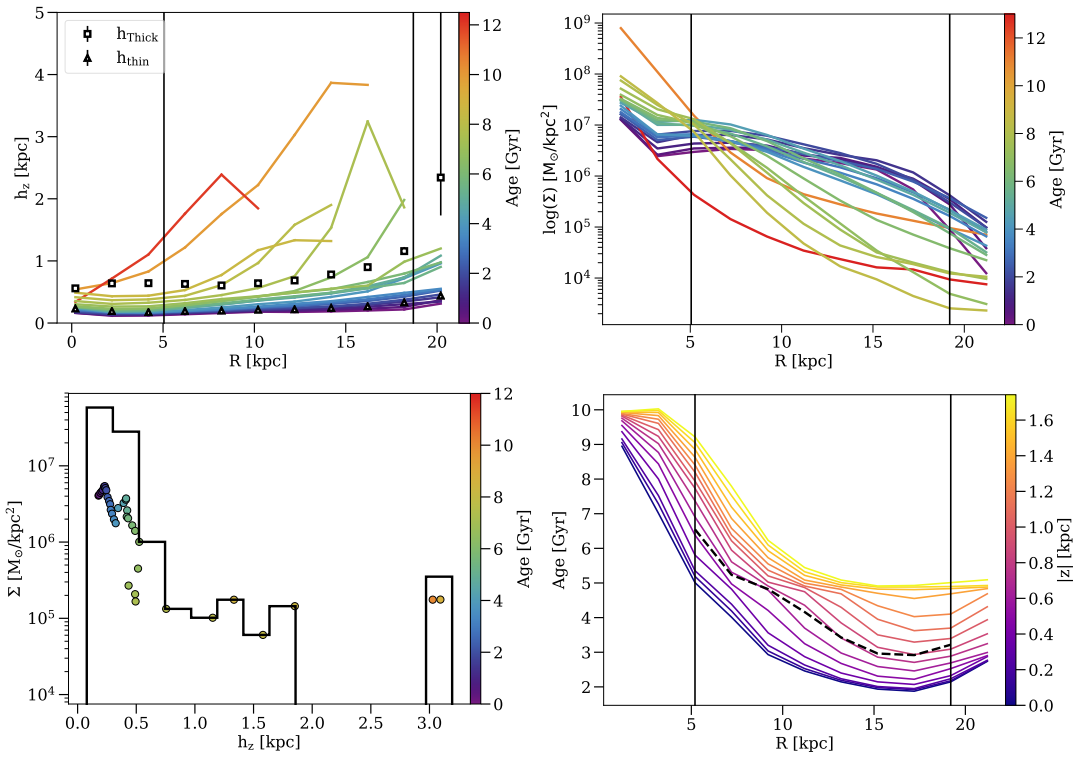


Figure 3.5: Case 1b, illustrated by g47: flaring MAPs and minimally flared thick disc. Panels represent the same as in Fig. 3.4.

g92, g128, and g148.

The other way to make a flat thick disc is our **case 1b**, when some MAPs flare considerably more than the rest, but they have low surface density compared to the rest of MAPs at the flaring radii, like for example in g47 illustrated in Fig. 3.5. In the upper left panel, it can be seen that MAPs above 6 Gyr old flare considerably towards the outskirts which could potentially make the global thick disc flare. Nevertheless, when I look at how much those MAPs contribute to the surface density in the upper right panel of Fig. 3.5, only MAPs younger than 5 Gyr old dominate the surface density in the outer part of the disc —again, due to the inside-out formation of the disc. Therefore, the flaring MAPs are important for the scale-height values of the inner disc, but do not have much influence on the scale-height values of the outskirts, producing very subtle or no thick disc flaring. I find 6 galaxies in our sample that fit in this category: g37, g38, g47, g62, g83 and g106.

Flared thick discs, on the other hand, are created when MAPs have a significant surface

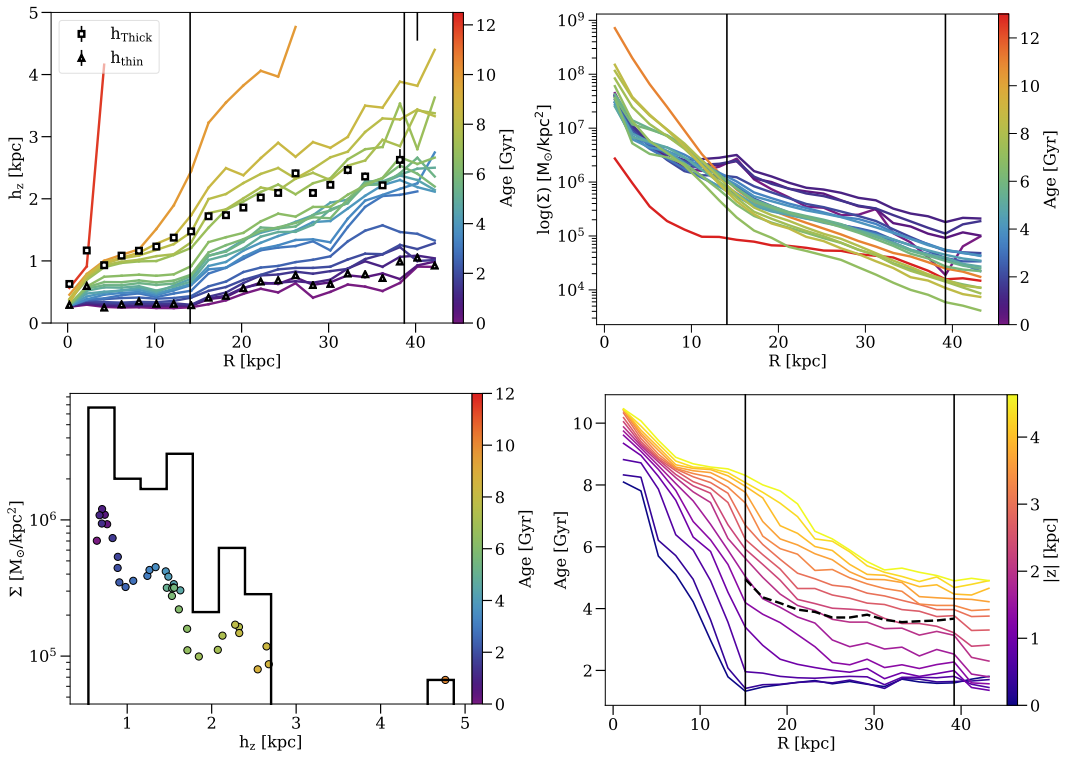


Figure 3.6: Case 2a, illustrated by g36: flaring MAPs and flaring thick disc. Panels represent the same as in Fig. 3.4.

density at the radius they start flaring. In this scenario, the scale-height of the global thick disc will progressively follow the flare of different MAPs, depending on how their respective surface densities and flaring levels combine, which is a result of the inside-out formation process of the disc. Galaxy g36 in Fig. 3.6 represents our **case 2a**. As can be seen in the upper left panel, MAPs older than 3 Gyr old flare considerably. There are even some gaps between the MAPs' scale-heights which are connected to mergers as discussed in Martig et al. (2014a). Similarly to case 1a and 1b represented in Figs. 3.4 and 3.5, as the surface density of the older MAPs gets lower with radius both in absolute values and relatively to younger MAPs, shown in the upper right panel of Fig. 3.6, the thick disc's scale-heights move across the gap between the MAPs' scale-heights and follow those of the younger components by the outskirts of the disc. This represents the most common flared thick disc scenario in our sample with 9 galaxies fitting into this category: g22, g36, g56, g57, g72, g124, g126, g136, and g147.

Cases **2b** and **2c** represent two particular scenarios of the mechanisms operating in case **2a**. In **case 2b**, only one or few flaring MAPs dominate the surface density all the way

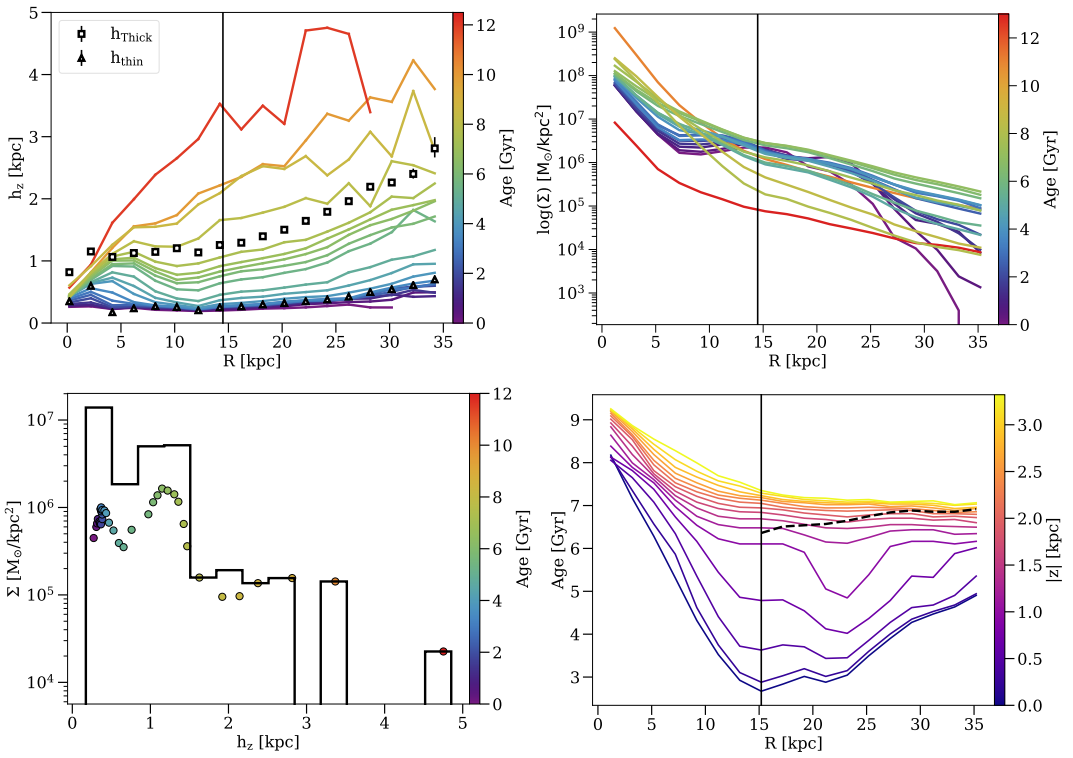


Figure 3.7: Case 2b, illustrated by g39: like case 2a with the particularity of having a few flaring MAPs dominating the surface density at all radii. The thick disc's scale-height follows those MAPs' flaring. Panels represent the same as in Fig. 3.4.

throughout the disc. If that is the case, then the thick disc's scale-height will follow closely the flaring of that particular MAP/MAPs. An example is g39, represented in Fig. 3.7. In the upper left panel of Fig. 3.7, the thick disc's scale-height follows MAPs around 7-7.5 Gyr old. If I look at the upper right panel of Fig. 3.7, I see that out of the MAPs contributing to the thick disc, MAPs between 6 and 7.5 Gyr old dominate by far the surface density at all radii. Therefore, these MAPs are going to dictate the flaring of the thick disc and its scale-heights are not going to go across multiple MAPs. Only 2 galaxies in our sample fit into this category: g39 and g44.

Finally, galaxy g102 represented in Fig. 3.8 shows our last flared thick disc scenario, **case 2c**. Although both MAPs and global thick disc are flared, instead of MAPs increasing their flaring and scale-heights progressively with age like cases 2a and 2b, a big group of MAPs have the same scale-heights. This can be seen in the upper left panel of Fig. 3.8. The upper right panel of Fig. 3.8 shows that in the thick disc, the surface density is dominated by different MAPs as a function of radius because of

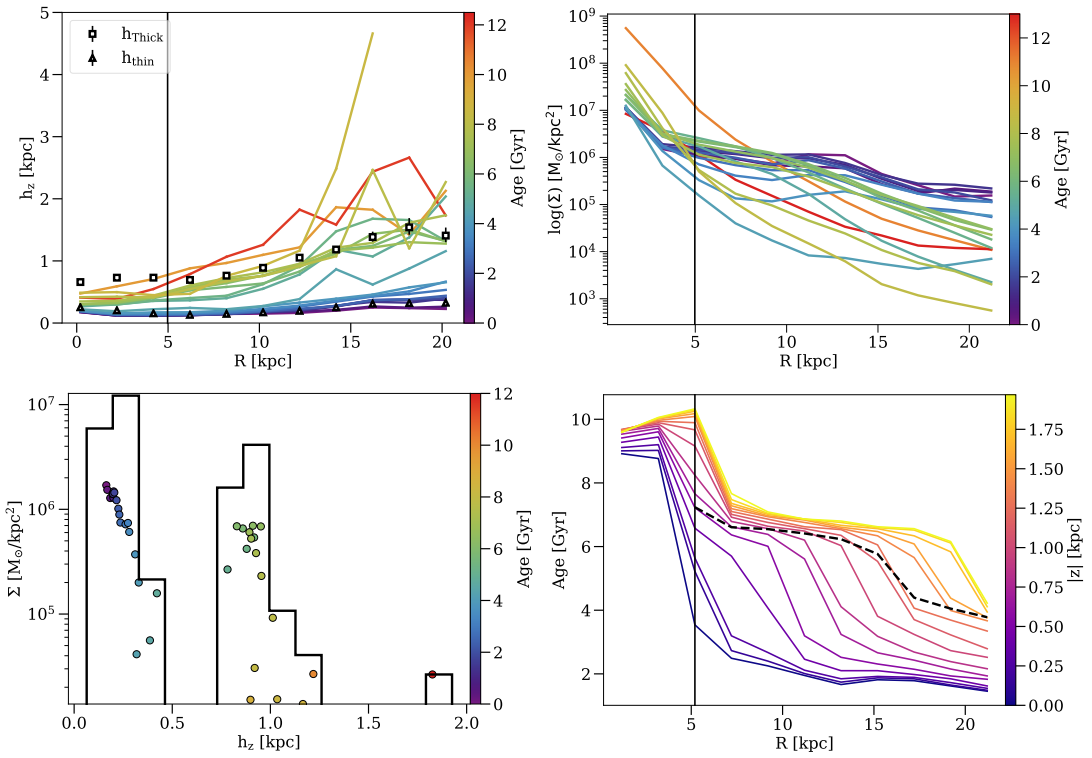


Figure 3.8: Case 2c, illustrated by g102: like case 2a with the particularity of a group of flaring MAPs having similar scale-heights and the thick disc's scale-height following those MAPs' flaring. Panels represent the same as in Fig. 3.4

the inside-out formation process of the disc. Nevertheless, since all these MAPs have roughly the same values of the scale-height at all radii, the thick disc's scale-heights will follow this group of MAPs. 4 galaxies from our sample fit into this category: g45, g48, g59, and g102.

### 3.4.3 Bimodal vs. continuous structure

Because of the different configurations of flaring MAPs and surface density changing in the radial direction, in some galaxies the thin and the thick discs will be formed by different groups of stellar populations, hence being two distinct components, whereas in some others the stellar populations forming the thin and the thick discs will be much more mixed —hence forming a thin-thick disc continuum. In the bottom left panel of Figs. 3.4 to 3.8, the surface density of each MAP colour-coded by age is represented against the value of their scale-height at $R_{1/2}$.

On the one hand, a thin/thick disc bimodality scenario is one where the disc has two components with comparable surface densities and each component has only certain MAPs. Galaxies g39 and g102 in Fig. 3.7 and 3.8 respectively are representative of this bimodality. In g102, the younger MAPs do not flare much and form the thin disc, whereas the older MAPs flare —and have the same scale-heights— and form the thick disc. Therefore, the thin and thick discs are clearly spatially divided and the stellar populations populating them are completely different regarding their age. Also, both disc components have a considerable amount of surface density. Galaxy g39 also shows a bimodality in its thin/thick disc. Contrary to g102, there are no big gaps between the MAPs' scale-heights and there is no group of MAPs with the same scale-height. However, a group of a few MAPs in the thick disc is so much more dominant in surface density than the rest, that this group creates a distinct massive thick disc component. Therefore, I inspected visually figures like the bottom left panel of Figs. 3.4 to 3.8 for all galaxies. I looked for either galaxies where the MAPs' scale-heights of the two groups are clearly separated, or they form two groups with similar surface density. I find a total of 8 galaxies in our sample that show clear thin/thick disc bimodality.

On the other hand, a continuum scenario is one where the transition between MAPs forming the thin disc and those of the thick disc is smooth, without clear massive distinct components. Galaxies g92 and g47 in Figs. 3.4 and 3.5 respectively are good examples: the scale-heights of MAPs increase progressively and no MAP dominates significantly over the others in terms of surface density. I looked for the galaxies where the MAP's surface density decreases smoothly with scale-height and age in figures like the bottom left panel of Figs. 3.4 to 3.8. I find a total of 13 galaxies in our sample show a continuous thin/thick disc structure.

Finally I find 6 galaxies in our sample that I classify as intermediate cases. These galaxies do not have a single gap in their MAPs' scale-heights but a few of them. However, because of the changing surface density with radius, sometimes the global thick disc's scale-heights are above a particular gap and sometimes below depending on radius. As a consequence, there is no clear group of MAPs which dictate the thick disc's scale-heights throughout the disc. Galaxy g36 in Fig. 3.6 is a good example of

the intermediate category. Looking at figures like the bottom left panel of Figs. 3.4 to 3.8 for all galaxies, the surface density of these galaxies' MAPs shows several peaks as a function of scale-height and age, but they are not clearly separated from one another in terms of scale-height.

### 3.4.4 Flaring of MAPs, flaring of thick discs, and bimodality

Having explained how the flaring of MAPs influences the flaring of the global thick disc, and creates continuous or bimodal structures, I show in this section how these features are interconnected.

I compute a parameter that quantifies the level of flaring of all MAPs and use it to analyse the whole galaxy sample. Since what matters is not only how flared a MAP is, but also how massive it is, we compute for each galaxy a mass-weighted average slope of MAPs as follows:

$$h_{\rm flaring} = \frac{\sum_n m_n \cdot ((h_{\rm outer} - h_{\rm inner})/R_n)}{\sum_n m_n}, \tag{3.1}$$

where $m_n$ is each MAP's total mass, $R_n$ is the radial extent of each MAP, and $(h_{\rm outer} - h_{\rm inner})$ is the difference between the MAP's scale-height at the beginning of the disc and the MAP's scale'height at the outermost radius. The resulting quantity that I denote as $h_{\rm flaring}$ is the averaged mass-weighted slope of all MAPs, hereafter the overall MAPs' flaring. In Fig. 3.9, the overall MAPs' flaring is computed for all the galaxies in our sample and compared to the flaring of their respective global thick disc. For this calculation, I leave out MAPs younger than 3 Gyr and older than 9 Gyr old since these do not contribute to the flaring of the thick disc as I previously argued in Sec. 3.4.1. It can be seen that, overall, MAPs always tend to flare more than their host thick discs. This is a consequence of the fact that MAPs that flare the most are not the most massive ones, especially at the flaring radii. Therefore, the global thick discs' scale-heights are going to be flattened by the MAPs that dominate the surface density at each radii, which are not the ones that flare the most. This is an example of a Yule-Simpson's paradox,

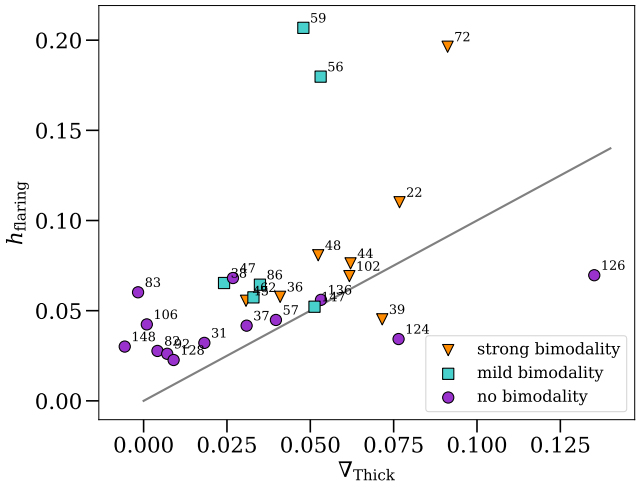


Figure 3.9: Mass averaged slope of all MAPs against thick disc slope. The marker shapes represent the bimodality of thin/thick disc: triangles represent a bimodal thin/thick structure, circles represent a continuum structure, and squares represent an intermediate case between continuum and bimodality. A black line shows a 1:1 line for comparison purposes. For almost all galaxies, MAPs are always more flared than the thick disc. All flat thick disc galaxies show no bimodality between thin and thick discs and their MAPs flare less than their flared thick disc counterparts, most of which show a bimodal structure.

characterised as "weak" by Minchev et al. (2019).

Finally, I study how flaring might connected with the bimodal or continuous structure of the disc. I represent the strength of the discs' bimodality with different marker shapes in Fig. 3.9. Galaxies are classified as having strong bimodality if MAPs can be grouped into two clearly differentiated groups, one forming the thin disc and another the thick disc (top left and bottom left panels of Figs. 3.4 to 3.8). Cases 2b and 2c are perfect examples of this group. Galaxies with no bimodality are those whose MAPs' scale-heights are smoothly distributed in the vertical direction, therefore the thin and thick disc belong to the same continuous structure. Cases 1a and 1b are perfect examples of this group. Finally, galaxies with mild bimodality are in between strong bimodality and no bimodality, where MAPs' scale-heights are somewhat grouped but there are not two distinct groups. Case 2a is a perfect example of this group. This classification was made by eye. It can be seen that most of the flat thick disc galaxies have a continuous disc structure, whereas galaxies with bimodal discs tend to have larger flaring factors $h_{\mathrm{flaring}}$ and more flared thick discs.

## 3.5 Age Gradients

A consequence of the combination of MAPs flaring and dominating the surface density in different disc radii is the creation of age gradients in the radial direction. In this section, I describe the age gradients in our galaxy sample and I explain how the different MAPs' flaring scenarios create radial age gradients.

### 3.5.1 Age Gradients in the Five Cases

I start by describing how the age gradients are created in our 5 cases. For that reason, from the mid-plane to 2 $\times h_{scale}$, I create 15 equally spaced horizontal slices 0.5 kpc wide and I compute the median age of the stellar particles in the same radial bins as when computing the scale-heights. The bottom right panels of Figs. 3.4 to 3.8 show the median stellar ages as a function of radius, colour-coded by the constant height of the slice. A black line represents a slice 0.5 kpc wide following the thick disc's scale-height.

In the cases 1a and 1b (flat thick discs), the MAP dominating the surface density is changing all the time as a function of radius as shown in the upper right panel of Figs. 3.4 and 3.5. This makes the median stellar age decrease with radius. In case 1a, because both the MAPs and the thick disc are flat, the age gradient through the thick disc is very similar to the age gradient at a constant height: in the bottom right panel of Fig. 3.4 it can be seen that the age gradient of the thick disc matches quite well the ones for heights of 0.5 and 0.75 kpc. Case 1b is similar to case 1a because of the small surface density of the flaring MAPs as explained previously.

Flared thick discs show a more diverse variety of age gradients. Case 2a is somewhat similar to cases 1a and 1b. Even though there are gaps, the MAPs' scale-heights increase with age gradually (see upper left panel of Fig. 3.6). At the same time, younger stellar populations have higher surface densities at larger radii. That is why at a given radius, the median stellar age increases smoothly with height, and decreases with radius. However, because MAPs are more extended in the vertical direction compared

to cases 1a and 1b, the thick disc's scale-heights cross through only a few MAPs, which cover a small age range. This, together with how these MAPs' surface densities are distributed radially, creates a flat age gradient as a function of thick disc's scale-height (e.g. for galaxy g36 shown in Fig. 3.6 the thick disc mean age only decreases from 5 Gyr to 4 Gyr over 25 kpc). Case 2b is different because a few MAPs dominate by far the surface density over the whole disc, and that conditions the thick disc flaring as mentioned in Sec. 3.4.2 (see again the upper left panel of Fig. 3.7). In the thick disc region, the radial age gradients are mildy negative or flat above ∼1 kpc, where the MAPs that dominate the surface density are found. When these MAPs' densities are combined to form the thick disc, the age gradient following the scale-height of the thick disc is going to be quite flat too. In the case of g39, a slightly positive age gradient results. Still, the gradient is small since it is determined only by a few MAPs with similar ages.

Case 2c has a different age gradient configuration from case 2a as well. Because several MAPs have the same scale-height, leaving a significant gap between the thin and thick disc, and because the thick disc MAPs have different radial surface density profiles, a characteristic feature is created in the age profiles (see bottom right panel of Fig. 3.8). A sudden drop in age can be seen in the horizontal slices at constant height, particularly pronounced at low radius. This represents the transition for that horizontal slice between the MAPs on one side of the gap to the other. This drop moves out in radius as height increases, driven by the flare in the thick disc. This feature should not be confused with the first drop in the very inner galaxy, which is caused by the transition from the old bulge to the disc. Also, the median age following the thick disc's scale-height decreases because the different MAPs living in the thick disc dominate the surface density at different radii as with cases 1a, 1b, and 2a.

### 3.5.2 Age Gradients in the Sample

Next, I show the age gradients of the whole sample. I compute the age gradient in the thick disc, $\nabla_{\rm age}$, by dividing the difference in age in the thick disc between $R_{\rm inner}$ and

$R_{\rm outer}$ by the extent of the thick disc. In Fig. 3.10, I represent $\nabla_{\rm age}$ as a function of the thick disc's scale-height slope, $\nabla_{\rm Thick}$, colour-coded with three different variables linked to the general properties of thick discs: mass of the galaxy in the top, thick disc mass ratio in the middle, and disc thickness in the bottom panel. The values in the colourbar indicate the 16th and 84th percentiles, so every point in dark blue or yellow belongs to the low and high tail of the distribution respectively. The marker shape represents the bimodality/continuous structure of the disc as in Fig. 3.9.

These figures show that flat thick disc galaxies are also low mass galaxies and have thinner discs. They also tend to have low thick disc mass fractions. Finally, all flat thick disc galaxies possess an age gradient. Above a certain level of thick disc flaring, galaxies have a wider range of behaviours, from no age gradient at all to very strong age gradients, as well as a wide range of masses, thick disk fractions and thicknesses. Although it might not be statistically significant, it is worth noting that about two thirds of galaxies with a flared thick disc have little or no age gradients. Finally, I have excluded galaxy g56 from the plot for visual purposes, as it has a gradient of 0.3 Gyr/kpc. g56 presents unusual age radial profiles that decrease with radius until close to $R_{\rm outer}$, where there is a sudden increase in age. This results in U-shaped profiles where the age at $R_{\rm outer}$ is higher than at $R_{\rm inner}$. Understanding the particular behaviour of this galaxy is not within the scope of this chapter, and therefore I treat g56 as an outlier.

I find that almost all of the most massive galaxies (above $1.1 \times 10^{11}$ $M_{\odot}$), galaxies with the highest thick disc mass ratios (above 45%), and the thickest discs (scale-height at $R_{1/2}$ above 1.8 kpc), have relatively flat age gradients in their thick discs. These 3 conditions are not strictly necessary for thick discs to have flat age gradients, but I find that most galaxies which have at least one of the three characteristics have an age gradient smaller than -0.1 Gyr/kpc.

So far I have referred to radial age gradients following the thick disc's scale-heights, which imply that I follow sometimes a steep line with radius. The age gradients change of course if I take a horizontal slice in the disc at a constant height above the midplane, which is what an observer would likely do. I select a slice 0.5 kpc wide at a height equal

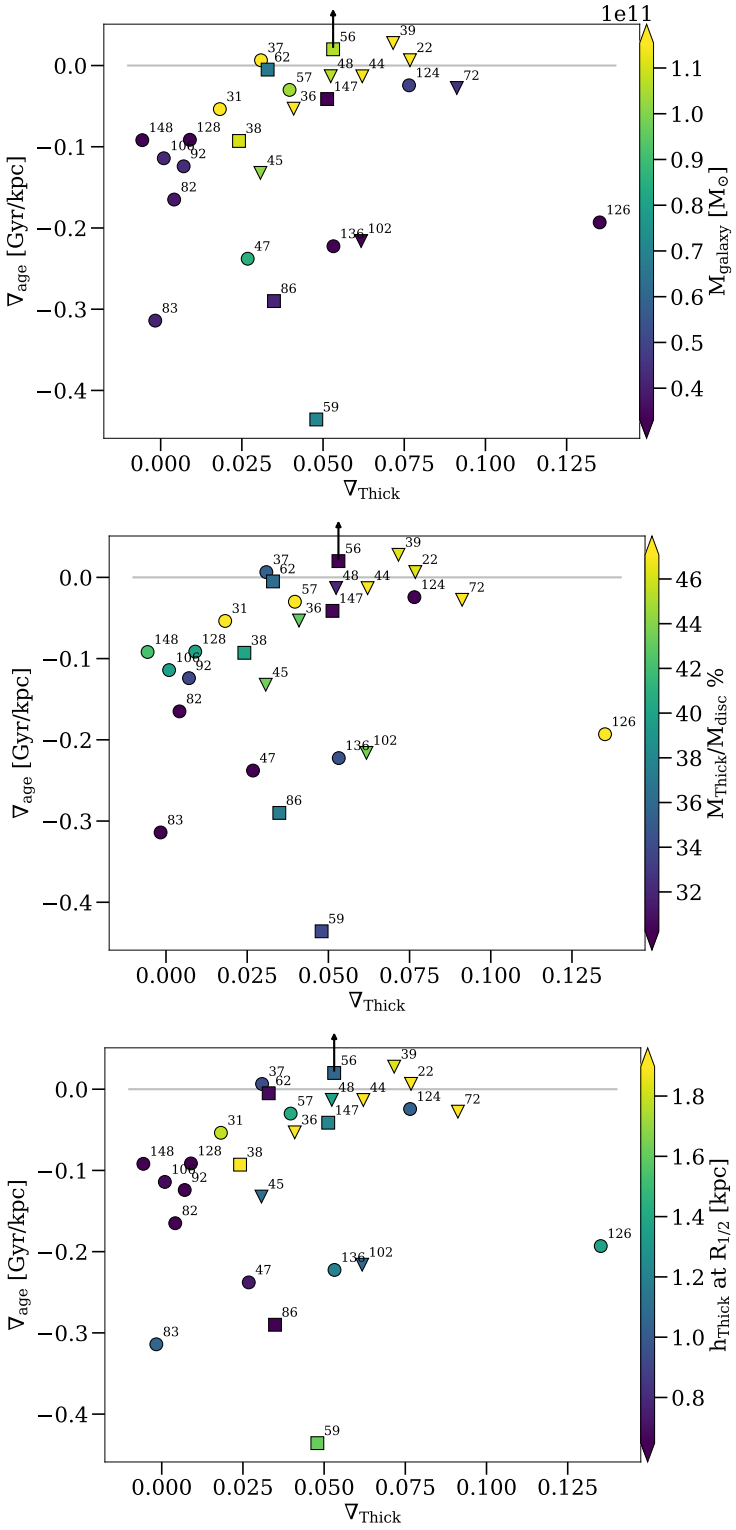


Figure 3.10: Age gradient following the thick disc' scale-heights against thick disc gradient, colour-coded by three different variables. *Top*: galaxy mass. *Middle*: mass thick disc ratio. *Bottom*: thickness of thick disc. The points' symbols represent the same as in Fig. 3.9. The grey solid line highlights the constant value 0, i.e., no age gradients. All flat thick discs have an age gradient, whereas flared thick discs are more diverse, although most of them tend to have a flat age gradient.

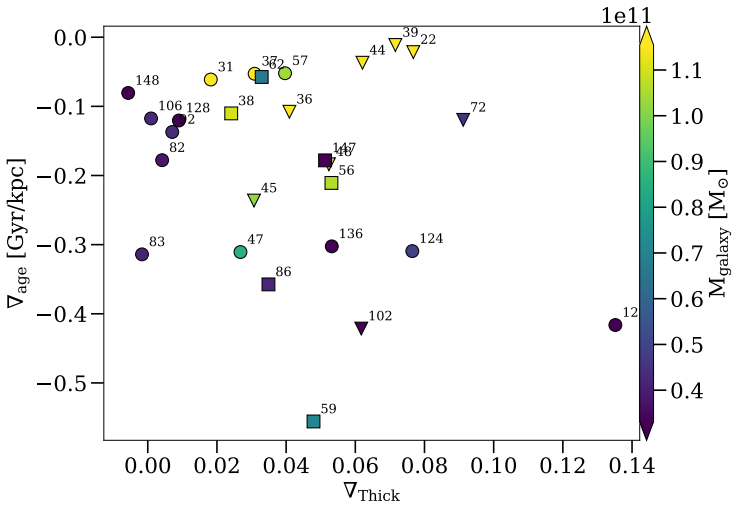


Figure 3.11: Age gradient at a constant height equal to the median value of $h_{\mathrm{Thick}}$ against slope of the thick disc. The markers' symbols represent the bimodality of the thick disc like in Fig. 3.9.

to the median value of the thick disc's scale-heights, and compute the age gradient. As can be seen in Fig. 3.11, this does not change the age gradients measured for galaxies with a flat thick disc — this is expected, since for those galaxies it is equivalent to measure the age at a constant height or along the thick disc scale-height. By contrast, the age gradient of galaxies with flared thick discs are generally stronger when measured at a constant height, except for the most massive galaxies with flat age gradients, which do not change much. I also note that galaxy g56 is not an outlier anymore if age gradients are measured at a constant height above the midplane.

## 3.6 Mergers and Formation Histories

While secular evolution and radial migration can in some cases induce some disc flaring (Minchev et al., 2012a; Martig et al., 2014a), interactions between discs and satellite galaxies are one of the main mechanisms causing flaring. How much flaring is induced depends on multiple factors such as the orbit and mass of the satellite, and the bulge fraction of the main galaxy (Kazantzidis et al., 2008, 2009; Qu et al., 2011; Moetazedian & Just, 2016). It is not within the scope of this work to explore meticulously how those different factors produce different effects on disc dynamics and flaring, but I can observe

some of their most noticeable effects, and explain some configurations of thick disc, MAPs, and age gradients.

The effect mergers have on thick disc flaring and age gradients are varied. For galaxies like g36 in case 2a, represented in Fig. 3.6, a merger will flare all MAPs born up to that point, whereas MAPs born after are going to be considerably less flared, creating a gap (Martig et al., 2014b). This is not necessarily enough to produce a flat age gradient along the thick disc. In galaxies like g102 in case 2c, the merger will make all the MAPs born up to that point flare with the same scale-heights, creating a thin/thick disc bimodality. Yet, there will be still an age gradient along the thick disc since the MAPs populating it still dominate the surface density at different radial distances. In other cases however, mergers will make one or few MAPs overmassive compared to the rest, creating a flat age gradient in the thick disc like galaxy g39 in case 2c.

In Fig. 3.12 I show the age gradient along the thick disc $\nabla_{\rm age}$ as a function of the thick disc's scale-height slope $\nabla_{\rm Thick}$ as I did in Fig. 3.10, but this time colour-coded by the stellar mass of the most massive merger in the last 9 Gyr in the upper panel, and the mass ratio of that merger in the bottom panel. The shape of the points has the same meaning as in Figs. 3.9 and 3.10. The stellar mass of the satellites is computed right before their first interaction with the disc of the main galaxy. Thus, I am not considering the initial mass of satellites and their disruption as they cross the galactic halo, which is a process that could be potentially altered by numerical resolution (van den Bosch et al., 2018). I also refer the reader to Martig et al. (2012, 2014a) for a more detailed discussion of some of the resolution tests that have been performed.

I find that galaxies with flat thick discs all had very quiescent merger histories: all of those galaxies (except g106 that had a 1:15 merger around 8 Gyr ago) only have mergers smaller than 1:30 in the last 9 Gyr. Radial age gradients along the disc are a natural consequence of an inside-out disc growing formation scenario. As the disc forms and grows gradually, younger MAPs are born and dominate the density towards the outer regions. For flat thick disc galaxies, which generally have quiescent merger histories, this configuration will remain intact as the MAPs' flaring is either minimal or happens at the radii with low surface density. Therefore, flat thick disc will tend to have a radial

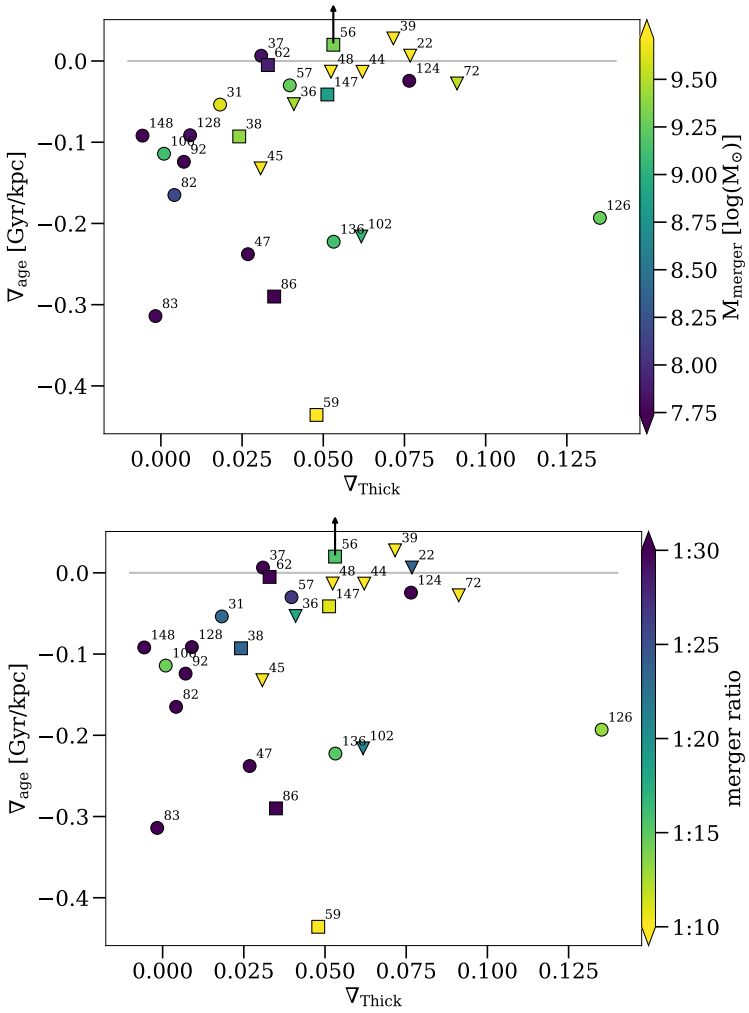


Figure 3.12: Age gradient following the thick disc's scale-height against the slope of the thick disc. *Top*: colour-coded by the mass of the most massive merger in the last 9 Gyr. *Bottom*: colour-coded by the mass ratio of the most massive merger in the last 9 Gyr (defined as the ratio between the stellar mass of the satellite and the main galaxy at the time of the merger) The symbols represent the bimodality of the thick disc like in Fig. 3.9. Galaxies with stronger mergers tend to have more flared thick discs with flatter age gradients.

age gradient along the disc, which is what I observe in Figs. 3.10 and 3.12.

Flared thick disc galaxies show more diversity. Galaxies with more massive mergers tend to have flat age gradients (less than –0.1 Gyr/kpc) and also tend to have some degree of flaring (more than 0.02). All the galaxies having merged with satellites whose stellar mass higher than $4.5 \times 10^9$ $M_\odot$ show either mild or strong bimodality, although there is no strong correlation between the degree of bimodality and the mass of the satellite. For instance, g59 underwent a massive merger but only shows mild bimodality. This could be due to different factors, like the merger's orbit: exploring this is not within the scope of this thesis, and future work will be needed on this matter. The bottom panel of Fig. 3.12 shows similar results. Most galaxies that underwent mergers with a mass ratio higher than 1:10 seem to have more flared thick discs with flat age gradients. These galaxies also show strong thin/thick disc bimodality. By contrast, I also find galaxies with a quiescent merger history but a flared thick disc and a flat age gradient. For these galaxies, there must be other mechanisms besides mergers causing both the flaring of the thick disc and the flat age gradient. In some of these galaxies, MAPs are born already with some degree of flaring, which has been reported in other cosmological simulations (e.g. Navarro et al., 2018). As for the others, MAPs were born in flatter configuration. The source of flaring for these MAPs can be internal heating mechanisms or external agents such flybys or multiple minor mergers throughout the life time of the galaxy. However, most galaxies in our sample have no more than one merger with a mass ratio above 1:30, and the few with more mergers (up to 4 above a merger mass ratio above 1:30) do not seem to be different from the rest of the galaxy sample.

Even though mergers are not the only mechanism for disc flaring, they play a key role in our sample. I do observe that if the merger is massive enough, or the mass ratio between the merger and the main galaxy is high enough, they can produce a flared thick disc, a flat age gradient, and a bimodal thin/thick disc structure. On the other hand, I observe that galaxies with a flat thick disc have a relatively quiescent merger history.

## 3.7 Conclusions

In this work I explored the structure of galactic thick discs using a sample of 27 simulated galaxies in their cosmological context (Martig et al., 2012). Minchev et al. (2015) explained how Mono-Age Populations (MAPs) create the thin and thick disc by a combination of three factors: the MAPs' level of flaring, the individual MAPs' surface density, and how these two change with radius. This interplay creates age radial gradients in the thick disc (as observed in the Milky Way, Martig et al., 2016). I expand on the work of Minchev et al. (2015), and use a sample of 27 simulated galaxies to explore: i) how the flaring of MAPs and the flaring of the global thick disc are connected, ii) whether the thin and thick discs are distinct components or a continuum, iii) what kinds of age gradients flaring MAPs form, iv) and how merger histories can potentially influence all the above. Our conclusions from this study can be summarised as follows:

- MAPs older than around 9 Gyr are very concentrated in the centre of the galaxy and barely contribute to the flaring of the thick disc. They do, however, increase the scale-height of the thick disc quite uniformly at all radii. MAPs younger than around 3 Gyr are very concentrated in the galactic plane and barely flare, therefore they will not contribute to the flaring of the thick disc either. Flaring of the thick disc is mainly driven by stellar populations between 3 and 9 Gyr old.

- Flat thick discs form when MAPs barely flare or when, due to inside-out formation, the flared MAPs do not carry a lot of surface density at the flaring radii compared to younger, less flared MAPs. The MAPs' scale-heights increase smoothly as a function of age, creating a continuous thin/thick disc structure as was found for the Milky Way (Bovy et al., 2012b), although mono-age and mono-abundance populations can be quite different (Minchev et al., 2016). I find that all flat thick discs exhibit a radial age gradient like the Milky Way (Martig et al., 2016), and they are galaxies with low mass (e.g. $M_{galaxy} \leq 5 \times 10^{10} M_{\odot}$), thinner global discs (e.g. average $h_{Thick} \leq 1$kpc), and lower thick disc mass ratios (e.g. $M_{thick}/M_{disc} \leq 40\%$). They also tend to have more quiescent merger histories,

with low mass or low mass ratio mergers, or mergers only at early times. In our sample, 12 galaxies have flat thick discs, which corresponds to 44% percent of the sample.

- Flared thick discs form when MAPs carry a significant amount of surface density where they flare. The flaring of the global thick disc can be driven by a sequence of different MAPs at different radii, or only MAPs spanning a couple of Gyrs if those MAPs dominate the surface density throughout the disc, or they all share the same scale-heights. If one of the two last cases happens, then a bimodal structure is created and thin and thick disc are distinct components in terms of the stellar populations inhabiting them. This effect is directly related with the merger history as Martig et al. (2014a) pointed out using the same galaxy sample. Flared thick discs are more diverse than their flat counterparts in terms of age radial profiles, although a high fraction of them show a small or flat age radial profile following their thick disc's scale-heights. This is especially the case for galaxies with high mass, high thick disc mass fractions, and the thickest global discs. I also find that galaxies that underwent very massive mergers or with high mass merger ratio tend to have flat age radial profiles. In our sample, 15 galaxies have flared thick discs, which corresponds to 56% percent of the sample.

Our sample of simulated galaxies thus shows a great diversity of thick disc structures, even though I only studied a relatively limited halo mass range and restricted ourselves to galaxies in isolated environments. I find a group of 6 galaxies that show characteristics close to the Milky Way, like radial age gradients in their thick discs, and minimal flaring of the global thick discs' scale-heights. These galaxies belong to the lower end of the distribution in our sample in terms of stellar mass ($M_{galaxy} \leq 5\times10^{10}M_{\odot}$), have average thick disc scale-heights ($h_{Thick} \leq 1$kpc), and are in the lower half of the distribution in terms of thick disc stellar mass ratio ($M_{thick}/M_{disc} \leq 40\%$). These galaxies have quiescent merger histories, with either none or a few very small mergers in terms of mass. This is also consistent with what is known about the Milky Way's merger history as its last significant merger in terms of mass happened around 8 Gyr ago or even more (e.g., Helmi et al., 2018b; Deason et al., 2018). Although there have been recent

interactions between the Milky Way and the Sagittarius dwarf galaxy, the latter still has not merged and therefore has induced changes in the MW's disc on a more local and smaller scale (e.g. two distinct geometrical thin and thick discs). Therefore, the Milky Way's merger history can be considered quiescent in the last Gyr, and thus comparable with this group of simulated galaxies in regards of the characteristics aforementioned.

The rest of the sample, i.e. flared thick disc galaxies, is a lot more diverse, depending on the galaxies' formation histories. Our results cannot be directly compared to galaxies in the Fornax cluster (Pinna et al., 2019a,b), but they could be used to interpret, for instance, the discovery in NGC 7572 of a very massive and flared thick disc (Kasparova et al., 2020): this probably results from a massive merger. In any case, the diversity found in this group of simulated galaxies seems to agree with the diversity found in nearby galaxies.

Our simulations suggest that thick discs can be successfully used to probe galaxies' merger histories, which I will study in more details in future work. As more and more data becomes available for thick discs in nearby galaxies, it will soon be possible to compare the Milky Way and its neighbours, to interpret their different structures, and to connect those with their formation histories. Ultimately, this can help discern how unique our Galaxy is in the context of its neighbouring galaxies and disc galaxies in general.

# Chapter 4

# No Memory of Past Warps in the Vertical Density Structure of Galaxies

*"Do not go gentle into that good night; Old age should burn and rave at close of day. Rage, rage against the dying of the light."*
– Dylan Thomas

## 4.1 Introduction

Many of the warp forming mechanisms (reviewed in Chapter 1) are often associated with disc heating and flaring (e.g., Gerssen & Shapiro Griffin, 2012; Minchev et al., 2015; Pinna et al., 2018). For instance, mergers have been proposed to create disc heating (Toth & Ostriker, 1992; Sellwood et al., 1998; Kazantzidis et al., 2008, 2009) and disc flaring (e.g., Villalobos & Helmi, 2008; Bournaud et al., 2009; Martig et al., 2014b). Another example is misaligned infall of gas, which can also cause disc heating and flaring (Scannapieco et al., 2009) as well as warping.

Therefore, disc heating and warping may happen simultaneously. Indeed, the outskirts

of the MW's disc seem to be both flaring (e.g., Amôres et al., 2017; López-Corredoira et al., 2018; Thomas et al., 2018) and warping (e.g., Chen et al., 2019; Yu et al., 2021). Khachaturyants et al. (2021) suggested that settled warp stars may contribute to the flaring of the youngest stellar populations observed at large galactocentric radii in the MW. In some cases, it could even be possible that the warps themselves might directly cause some vertical heating: bending waves, a phenomenon closely related to warping, have been proposed to heat discs (Khoperskov et al., 2010; Griv, 2011).

However, heating and warping do not necessarily always happen together. In the case of satellite-galaxy interactions, whether the disc tilts or gets heated depends on different properties of the satellite, including its orbital properties (Velázquez & White, 1999). Shen & Sellwood (2006) similarly found in simulations that in a satellite-galaxy interaction, the host galaxy's disc tilts remarkably rigidly, so that vertical heating is very limited.

Thus, it is worth exploring the connection between warping and disc heating/flaring. In this chapter, I use the sample of simulated galaxies from Martig et al. (2012) to explore how much disc vertical heating happens during warps, and how warps affect the vertical stellar density structure of galactic discs. The chapter is divided as follows: in section 4.2 and 4.3 I describe the methods to characterise the warps and the vertical structure of discs. In section 4.4 I describe different properties of the warps, including how they form. In section 4.5, I address the connection between warps, disc heating, and disc flaring; and summarise our conclusions in section 4.6.

The work presented in this chapter has been published in García de la Cruz et al. (2021a).

## 4.2 Methods: warp selection and characterization

### 4.2.1 Alignment of the galactic plane

In order to study warps, I need to globally align the galactic disc in the XY plane. For this, I first compute the total angular momentum of all stellar particles inside a sphere of radius 20 kpc. I then rotate all particles to align this angular momentum with the Z axis. To refine the alignment of the disc in the XY plane, I rotate the disc a second time by computing again the total angular momentum's direction but, this time, within a cylinder with radius equal to $R_{25}$ and height equal to 6 times the estimated disc thickness $h_{\rm scale}$. This estimated disc thickness is defined as the standard deviation of the vertical position of stars located at half the optical radius of the galaxy, $R_{25}$, also used and described in García de la Cruz et al. (2021b). $h_{\rm scale}$ is computed after the first alignment. Because the misalignment left after the first rotation is little, and $h_{\rm scale}$ is computed at $R_{25}/2$ and not at the edge of the disc, $h_{\rm scale}$ is not very much affected by the second alignment.

### 4.2.2 Identifying warps

After I ensure the discs are properly aligned with the XY plane, I create maps of the mean vertical position of stellar particles and use those maps to visually identify the presence of warps. By a warp, I define a wide azimuthal area of the outer part and/or edge of the disc that is shifted either up or bottom from the galactic plane (see examples in Fig. 4.1). This definition does not include complex vertical corrugation patterns that may not take place in inner parts of the disc or small areas in terms of azimuthal extension. I only select warps that clearly start within $R_{25}$. I track each galaxy as a function of time, and note when warps start and end. Our final sample consists of 11 warps: 5 that have ended by redshift $z = 0$ and 6 that are still ongoing. These 11 galaxies are included in Table 4.1.

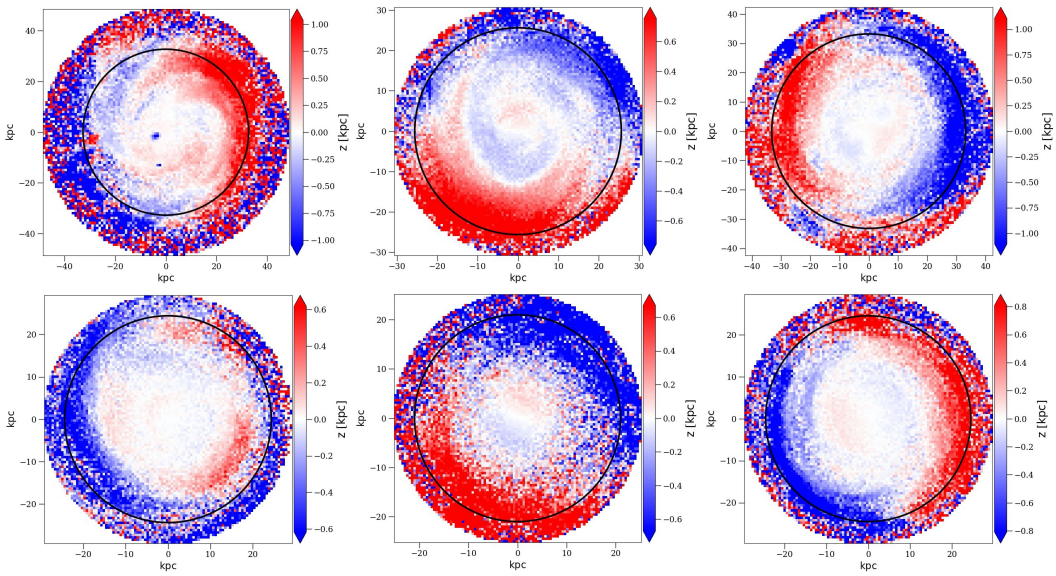


Figure 4.1: A sample of vertical position maps where warps are detected. From left to right and top to bottom: **g38**, **g83**, **g39**, **g62**, **g126**, and **g48**. Each pixel is colour-coded by the stellar particles' mean vertical position of stellar particles. The black circle corresponds to $R_{25}$, which we use to define the edge of the disc. The left column shows two examples of L-shaped warps (or one-sided), while the rest shows S-shaped warps (or two-sided).

### 4.2.3 Characterizing warps

Once I have identified the snapshots where the galactic disc is warped, I proceed to characterise the warps. For that, I divide the disc into 10 azimuthal sectors, and each sector into overlapping radial bins 2 kpc wide every 0.5 kpc. For each of these azimuthal and radial sectors, I bin the stellar particles into 100 vertical bins up to 5 times $h_{\rm scale}$ above and below the galactic plane, and identify the peak of the vertical density. An example of this can be seen in Fig. 4.2.

I compute the maximum height above the midplane reached by the warp. I also compute the angle between the galactic plane and a line joining the maximum of the warp to the galactic center: I will call this the warp angle $\theta$.

From all the information extracted in this process and represented in Fig. 4.2, I also extract the onset radius of the warp, as it can clearly be seen when the peak of the vertical stellar density starts to shift away from the galactic plane. I record the value of the warp angle, height and onset radius throughout the warp's life.

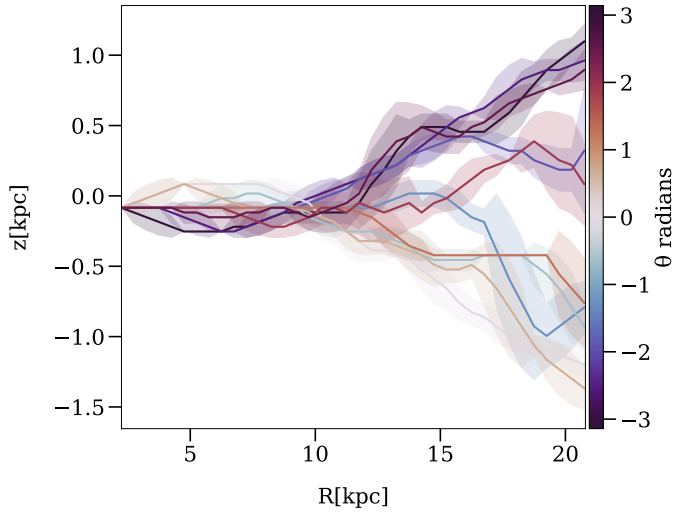


Figure 4.2: Mean vertical position of the stellar density peak as a function of radius colour-coded for different azimuthal angles for galaxy **g126**. Shaded areas represent the dispersion around the mean vertical position. The values at the largest radius are used to compute the maximum warp height and angle given in Table 4.1. I define the onset radius of the warp as the radius where the vertical position of the stars starts deviating from 0 for different azimuthal angles (this would be ∼11 kpc for galaxy **g126** shown here).

## 4.3 Vertical density profiles & scale-heights

I analyse the vertical density distribution for stars in the disc both inside and outside the warped region of the disc. To compute a single vertical density profile at a given radius, I first need to correct for the different vertical shifts in vertical density as a function of azimuth caused by the warp itself. For that, after dividing the disc into different azimuthal and radial bins as described in Sec. 4.2.3, I compute the dispersion of the vertical position of the stars in every disc region. Then, I compute the median value of the vertical position from all stellar particles whose vertical position is smaller than the previously computed vertical dispersion. Finally, I shift uniformly all the stellar particles within the region by this median value. With this, the peak of the vertical stellar density is aligned with the galactic plane of the galaxy for a given radius and azimuthal sector. An example of this technique is shown in Fig. 4.3. After correcting for the vertical shift caused by the warp in different azimuthal sectors, I fit the density profiles with a double sech$^2$ representing a thin and thick disc following the method explained in Chapter 2, and applied in Chapter 3.

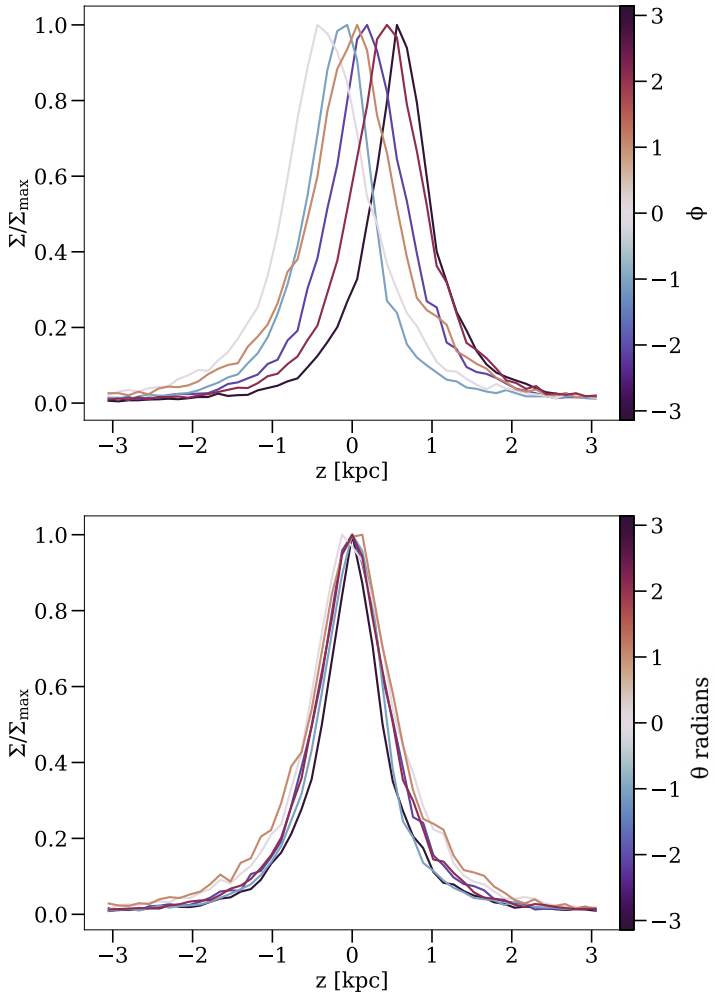


Figure 4.3: *Top:* normalised vertical stellar density for different azimuthal angles within a stellar ring in the disc for galaxy **g83**. *Bottom:* the result of shifting uniformly all stellar particles in the given azimuthal angle following the method described in Sec. 4.3. This shows density profiles that are very similar in the different angular sectors of the disc, with only small variations at large height. I apply this methodology for all the analysis in this work.

## 4.4 Warp formation processes and characteristics

After identifying and characterising the galactic warps as described in Sec. 4.2, our final sample consists of 11 warps: 5 that have ended by redshift $z = 0$ and 6 that are still ongoing. In this section, I first present the mechanisms creating the warps, and then discuss the shape, duration and amplitude of the warps.

I find that the different warp formation processes can be grouped into two categories. Warps belonging to the first group arise when the stellar particles living in the disc experience a shift of their vertical position. In order words, the warp is made of stellar particles that already existed in the disc prior to the warp itself. The two main channels to create such a warp are vertical instabilities in the absence of satellite galaxies or through an interaction with a satellite galaxy, i.e. a flyby or a merger. On the other hand, warps belonging to the second group form when new stellar material is added to the galaxy in off-plane orbital configurations. This can happen either because stars are accreted onto the disc, or because stars are born already in an off-plane configuration out of a bent gas disc. Below, I provide a more detailed description of the formation of the warps from our sample (see also a summary in Table 4.1):

*Internally-driven warps*

In two galaxies, I notice warps that appear while no massive satellite is visible in our stellar density maps, which extent to 80 kpc distance from the galactic centre. A bending wave starts expanding from the inner disc outwards. When this bending wave reaches the outermost part of the disc, it has widened enough to form an L-shaped warp. The origin of this feature is difficult to determine: it could be triggered by some of the dark matter halos orbiting the galaxy (Widrow et al., 2014; Chequers et al., 2018), but could also be driven by spiral arms (Faure et al., 2014), or result from an internal bending instability (Revaz & Pfenniger, 2004). In any case, I cannot discern the true agent behind warp formation and further analysis will be done to clarify the cause of the warp. I find two warps belonging to this category: **g38**, **g128**.

Table 4.1: Summary of the general features of our warp sample. In the final time column, the symbol "-" means the warp is ongoing by $z = 0$. In the symmetry/shape column, "L" means the warp is one-sided, while "S" means is two-sided, with each side going in opposite directions.

| galaxy ID | initial time Gyr | final time Gyr | symmetry/shape | max. \|z\| kpc | max. $\|\theta\|$ ∘ | likely warp agent |
|---|---|---|---|---|---|---|
| g38 | 11.9 | 12.4 | L | 1.40 | 2.45 | internally driven |
| g128 | 9.8 | 10.1 | L | 0.61 | 2.10 | internally driven |
| g35 | 13.1 | - | L | 3.07 | 6.08 | satellite |
| g62 | 13.0 | - | S | 1.59 | 3.74 | satellite |
| g83 | 12.3 | - | S | 1.69 | 3.76 | satellite |
| g126 | 12.1 | - | S | 1.97 | 6.12 | satellite |
| g148 | 11.9 | 13.3 | S | 0.63 | 4.08 | satellite |
| g48 | 9.8 | - | S | 5.43 | 12.25 | stellar ring |
| g59 | 11.1 | - | S | 7.60 | 21.68 | stellar ring |
| g102 | 9.8 | 12.6 | S | 2.93 | 8.9 | stellar ring |
| g39 | 8.0 | 9.7 | S | 6.69 | 11.55 | accretion |

*Interactions with satellites*

These warps are created by the interaction between a satellite and the host galaxy, either a merger or a flyby. Galaxies belonging to this category mostly form S-shaped warps.

**g35**: a satellite with $M_\star \sim 1.9 \cdot 10^7 M_\odot$ stellar mass crosses the disc at t ~ 12.8 Gyr and shortly after this, a warp appears at t ~ 13.1 Gyr on the side of the disc through which the satellite has passed (this is the only L-shaped warp of this category).

**g62**: a satellite $M_\star \sim 2.9 \cdot 10^6 M_\odot$ crosses the disc at t ~ 11.8 Gyr creating multiple vertical bending waves. Around t ~ 13.0 Gyr, a warp develops on one side of the disc (L-shaped) and then shortly evolves into an S-shaped warp.

**g83**: a satellite with $M_\star \sim 3.6 \cdot 10^5 M_\odot$ flies by the disc in a polar orbital configuration with pericenter ~ 46 kpc from the galaxy's centre at t ~ 11.4 Gyr, creating a warp at t ~ 12.3 Gyr. A second pass at t ~ 13.4 Gyr increases the amplitude of the warp.

**g148**: a satellite with $M_\star \sim 1.6 \cdot 10^6 M_\odot$ at t ~ 11 Gyr flies by in a low-inclination orbit at t ~ 11 with pericentre ~ 14 kpc from the galaxy's centre, creating a warp at t ~ 11.9 Gyr.

**g126**: a 1:10 merger at t ~ 10.5 Gyr creates vertical oscillations propagating from the inner to the outer disc. The warp forms at t ~ 12.1 Gyr when these vertical oscillations reach the outer disc. A stellar ring forms later on, at t ~ 12.5 Gyr, in a slightly bent configuration, which reinforces the warp and increases its duration.

*Accretion on an inclined orbit*

**g39**: a 1:20 merger at t ~ 7.5 Gyr scatters around stellar particles both belonging to the satellite and the host galaxy in off-plane configurations. Around half a Gyr later, at t ~ 8 Gyr, the disc grows and the off-plane material falls back onto the disc, forming an S-shaped warp.

*Formation of an inclined stellar ring*

These warps form when a massive merger perturbs the gas disc, which ends up misaligned with respect to the stellar disc. Later on, a flyby triggers star formation in the outer regions of the inclined gas disc, forming an inclined stellar ring. The gravitational interaction between the stellar disc and the stellar ring pulls the latter down to the galactic plane. The warp is the product of this mixing between the aligned stellar disc and the off-plane stellar material. As with warps created from interactions with satellites, these warps are also S-shaped. A visual representation of this process can be found in Fig. 4.4. The top row of Fig. 4.4 records the merger of the satellite. On the right top panel, it can be seen how both the stellar but especially the gas disc are inclined. On the middle row of Fig. 4.4, the stellar ring forms and starts to break as the galaxy centre exerts gravity force towards it. Finally, on the bottom row of Fig. 4.4, the stellar ring has merged with the outer disc and the warp is fully formed.

**g48**: a 1:4 merger happens at t ~ 8 Gyr. About 1.5 Gyr later, at t ~ 9.8 Gyr, a stellar ring forms following a flyby from another satellite.

**g59**: a 1:4 merger at t ~ 7.5 Gyr spreads gas around the galaxy. During the next Gyr, flybys from two massive satellites keep the gas bent until, finally, it condenses and forms stars at t ~ 11.1 Gyr. A stellar ring forms in a bent configuration, and as with **g48**, this stellar ring creates the warp.

**g102**: a 1:15 merger happens at t ~ 8 Gyr. About 1 Gyr later, two satellites fly by close to the disc and, shortly after this, an inclined stellar ring develops outside of $R_{25}$ at t ~ 9.8 Gyr. This structure progressively falls onto the disc, creating the warp.

I record the shape and duration of all these warps. I consider the warp has ended when the vertical shift from the galactic plane at the edges of the disc has disappear by eye. I also compute the maximum height above the midplane reached by the warp as well as the maximum warp angle. All these properties are summarised in Table 4.1. The values I find for most warp angles are comparable to those found in observations (e.g., Sánchez-Saavedra et al., 2003; Ann & Park, 2006; Reshetnikov et al., 2016) and in other simulations (e.g., Gómez et al., 2017). Only one galaxy, **g59**, is a clear outlier

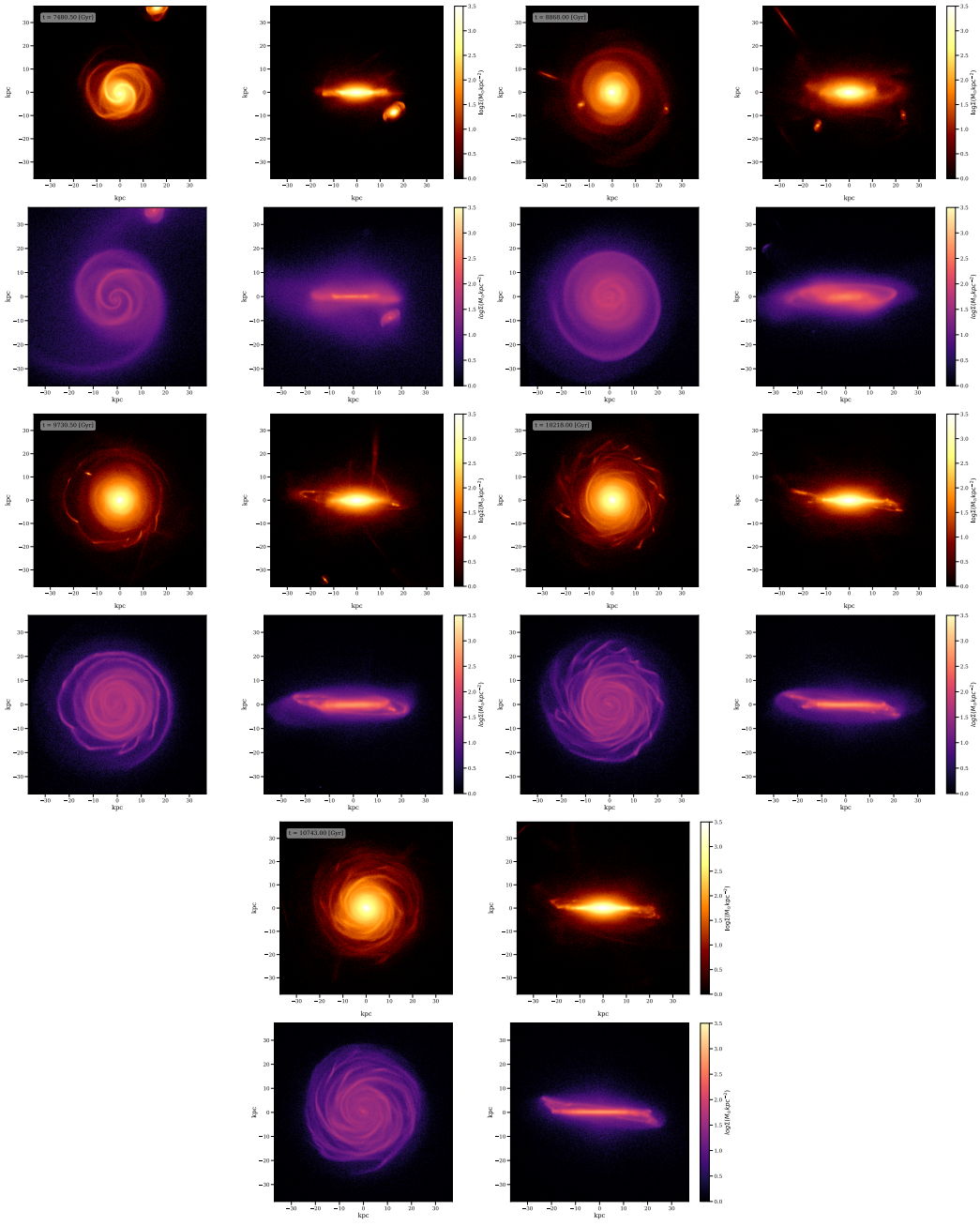

Figure 4.4: Density maps of stellar particles (orange and yellow) and gas particles (purple and pink) for galaxy g48 seen face on and edge on. The time sequence indicated by the text box on the face on maps of stellar particles shows the process described in Sec. 4.4 where, after the merger, the inclined gas condenses and forms a stellar outer ring in an off-plane configuration which later on transforms into a warp.

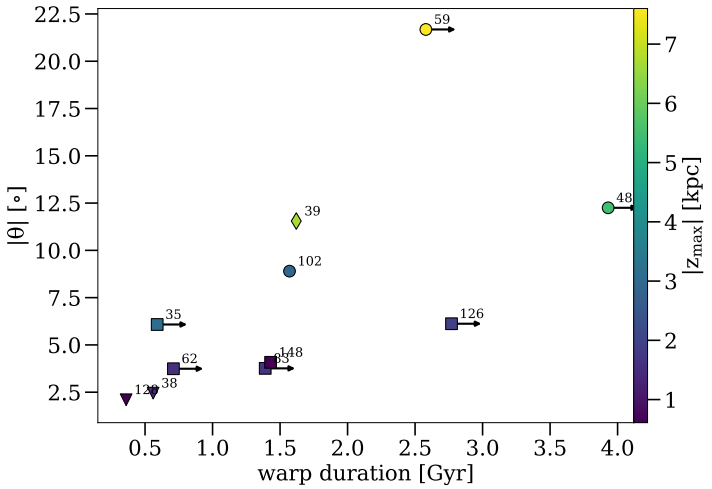


Figure 4.5: Maximum warp angle as a function of the duration of the warp, colour-coded by the maximum height over the galactic plane. The shape of points represents the origin of the warp: triangles are internally-driven, squares are satellite interactions, diamonds are stellar accretion from inclined orbits, and circles are stellar rings being born in off-plane configurations.

with a very strong warp when compared with observational studies. Such strong warps are rarely observed, but they exist (see e.g., Sánchez-Saavedra et al., 2003), and are not rare in simulations (Kim et al., 2014).

In Fig. 4.5, I show the warp angle as a function of warp duration (the symbols indicate the origin of the warp, and the colour code the maximum height in kpc reached by the warp). For warps that are ongoing at $z = 0$ (indicated by an arrow), the measured duration is only a lower limit, but I still find a general correlations between warp amplitude and duration. I find that internally-driven warps have the shortest duration, around 0.5 Gyr. Their maximum amplitudes are also the smallest within the sample, not reaching above $\sim 2.5°$ or 1.5 kpc. By contrast, warps driven by gravitational interactions between satellites and their host galaxies (flybys or mergers) can last longer than 1 Gyr, in agreement with Shen & Sellwood (2006). The longest warp within this category is found in **g126**: as described earlier, this is a special case where the warp is reinforced by the creation of an inclined stellar ring. Compared to internally-driven warps, warps created by interactions reach slightly higher angles above the mid-plane, up to $\sim 7°$ (corresponding to maximum heights below 3 kpc). This general trend was also observed by Schwarzkopf & Dettmar (2001). Finally, warps produced by off-plane stellar rings or by off-plane stellar accretion have the longest duration within the sample, lasting

several Gyr. These warps also reach the largest heights above the galactic plane.

## 4.5 Monitoring disc heating during warps

In this section, I examine the evolution of the vertical density structure of discs during warps, from 0.5 Gyr before a warp starts to 0.5 Gyr after it ends (for the warps that end before $z = 0$). By doing this, I try to minimize the effect that other processes like mergers may have on the disc, and limit our analysis to the warp only. I first study whether the vertical density structure of the warped region is distinct from the one in the unwarped inner part of the disc. I then follow the time evolution of both the thickness of the disc and the vertical velocity dispersion to understand if the warped region of the disc experiences more vertical heating than the inner disc.

### 4.5.1 Inner-outer disc transition

I examine the evolution of the scale-heights of the thin disc, thick disc, and mono-age populations during different epochs: before the warp starts, during the warp, and (when possible) after the warp has ended. I study whether scale-heights behave differently within the warped region of the disc. I find two main cases within our galaxy sample, which are represented in Figs. 4.6 and 4.7 respectively, and explained below: in the first case, the scale-heights never behave very differently within the warped region of the disc. Therefore, in terms of the scale-heights, there is no transition between the non-warped and the warped regions of the disc. In the second case, during the warp, the scale-heights behave very differently within the warped region of the disc. Hence, there is a transition between the non-warped and the warped regions of the disc in terms of the vertical stellar density.

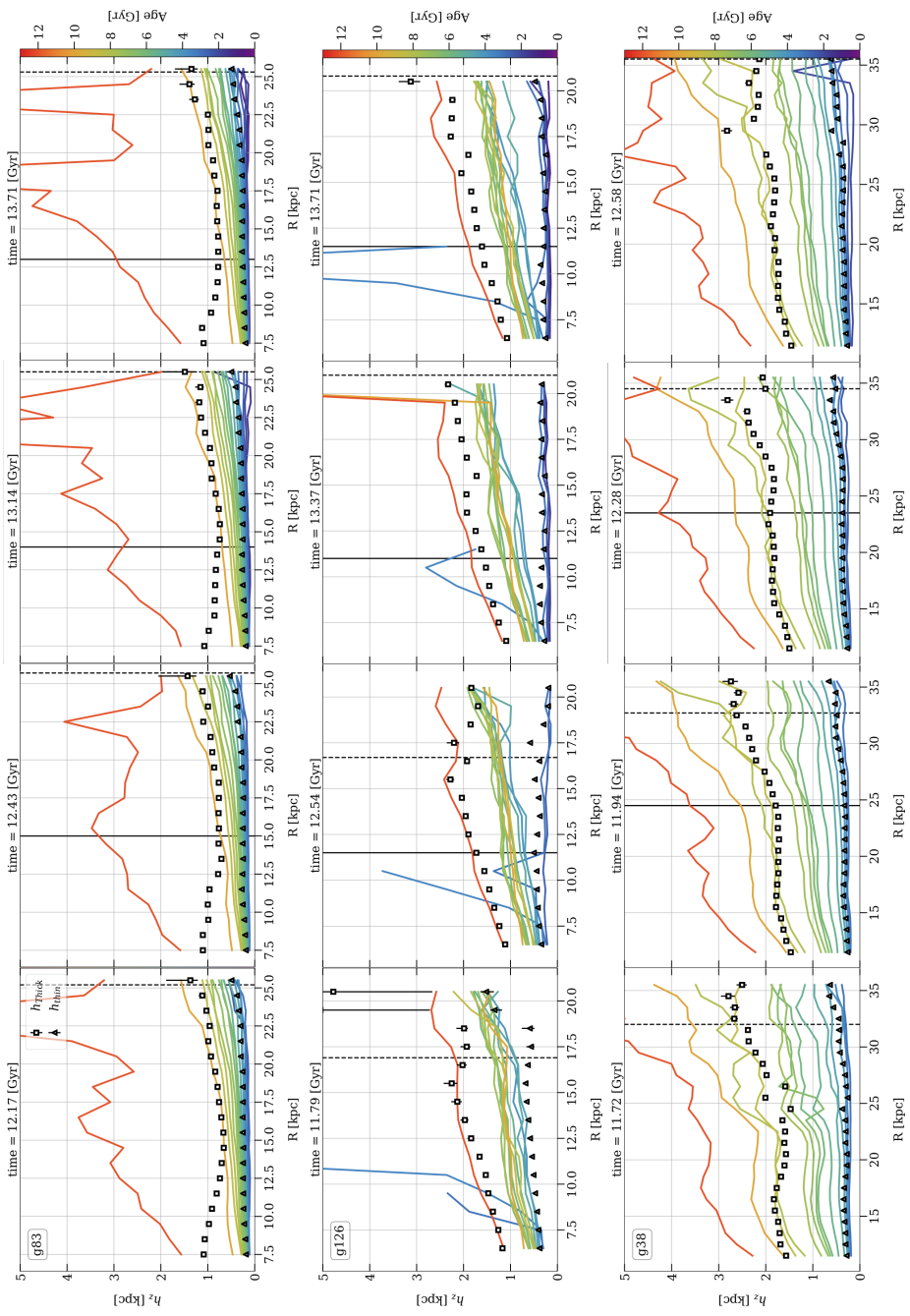


Figure 4.6: Values of the scale-height against radius for the thin disc (triangles), thick disc (squares), and mono-age populations (solid lines) colour-coded by age. Mono-age populations from 9 to 11 Gyr and from 11 to 13 Gyr are binned together, every other mono-age population spans 0.5 Gyr. The x-axis spans from the beginning of the disc to $R_{25}$ at the cosmological time of the rightmost panel. The solid vertical black line represents the onset radius of the galactic warp, while the dashed vertical black line marks the value of $R_{25}$ at the time of the snapshot indicated above each panel. The top row represents galaxy **g83**, where the warps starts at 12.3 Gyr and is still in place by $z = 0$. The thick disc stays flat all along. The middle row represents galaxy **g126**, whose warps starts at 12.1 Gyr and is still active by $z = 0$. Both the flaring of the thick disc and MAPs are preserved throughout the warp. The bottom row represents galaxy **g38**, whose warp starts at 11.9 Gyr and fades away at 12.5 Gyr. The scale-heights of both thin and thick disc, as well as MAPs do not experience major changes during the warp.

**The vertical density structure is preserved at all times**

In this category, I find galaxies whose warps are either internally-driven or created by an interaction with a satellite. In those cases, the scale-heights of mono-age populations and of the thin and thick disc behave similarly in the inner non-warped region and in the outer warped region of the disc. For instance, in case of a flat thick disc, *top row* of Fig. 4.6, the scale-heights of the thick disc are similar in the inner and outer disc. In case of a flared thick disc, *middle row* and *bottom row* of Fig. 4.6, the scale-heights continuously increase as a function of radius (both for the global thick disc and most of the mono-age populations). The scale-heights sometimes flatten slightly in the very outer disc (outside of $R_{25}$, marked by the dashed black line in Fig. 4.6), but otherwise they behave similarly in the warped and unwarped regions. For the case of **g126** in particular, the flaring displayed in the leftmost panel of the *middle row* is the product of the merger at $t \sim 10.5$ Gyr. Yet, no increase of flaring is observed during the warp's lifetime. In fact, the rest of the panels of the *middle row* show new generations of stars being born in cold and flat configurations also within the warp. Lastly, the *bottom row* of Fig. 4.6 is also showing that, after the warp is gone, the vertical structure of the disc does not keep a memory of the warp.

It is interesting to notice that warps in this category are created when stellar particles already living in the disc before the warp get bent. The fact that the geometrical thin/thick disc structure holds without being strongly affected by the warp means that all the stellar particles are shifted uniformly for a given radius and azimuthal region of the disc.

**The vertical stellar density is temporarily altered during the warp**

In galaxies whose warp is produced by stellar material either being accreted or born in off-plane configurations, the vertical stellar density temporarily changes from the inner and non-warped disc to the outer and warped disc. In particular, during the warp, the warped region of the disc is not well described by a double $\mathrm{sech}^2$ density profile, which in practice leads to large uncertainties on the thick disc scale-heights in the warped

region (as shown in Fig. 4.7).

An example of this category is **g39**, which is illustrated in the *top row* of Fig. 4.7. After a merger at t~7.5 Gyr, the vertical density within the disc settles down except close to the disc's edge $R_{25}$ (see leftmost panel). Later, the warp forms when material spread by the merger is accreted. The amount of material being accreted is such that the stellar vertical density is not well described by a double sech$^2$ anymore, hence the large uncertainties in the thick disc's scale-heights within the warp (see two middle panels). After the warp is gone, the disc settles back into a double sech$^2$ structure (see rightmost panel).

A similar inner-outer disc transition is observed for galaxies which formed an outer ring structure off plane, like galaxy **g48** illustrated in the *bottom row* of Fig. 4.7. At t~9.7 Gyr, the disc beyond 14 kpc is poorly described by a double sech$^2$ (see leftmost panel). This is due to the aftermath of a merger at t~8 Gyr, which induced vertical perturbations (although not in the form of a warp). Yet, once the disc recovers from the merger, the double sech$^2$ structure starts to reappear. A warp then develops in the outer disc because of an interaction with another satellite, leading to the formation of an inclined stellar ring. In this region, the disc structure is altered asymmetrically by the high amount of stellar material at high z above or below the galactic plane (see two middle panels). However, once this material settles down within the disc, the double sech$^2$ reappears even before the warp is fully gone (see rightmost panel).

Regardless of the accreted/in-situ origin of the material, warps that fall into this category are created because of new material is added to the disc at large height, as opposed to those where stars in the disc get bent. Here, the double sech$^2$ structure is not preserved within the warp region, but it reappears after the off-plane material settles down within the disc. Therefore, once the warp is gone, the thin and thick disc structure is recovered, with no sign of where the warp's onset radius used to be.

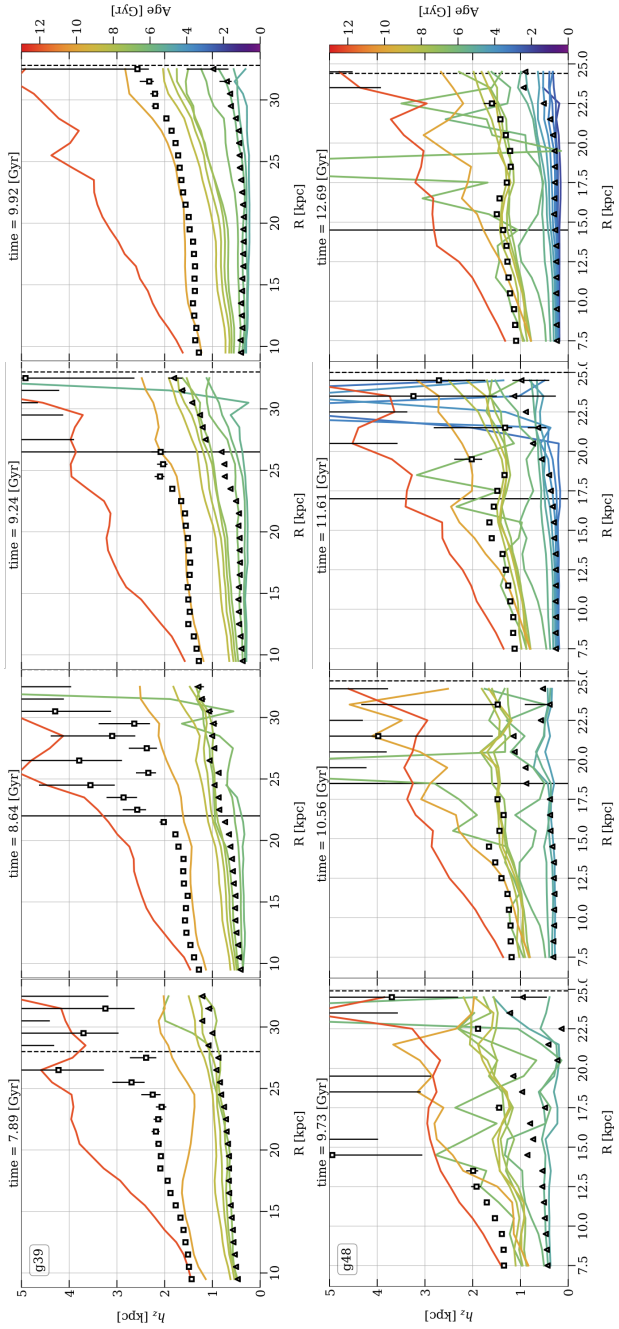


Figure 4.7: Similar to Fig 4.6 but for two galaxies whose disc's vertical density profile is altered during the warps. The top row represents galaxy **g39**, where the warp starts at 8 Gyr and ends at 9.7 Gyr. In the warped region (beyond the solid vertical line), the vertical density structure is no longer well described by a double sech$^2$, hence the large uncertainties in the thick disc's scale-heights. However, as the warp fades away, the global thin/thick disc structure is recovered throughout the disc and no sign of the past warp is seen. The bottom row represents galaxy **g48**, where the warp starts at 9.8 Gyr and is still present at $z = 0$. The same effect can be seen, with the thin and thick disc structure recovered for almost all radii even before the warp has finished.

### 4.5.2 Disc heating

In order to clarify whether disc heating or flaring take place during warps, I follow the time evolution of the dispersion of the vertical position and vertical velocity of the stellar particles in two radial bins: one in the inner and non-warped part of the disc, and the other in the outer and warped part of the disc. I monitor the evolution of these quantities only half a Gyr before and after the warp to minimize the effects of other disc heating agents.

On the top row of Fig. 4.8 I show the dispersion of the vertical position in a region within the inner disc (*top*) and outer disc (*bottom*). Clearly, the disc thickness does not change as a function of time for most galaxies, both in the inner and outer region of the discs. The few cases where there is a significant change are the galaxies for which warps last the longest. For these few galaxies, the disc actually becomes thinner with time, because of new generations of stars being born in a much colder configuration. This is seen both in the inner and outer disc.

A similar effect is observed on the bottom row of Fig. 4.8. The vertical velocity dispersion does not increase because of the warp (both in the inner and outer disc). In many cases, the vertical velocity dispersion does not change at all. For galaxies that I track over longer periods of time, I see $\sigma_{\mathrm{v_z}}$ decrease because of the formation of young stars in a cold configuration.

From this, I conclude that disc heating does not happen during warps, even in the outer regions. This can be due to a few different reasons. First, in cases of warps triggered by interactions, I find that heating happens on faster timescales than warping: warps need a few dynamical timescales to emerge. This means that disc heating is finished before the warp starts. An example of this is galaxy **g126** in the *middle row* of Fig. 4.6: a merger happens at t$\sim$10.5 Gyr and creates flaring before the warp starts at t$\sim$12.1 Gyr (see leftmost panel of *middle row* of Fig. 4.6). Then, the warp develops and no further heating or flaring is observed. The effect can also be seen in Fig. 4.9, where both $\sigma_z$ and $\sigma_{v_z}$ increase noticeably during the merger, but this sudden increase stops before the warp formation. After warp formation, $\sigma_z$ and $\sigma_{v_z}$ barely increase or adopt a smoother

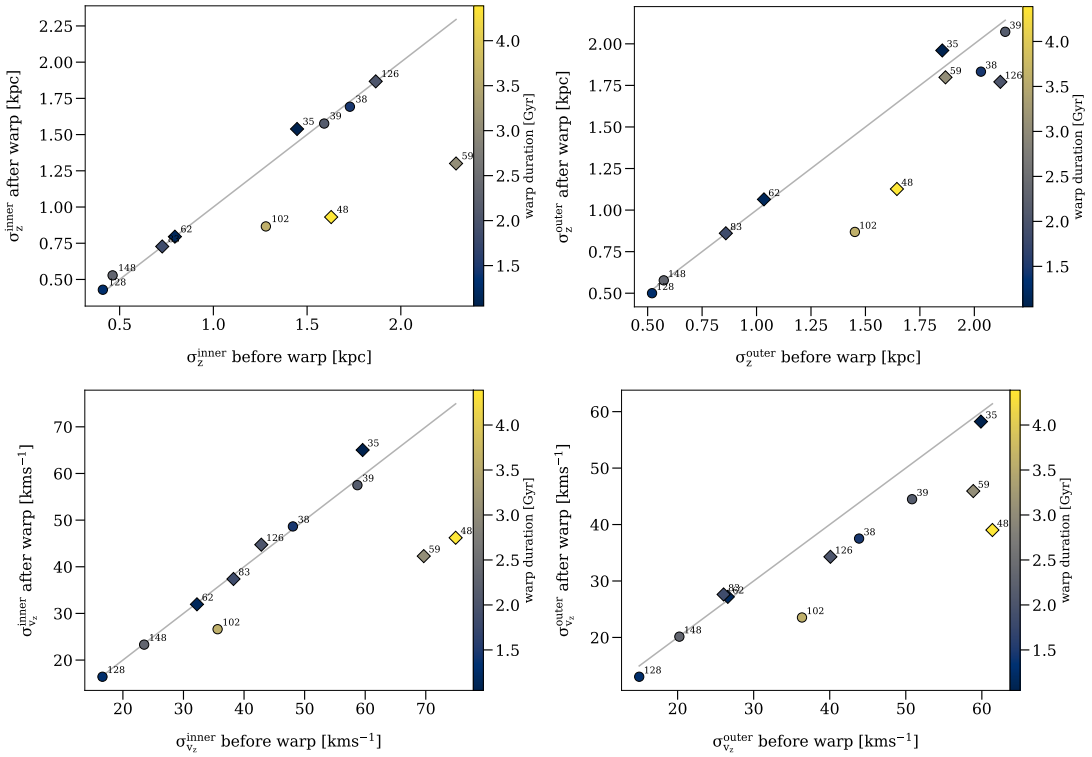


Figure 4.8: *Top row:* standard deviation of the vertical position of the stellar particles before and after the warp within a region in the non-warped part of the disc (left), and outer and warped part of the disc (right). Points are colour-coded by the duration of the warp, and the shape represents whether the warp is finished (circles) or not (diamonds). *Bottom row*: equivalent of the top row for the vertical velocity dispersion. These plots show that there is no disc heating during the warp. For most galaxies, both the disc thickness and the vertical velocity dispersion are nearly constant as a function of time, while they decrease for warps with the longest duration due to new generations of stars being born in colder configurations during the warp's lifetime.

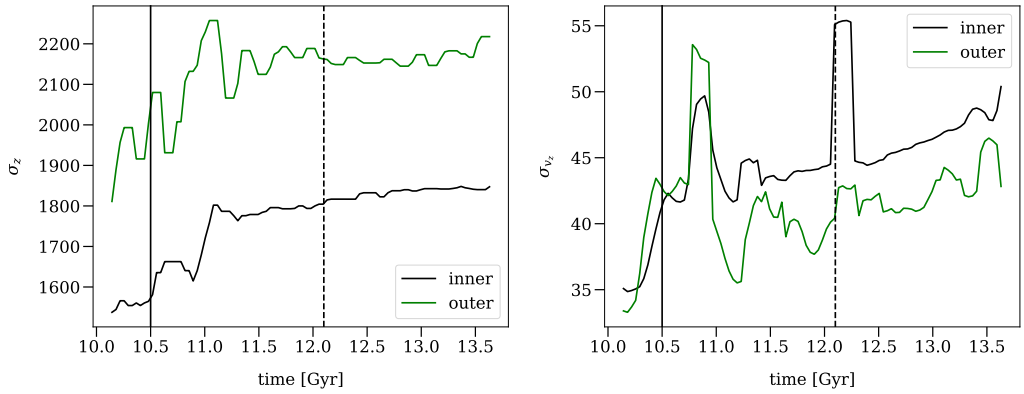


Figure 4.9: For galaxy **g126**, evolution over time of the vertical position dispersion on the left panel and vertical velocity dispersion on the right panel, for stellar particles living in the disc. The black line represents the inner disc and the green line represents the outer disc, being the stellar particles selected in a similar manner as in Fig. 4.8. The vertical solid black line indicates the time of the merger while the vertical dotted black line indicates the time of warp formation.

increase trend. The trend seen in Fig. 4.9 correspond only to stars being born before the merger. So, if all stars were included, the trends observed would be even shallower, since the youngest stars born after the merger would have colder configurations and would bring $\sigma_z$ and $\sigma_{v_z}$ down. Second, not all galaxy-satellite interactions may cause vertical disc heating as pointed out by Velázquez & White (1999). Finally, while Khoperskov et al. (2010) and Griv (2011) suggested that bending waves can cause vertical disc heating, I find that warps are not a source of vertical heating in our simulations. Thus, warps only correspond to a global shift of the vertical structure of the disc or to an asymmetrical alteration of the vertical density, and when warps disappear discs recover their initial vertical structure.

## 4.6 Conclusions

In this Chapter, I analysed the connection between disc heating and warping using the simulations from Martig et al. (2012). I chose a subsample of 6 simulated galaxies with warps present at $z = 0$, as well as 5 other galaxies which underwent warps in the past. I computed scale-heights for mono-age populations as well as for thin and thick discs after correcting for the warps' vertical shift as explained in Sec. 4.2 and represented in

Fig. 4.3.

I found that for warps either internally driven or created by interactions, the scale-heights of the geometrical thin and thick disc, and of mono-age populations, are not affected by the warp: whether the thin and thick disc are flat or flared, the trend is always preserved all the way through the disc. In other words, for warps formed when the stars are shifted off-plane, the warp seems to affect uniformly all the stellar disc, and does not alter the structure of the vertical stellar density. I also noted that these warps tend to have shorter lifetimes and reach lower heights above/below the galactic plane.

On the other hand, galaxies whose warps are created by the accretion or the formation of stars in off-plane configurations show a vertical stellar density structure that temporarily changes between the inner and non-warped region of the disc and the warped one. While the non-warped region keeps having a double $\mathrm{sech}^2$ density profile, this is altered asymmetrically in the warped region due to the off plane material. However, once the warp fades away, the double $\mathrm{sech}^2$ is recovered and the trends of the thin/thick disc scale-heights as well as of mono-age populations are coherent throughout the disc, without a signature of a pre-existing warp. Additionally, these warps tend to last longer and reach larger heights above/below the galactic plane than the others.

Finally, I found that for all warps the disc thickness and the vertical velocity dispersion do not increase during the warp, indicating that there is no disc heating happening during warps. This can be either because the disc heating induced by the warp agent takes place before warp formation, or because neither the warp agent nor the warp itself are a source of disc heating. Also, when warps last for a long time, the new generations of stars born during the warp usually have colder configurations than older stars, and act as disc cooling agents.

These results suggest that depending on their origin, warps may or may not alter the vertical stellar structure of the stellar disc. Nevertheless, once warps disappear, they do not leave any imprint in the stellar populations living in the disc. Therefore, in terms of stellar vertical density structure and vertical heating in the disc, galaxies do not hold any

memory of warps they might have experienced in the past. Given the relatively small size of our galaxy sample, further work using larger samples from different simulations would greatly help confirm these results.

# Chapter 5

# Conclusions and Future Work

*"Science is not only compatible with spirituality; it is a profound source of spirituality."*

– Carl Sagan

## 5.1 Summary and conclusions

In this thesis, I have analysed the vertical stellar density structure of disc galaxies in cosmological zoom-in simulations. I have studied how, depending on the merger history, the vertical stellar density in discs give rise to different types of thin and thick discs, and how some of their features are also linked to the host's evolutionary history. In addition, I have studied how warps, depending on their origin, influence the vertical stellar density of the disc and what kind of imprints warps may or not leave. Therefore, I have used different galaxy disc features related to the vertical stellar density to perform galactic archaeology. The results are summarised below.

### 5.1.1 Flaring of thick discs of galaxies

Minchev et al. (2015) showed that flat thick disc can be made of different Mono-Age Populations (MAPs) with different levels of flaring and radial surface density distribution, indicating that thick disc are indeed complex structures. I expanded the analysis of Minchev et al. (2015) and analysed in depth 27 simulated MW-like galaxies from Martig et al. (2012) to connect the different flaring configurations of MAPs with the flaring of the global thick disc. I also connected this with the galaxy's merger history, the age structure, and with whether the thin and thick discs are two different components.

Flat thick discs form when MAPs barely flare or when, due to inside-out formation, the flared MAPs do not carry a lot of surface density at the flaring radii compared to younger, less flared MAPs. Galaxies with flat thick discs have some common features: they all have radial age gradients, and the thin and thick discs form a continuous structure. This group of galaxies have quiescent merger histories in the past 9 Gyr. This is in agreement with what we know about the MW, including the discovery of the last major building block of the Galaxy, Gaia-Enceladus, merging at early cosmological times.

On the other hand, flared thick discs form when MAPs carry a significant amount of surface density where they flare. The flaring of the global thick disc can be driven by a sequence of different MAPs at different radii, or if a group of MAPs share the same scale-heights. If the last case happens, then a bimodal structure is created and thin and thick discs are distinct components in terms of the stellar populations inhabiting them. This effect is directly related to the merger history as Martig et al. (2014a) pointed out using a smaller sample. Flared thick discs are more diverse than their flat counterparts in terms of age radial profiles, although a high fraction of them show small or flat age radial profiles in their thick disc. This is especially the case for galaxies that underwent mergers with high mass ratios, which also show mild or strong bimodality in their thin and thick discs.

These results help us understand the emerging picture where thick discs are more varied

and complex than previously thought. Furthermore, because of the recent increase in the amount and quality of data for both the MW and nearby galaxies, it is now possible to compare the MW to its neighbours. This analysis provides the framework to interpret the differences we see between the MW and other galaxies, and to understand some of the specific features observed in the MW.

### 5.1.2 Vertical density structure in galactic warps

Many of the warp-creating mechanisms (e.g., Shen & Sellwood, 2006) are often associated with disc heating and flaring (Pinna et al., 2019b). However, heating and warping do not necessarily always happen together. In the case of satellite-galaxy interactions, whether the disc tilts or gets heated might depend on different properties of the satellite, including its orbital properties (Velázquez & White, 1999). Hence, I explored the connection between warping and disc heating/flaring. I studied how much disc vertical heating happens during warps, and how warps affect the vertical stellar density structure of galactic discs.

I find that for warps made of pre-existing stellar particles shifted off-plane, the scale-heights do not change within the disc's warped region: discs bend rigidly. For warps made of off-plane new stellar material (either born in-situ or accreted), the warped region of the disc is temporally not well described by a double $\text{sech}^2$ density profile. Yet, once the warp is gone, the thin and thick disc structure is recovered, with their scale-heights following the same trends as in the region that was never warped. Finally, I find that the overall thickness and vertical velocity dispersion do not increase during a warp, regardless of the warp's origin. This holds even for warps triggered by interactions with satellites, which cause disc heating but before the warp forms.

Therefore, these results suggest that the vertical structure of galaxies does not hold any memory of past warps. Also, this study is suggesting that the vertical density profiles in warps (and whether they are well described by double $\text{sech}^2$ or not) can be linked to the origin of the warp, and that this could potentially be used to constrain the origin of warps in nearby galaxies and in the MW.

## 5.2 Future work

### 5.2.1 Characterising the vertical stellar distribution in the disc outskirts

The outskirts of the MW are known to be out of equilibrium. This could be due to different factors added together, like the actions of the bar and spiral arms (Antoja et al., 2018; Bland-Hawthorn et al., 2019), and the interaction with the Sagittarius dwarf galaxy and the Magellanic Clouds (Binney, 2019; Laporte et al., 2019; Poggio et al., 2020). Evidence of the messiness of the MW's outskirts is further supported by the recent analysis made by Antoja et al. (2021) using Gaia EDR3, where complex velocity patterns and asymmetries have been found at large radii.

Gaia DR3 will have one of the most complete mappings of the outskirts of the MW which, combined with new spectroscopic surveys like 4MOST or WEAVE, makes the perfect time to explore and study the Galactic disc at large radii.

Although flaring in the inner disc ($\leq$11 kpc) is highly disfavoured (Mateu & Katherina Vivas, 2018), whether the outer geometrical thick disc of the Galaxy flares and the amplitude of the flaring is still a matter of debate (e.g., Amôres et al., 2017; López-Corredoira et al., 2018). As mentioned in Chapter 3, I established a connection between the flaring of the geometrical thick disc and the flaring of the MAPs in the disc. Thus, since upcoming spectroscopic surveys like WEAVE or 4MOST will provide great-quality data on chemical abundances of the MW's disc stars, the study of the flaring of different mono-abundance stellar populations could be done, establishing the connection between the stellar density of these populations, their scale-height, and the scale-height of the Galactic geometrical thick disc (as done in Chapter 3). The radial density profiles of mono-abundance populations are directly connected to the star formation history and the merger history of the galaxy. Therefore, these results could be supported with simulations to derive conclusions on how external interactions and the star formation history of the Galaxy shaped the current geometrical outer thick disc.

In addition to the potential flaring in the outer disc, it is well known that a warp exists at large radii (Romero-Gómez et al., 2019). Because of the warp, it is not clear if the vertical density of the disc is still well represented by a geometrical thin and thick disc, in other words, a double $\text{sech}^2$. In Chapter 4, I explain that whether a double $\text{sech}^2$ is preserved or not within warps depends on the warp's origin. Therefore, the vertical stellar density at large radii could be studied in order to see if the thin-thick structure is altered, possibly shedding some light into the nature of the origin of the Galactic warp. Also, this would enable to disentangle flaring and warping, and obtain more robust estimations of the mono-abundance populations' and thick disc's scale-heights.

On top of positions, velocities, and even colours, Gaia DR3 will provide spectra with the Radial Velocity Spectrometer (RVS) for a subsample of stars as faint as magnitudes $G \sim 16$ (Recio-Blanco et al., 2016). Although the signal-to-noise ratio will not be enough to extract information about chemical abundances for all the stars, WEAVE and/or 4MOST will complement Gaia such that almost all stars with magnitudes between $12 < G < 16$ will have spectra with enough signal-to-noise ratio to derive some of their chemical abundances. This information, combined with machine learning techniques, could be used to unveil the accreted stellar population of the disc, and subsequently discern how much the accreted stars of the MW are shaping both the flaring and the warp of the Galactic disc at large radii.

By the end of this project, a comprehensive view of the geometrical thick disc of the MW at large radii would be obtained, including its flaring and warping. The origins of these two features would be explored by quantifying the contribution of the accreted stars in the outer disc.

### 5.2.2 Mapping the age structure in the disc of the Milky Way

For stars within 3 kpc from the sun, the signal-to-noise ratio will be good enough to determine stellar ages thanks to the WEAVE HR survey. For larger distances, ages can be determined through more indirect methods from the WEAVE LR survey (although with lower precision), and it will look further out in the outer disc, $R_g > 14$ kpc.

Similarly, 4MOST Milky Way Disc and Bulge High-Resolution Survey (4MIDABLE-HR) and 4MOST Milky Way Disc and Bulge Low-Resolution Survey (4MIDABLE-LR) will provide spectra with enough resolution to derive ages through more direct or indirect methods for similar distances. This could be used to improve and expand on the work by Martig et al. (2016) on the radial age gradient of the MW's disc. Besides a better characterization of the age distribution within 3 kpc from the sun, the radial age gradient for larger galactrocentric radii could be explored (even beyond $R_g \sim 14$ kpc). In Chapter 3, I linked the radial age gradient of a galaxy with the radial density distribution of their MAPs and their flaring within the galaxy's disc, which is also connected to the merger history of the galaxy itself. Therefore, by characterising the age distribution at each radius and height, I would put constraints on the outer Galactic disc's star formation history. Furthermore, it would be possible to connect the age structure of the Galactic geometrical thick disc with its flaring as in Chapter 3, since the flaring would have been already characterised from the previous project.

In addition, Ivan Minchev and collaborators developed a method to estimate the birth radius of a star given its metallicity and its age (Minchev et al., 2018). It would then be possible to constrain the amount of radial migration in the outer disc, which has great potential. For example, it would help understand how the MW's disc grew in the radial direction and how much of it was born in situ. Particularly, it could help understand the growth and evolution of the geometrical thick disc. For instance, on top of constraining how much accretion there is, I would quantify how much stars born in situ contribute to the MW's thick disc mass budget versus stars migrating from inward/outward parts of the disc. In a possible collaboration with Ivan Minchev, up-to-date chemical-dynamical models could be produced to support and better interpret the data (as has been previously done (e.g., Minchev et al., 2013)). These results could also allow for testing disc thickening models.

Furthermore, radial migration is an important process for the evolution of our Galaxy, especially connected/enhanced by mergers (Hayden et al., 2018). Hence, constraining the radial migration in the outer disc would help have a holistic picture of the evolution of the MW, especially its interactions with neighbouring objects (e.g. the fact that the

Sagittarius dwarf galaxy may have influenced the star formation history of the disc (Ruiz-Lara et al., 2020)).

### 5.2.3 Accretion and radial migration from simulations

The results obtained above would be compared to simulations of MW-like galaxies, both from the sample from Martig et al. (2012) and/or the publicly available simulations. For instance, I would study how the accreted stellar populations distribute in the disc depending on the mergers' orbital parameters and shed light on the accretion events of the MW. Also, the most analogous galaxies to the MW can be compared with the rest of the sample, describing what they have in common and what makes them different from the MW. A similar exercise can be done by quantifying the amount of stellar migration in the stellar disc. Therefore, these comparisons would not only support the results from the observations of the MW, but would also help understand how common the MW is, putting the MW in the context of its neighbouring galaxies.

### 5.2.4 Connecting the density profile of the MW with the age radial profile of the disc

Studies like Ruiz-Lara et al. (2017) addressed the topic of density profiles in the outskirts of galaxies from a theoretical perspective. Yet, more work using cosmological simulations needs to be done to connect the shape of density profiles to other features of galaxies, like their merger history. The redistribution of stars in the radial direction during the galaxy's life is connected to the density profile type in the outskirts as well as the radial age gradient of the disc (e.g. the U-shape profiles found in external galaxies). In the simulations from Martig et al. (2012), a diversity of age radial profiles has been found. In Chapter 3, this diversity has been explained in terms of the spatial distribution of the different stellar populations and it has been linked to the merger history of the galaxies. Among this diversity, there are simulated galaxies that present an age radial gradient with a similar shape to the one found in the MW by Martig et al. (2016), and

those properties linked with also resemble the MW. By comparing this structure with that of the simulations, I would be able to find analogues within the sample and look into the similarities of these analogues to extrapolate the properties of the MW.

First, both the radial density profile and the shape of the age radial profile of the MW at large radii would be studied. Then, different aspects of the simulated galaxy's outskirts would be studied in detail, like the shape of the density profile (e.g. up-bending, down-bending) and the amount of radial migration. Likewise, I would look into the redistribution of stars within the disc across cosmic time and how this affected both the density profile and the age radial profile. I would then establish connections between the age radial profiles and the radial density profiles. Then, comparisons between the MW and simulations would be made to find MW analogues regarding both the radial density profile and the age radial profile of the disc at large radii. Once the MW analogues are found, I would be able to gain insights into how the redistribution of stars affects both the stellar density profile and the radial age profile, and find what all the MW analogues have in common and set them apart from other galaxies in the simulations.

By the end of this work, I would have characterised the density profile and the age radial profile of the MW. Moreover, I would have compared both the density profile and the age radial profile in the outskirts of the MW with that of the simulated galaxies. With this comparison, I would gain insights into how the redistribution of stars within the disc played a role in making the features we observe with Gaia DR3.

## 5.3 Concluding remarks

The vertical stellar density is the key to explaining many properties of galactic discs. It is also heavily influenced by various processes in galaxy evolution. In this thesis, I have connected the merger history of galaxies with some of these properties defined by the vertical stellar density. I have also connected warps with the vertical stellar density, analysing how it is affected during and after warps depending on the warp's origin.

These findings can be tested both for the Milky Way and its neighbouring galaxies with on-going and up-coming spectroscopic surveys, enabling two things: first, performing galactic archaeology and unveil information from the past of these galaxies; second, constraining what Milky Way analogues are and place the Milky Way in the context of its neighbouring galaxies, shedding light into the question of whether our Galaxy is common or uncommon in the universe.

# Bibliography

Abadi M. G., Navarro J. F., Steinmetz M., Eke V. R., 2003, The Astrophysical Journal, 597, 21

Abraham R. G., Merrifield M. R., Ellis R. S., Tanvir N. R., Brinchmann J., 1999, Monthly Notices of the Royal Astronomical Society, 308, 569

Adibekyan V. Z., Sousa S. G., Santos N. C., Delgado Mena E., González Hernández J. I., Israelian G., Mayor M., Khachatryan G., 2012, Astronomy and Astrophysics, 545, A32

Aguerri J. A., Méndez-Abreu J., Corsini E. M., 2009, Astronomy & Astrophysics, 495, 491

Amôres E. B., Robin A. C., Reylé C., 2017, Astronomy and Astrophysics, 602, 67

An D., et al., 2013, The Astrophysical Journal, 763, 65

Ann H. B., Park J. C., 2006, New Astronomy, 11, 293

Antoja T., et al., 2018, Nature, 561, 360

Antoja T., et al., 2021, Astronomy and Astrophysics, 649, 115

Athanassoula E., 2003, Monthly Notices of the Royal Astronomical Society, 341, 1179

Athanassoula E., Rodionov S. A., Peschken N., Lambert J. C., 2016, The Astrophysical Journal, 821, 90

Aumer M., Binney J. J., 2009, Monthly Notices of the Royal Astronomical Society, 397, 1286

Aumer M., White S. D., 2013, Monthly Notices of the Royal Astronomical Society, 428, 1055

Aumer M., Binney J., Schönrich R., 2017, Monthly Notices of the Royal Astronomical Society, 470, 3685

Barazza F. D., Jogee S., Marinova I., 2008, The Astrophysical Journal, 675, 1194

Barber C., Starkenburg E., Navarro J. F., McConnachie A. W., Fattahi A., 2013, Monthly Notices of the Royal Astronomical Society, 437, 959

Barden M., et al., 2005, The Astrophysical Journal, 635, 959

Bartko H., et al., 2009, Astrophysical Journal, 697, 1741

Battaner E., Jiménez-Vicente J., 1998, Astronomy and Astrophysics, 332, 809

Battaner E., Florido E., Sanchez-Saavedra M., 1990, Astronomy and astrophysics, 236, 1

Baugh C. M., 2006, Reports on Progress in Physics, 69, 3101

Baugh C. M., Cole S., Frenk C. S., 1996, Monthly Notices of the Royal Astronomical Society, 283, 1361

Baugh C. M., Benson A. J., Cole S., Frenk C. S., Lacey C. G., 1999, Monthly Notices of the Royal Astronomical Society, 305, L21

Belokurov V., 2013, New Astronomy Reviews, 57, 100

Bender R., Burstein D., Faber S. M., 1993, ApJ, 411, 153

Bennett M., Bovy J., 2019, Monthly Notices of the Royal Astronomical Society, 482, 1417

Bensby T., Feltzing S., Lundström I., 2003, Astronomy and Astrophysics, 410, 527

Bensby T., Feltzing S., Lundström I., Ilyin I., 2005, Astronomy and Astrophysics, 433, 185

Bensby T., Feltzing S., Oey M. S., 2014, Astronomy and Astrophysics, 562, A71

Benson A. J., Bower R., 2011, Monthly Notices of the Royal Astronomical Society, 410, 2653

Bigiel F., Leroy A., Walter F., Brinks E., De Blok W. J., Madore B., Thornley M. D., 2008, Astronomical Journal, 136, 2846

Binney J., 1977, The Astrophysical Journal, 215, 483

Binney J., 2019, Proceedings of the International Astronomical Union, 14, 101

Binney J., Gerhard O. E., Stark A. A., Bally J., Uchida K. I., 1991, Monthly Notices of the Royal Astronomical Society, 252, 210

Birnboim Y., Dekel A., 2003, Monthly Notices of the Royal Astronomical Society, 345, 349

Bizyaev D. V., Kautsch S. J., Mosenkov A. V., Reshetnikov V. P., Sotnikova N. Y., Yablokova N. V., Hillyer R. W., 2014, Astrophysical Journal, 787, 24

Bland-Hawthorn J., Gerhard O., 2016a, Annual Review of Astronomy and Astrophysics, 54, 529

Bland-Hawthorn J., Gerhard O., 2016b, Annual Review of Astronomy and Astrophysics, 54, 529

Bland-Hawthorn J., et al., 2019, Monthly Notices of the Royal Astronomical Society, 486, 1167

Blanton M. R., Eisenstein D., Hogg D. W., Schlegel D. J., Brinkmann J., 2005, The Astrophysical Journal, 629, 143

Blumenthal G. R., Faber S. M., Primack J. R., Rees M. J., 1984, ] 10.1038/311517a0, 311, 517

Bonaca A., Conroy C., Wetzel A., Hopkins P. F., Kereš D., 2017, The Astrophysical Journal, 845, 101

Bosma A., 1981, The Astronomical Journal, 86, 1825

Bournaud F., 2015

Bournaud F., Combes F., 2002, Astronomy and Astrophysics, 392, 83

Bournaud F., Combes F., 2003, Astronomy and Astrophysics, 401, 817

Bournaud F., Jog J., Combes F., 2007, Astronomy & Astrophysics, 476, 1179

Bournaud F., et al., 2008, Astronomy & Astrophysics, 486, 741

Bournaud F., Elmegreen B. G., Martig M., 2009, Astrophysical Journal, 707, L1

Bovy J., Rix H. W., Hogg D. W., 2012a, Astrophysical Journal, 751, 131

Bovy J., Rix H. W., Liu C., Hogg D. W., Beers T. C., Lee Y. S., 2012b, Astrophysical Journal, 753, 148

Bower R. G., Benson A. J., Malbon R., Helly J. C., Frenk C. S., Baugh C. M., Cole S., Lacey C. G., 2006, Monthly Notices of the Royal Astronomical Society, 370, 645

Bromm V., Loeb A., 2003, Nature 2003 425:6960, 425, 812

Brook C. B., Kawata D., Gibson B. K., Freeman K. C., 2004, The Astrophysical Journal, 612, 894

Brook C. B., Gibson B. K., Martel H., Kawata D., 2005, The Astrophysical Journal, 630, 298

Burkert A., 1995, The Astrophysical Journal, 447, L25

Burstein D., 1979, The Astrophysical Journal, 234, 829

Busha M. T., Marshall P. J., Wechsler R. H., Klypin A., Primack J., 2011, Astrophysical Journal, 743, 40

Callingham T. M., et al., 2019, Monthly Notices of the Royal Astronomical Society, 484, 5453

Carlberg R. G., Oronto T., And O., Freedman W. L., Campanas L., 1985, ApJ, 298, 486

Carollo C. M., Carollo Marcella C., 1999, ApJ, 523, 566

Carollo D., et al., 2008, Nature, 451, 216

Catalán-Torrecilla C., et al., 2017, The Astrophysical Journal, 848, 87

Cen R., Miralda-Escude J., Ostriker J. P., Rauch M., 1994, The Astrophysical Journal, 437, L9

Ceverino D., Dekel A., Bournaud F., 2010, Monthly Notices of the Royal Astronomical Society, 404, 2151

Ceverino D., Dekel A., Mandelker N., Bournaud F., Burkert A., Genzel R., Primack J., 2012, Monthly Notices of the Royal Astronomical Society, 420, 3490

Chen X., Wang S., Deng L., de Grijs R., Liu C., Tian H., 2019, Nature Astronomy, 3, 320

Cheng X., et al., 2020, The Astrophysical Journal, 905, 49

Chequers M. H., Widrow L. M., 2017, Monthly Notices of the Royal Astronomical Society, 472, 2751

Chequers M. H., Widrow L. M., Darling K., 2018, Monthly Notices of the Royal Astronomical Society, 480, 4244

Chiappini C., Matteucci F., Meynet G., 2003, Astronomy and Astrophysics, 410, 257

Clarkson W., et al., 2008, The Astrophysical Journal, 684, 1110

Cole S., Lacey C. G., Baugh C. M., Frenk C. S., 2000, Monthly Notices of the Royal Astronomical Society, 319, 168

Cole S., et al., 2005, Monthly Notices of the Royal Astronomical Society, 362, 505

Comerón S., et al., 2011, Astrophysical Journal, 741, 28

Comerón S., et al., 2012, Astrophysical Journal, 759, 98

Comerón S., Elmegreen B. G., Salo H., Laurikainen E., Holwerda B. W., Knapen J. H., 2014, Astronomy and Astrophysics, 571, 58

Comerón S., Salo H., Janz J., Laurikainen E., Yoachim P., 2015, A&A, 584, 34

Comerón S., Salo H., Peletier R. F., Mentz J., 2016, A&A, 593, 6

Comerón S., Salo H., Knapen J. H., 2018, Astronomy and Astrophysics, 610, 5

Cook B. A., Conroy C., Pillepich A., Rodriguez-Gomez V., Hernquist L., 2016, The Astrophysical Journal, 833, 158

Courteau S., de Jong R. S., Broeils A. H., 1995, ApJL, 457, L73

Courteau S., Dutton A. A., van den Bosch F. C., MacArthur L. A., Dekel A., McIntosh D. H., Dale D. A., 2007, The Astrophysical Journal, 671, 203

Croft R. A. C., Weinberg D. H., Bolte M., Burles S., Hernquist L., Katz N., Kirkman D., Tytler D., 2002, The Astrophysical Journal, 581, 20

Daddi E., et al., 2005, The Astrophysical Journal, 626, 680

Daddi E., et al., 2007, The Astrophysical Journal, 670, 156

Dalcanton J. J., Bernstein R. A., 2002, The Astronomical Journal, 124, 1328

Davis M., Efstathiou G., Frenk C. S., White S. D. M., 1985, ] 10.1086/163168, 292, 371

De Grijs R., Peletier R. F., 1997, Astronomy and Astrophysics, 320, 21

De Jong J. T., Yanny B., Rix H. W., Dolphin A. E., Martin N. F., Beers T. C., 2010, Astrophysical Journal, 714, 663

De Simone R. S., Wu X., Tremaine S., 2004, Monthly Notices of the Royal Astronomical Society, 350, 627

Deason A. J., Belokurov V., Koposov S. E., Lancaster L., 2018, The Astrophysical Journal, 862, L1

Debattista V. P., Sellwood J. A., 1999, The Astrophysical Journal, 513, L107

Deeley S., et al., 2017, Monthly Notices of the Royal Astronomical Society, 467, 3934

Dekel A., Birnboim Y., 2006, Monthly Notices of the Royal Astronomical Society, 368, 2

Dekel A., et al., 2009, Nature, 457, 451

Di Matteo P., Lehnert M. D., Qu Y., Van Driel W., 2011, Astronomy & Astrophysics, 525, L3

Donohoe-Keyes C. E., Martig M., James P. A., Kraljic K., 2019, Monthly Notices of the Royal Astronomical Society, 489, 4992

Dunkley J., et al., 2009, Astrophysical Journal, Supplement Series, 180, 306

Durbala A., Sulentic J. W., Buta R., Verdes-Montenegro L., 2008, Monthly Notices of the Royal Astronomical Society, 390, 881

Eadie G., Jurić M., 2019, The Astrophysical Journal, 875, 159

Eisenstein D. J., Hut P., 1998, The Astrophysical Journal, 498, 137

Elbaz D., et al., 2007, Astronomy and Astrophysics, 468, 33

Ellison S. L., Nair P., Patton D. R., Scudder J. M., Mendel J. T., Simard L., 2011, Monthly Notices of the Royal Astronomical Society, 416, 2182

Elmegreen B. G., Bournaud F., Elmegreen D. M., 2008, The Astrophysical Journal, 688, 67

Elmegreen B. G., Elmegreen D. M., Tompkins B., Jenks L. G., 2017, The Astrophysical Journal, 847, 14

Eskridge P. B., et al., 2000, The Astronomical Journal, 119, 536

Fakhouri O., Ma C. P., 2008, Monthly Notices of the Royal Astronomical Society, 386, 577

Falcón-Barroso J., et al., 2006, Monthly Notices of the Royal Astronomical Society, 369, 529

Fathi K., Allen M., Boch T., Hatziminaoglou E., Peletier R. F., 2010, Monthly Notices of the Royal Astronomical Society, 406, 1595

Faure C., Siebert A., Famaey B., 2014, Monthly Notices of the Royal Astronomical Society, 440, 2564

Ferguson H. C., Dickinson M., Williams R., 2000, Annual Review of Astronomy and Astrophysics, 38, 667

Ferguson H. C., et al., 2004, The Astrophysical Journal, 600, L107

Feuillet D. K., Frankel N., Lind K., Frinchaboy P. M., García-Hernández D. A., Lane R. R., Nitschelm C., Roman-Lopes A., 2019, Monthly Notices of the Royal Astronomical Society, 489, 1742

Fisher D. B., Drory N., 2008, The Astronomical Journal, 136, 773

Fisher D., Franx M., Illingworth G., 1996, ApJ, 459, 110

Font A. S., et al., 2020, Monthly Notices of the Royal Astronomical Society, 498, 1765

Foreman-Mackey D., Hogg D. W., Lang D., Goodman J., 2013, Publications of the Astronomical Society of the Pacific, 125, 306

Freeman K., Bland-Hawthorn J., 2002, Annual Review of Astronomy and Astrophysics, 40, 487

Frenk C. S., White S. D. M., 2012, Annalen der Physik, 524, 507

Fuhrmann K., 1998, Astronomy and Astrophysics, 338, 161

Gadotti D. A., 2011, Monthly Notices of the Royal Astronomical Society, 415, 3308

García Pérez A. E., et al., 2016, The Astronomical Journal, 151, 144

García-Ruiz I., Sancisi R., Kuijken K., 2002, Astronomy and Astrophysics, 394, 769

García de la Cruz J., Martig M., Minchev I., 2021a, arXiv, 000, arXiv:2111.01522

García de la Cruz J., Martig M., Minchev I., James P., 2021b, Monthly Notices of the Royal Astronomical Society, 501, 5105

Gerhard O., 2002, Space Science Reviews 2002 100:1, 100, 129

Gerssen J., Shapiro Griffin K., 2012, Mon. Not. R. Astron. Soc, 423, 2726

Gillessen S., et al., 2017, The Astrophysical Journal, 837, 30

Gilmore G., Reid N., 1983, Monthly Notices of the Royal Astronomical Society, 202, 1025

Gómez F. A., White S. D., Grand R. J., Marinacci F., Springel V., Pakmor R., 2017, Monthly Notices of the Royal Astronomical Society, 465, 3446

Grand R. J., Kawata D., Cropper M., 2014, Monthly Notices of the Royal Astronomical Society, 439, 623

Grand R. J. J., Springel V., Gómez F. A., Marinacci F., Pakmor R., Campbell D. J. R., Jenkins A., 2016, MNRAS, 459, 199

Grand R. J., et al., 2017, Monthly Notices of the Royal Astronomical Society, 467, 179

Gregory P., 2010, English

Griv E., 2011, Mon. Not. R. Astron. Soc, 415, 1259

Guérou A., Emsellem E., Krajnović D., McDermid R. M., Contini T., Weilbacher P. M., 2016, Astronomy and Astrophysics, 591, A143

Hammer F., Flores H., Puech M., Yang Y. B., Athanassoula E., Rodrigues M., Delgado R., 2009, Astronomy & Astrophysics, 507, 1313

Hart R. E., et al., 2016, Monthly Notices of the Royal Astronomical Society, 461, 3663

Hayden M. R., et al., 2015, Astrophysical Journal, 808, 132

Hayden M. R., et al., 2018, Astronomy and Astrophysics, 609, 79

Haywood M., Di Matteo P., Lehnert M. D., Katz D., Gómez A., 2013, Astronomy and Astrophysics, 560, A109

Heald G., et al., 2011, A&A, 526

Heckman T. M., Armus L., Miley G. K., 1990, ApJS, 74, 833

Helmi A., Babusiaux C., Koppelman H. H., Massari D., Veljanoski J., Brown A. G., 2018a, Nature, 563, 85

Helmi A., Babusiaux C., Koppelman H. H., Massari D., Veljanoski J., Brown A. G., 2018b, Nature, 563, 85

Holmberg J., Nordström B., Andersen J., 2007, Astronomy & Astrophysics, 475, 519

Holtzman J. A., et al., 2015, Astronomical Journal, 150, 148

Hopkins P. F., Quataert E., Murray N., 2012, Monthly Notices of the Royal Astronomical Society, 421, 3522

Horta D., et al., 2020, Technical report, Evidence from APOGEE for the presence of a major building block of the halo buried in the inner Galaxy, `https://github.com/jobovy/galpy`. `https://github.com/jobovy/galpy`

Hubble E., 1926, Contributions from the Mount Wilson Observatory / Carnegie Institution of Washington, vol. 324, pp.1-49, 324, 1

Ibata R., Mouhcine M., Rejkuba M., 2009, Monthly Notices of the Royal Astronomical Society, 395, 126

Ideta M., Hozumi S., Tsuchiya T., Takizawa M., 2000, Monthly Notices of the Royal Astronomical Society, 311, 733

Inoue A. K., Shimizu I., Iwata I., Tanaka M., 2014, Monthly Notices of the Royal Astronomical Society, 442, 1805

Inoue S., Dekel A., Mandelker N., Ceverino D., Bournaud F., Primack J., 2016, Monthly Notices of the Royal Astronomical Society, 456, 2052

Iršič V., et al., 2016, Monthly Notices of the Royal Astronomical Society, p. stw3372

Jaynes E., Bretthorst G., 2003, Language, p. 727

Jenkins A., 1992, Monthly Notices of the Royal Astronomical Society, 257, 620

Jiang I. G., Binney J., 1999, Monthly Notices of the Royal Astronomical Society, 303, L7

Jogee S., et al., 2009, The Astrophysical Journal, 697, 1971

Jungwiert B., Combes F., Palous J., 2001, Astronomy and Astrophysics, 376, 85

Jurić M., et al., 2008, The Astrophysical Journal, 673, 864

Kafle P. R., Sharma S., Lewis G. F., Bland-Hawthorn J., 2014, Astrophysical Journal, 794, 59

Kalberla P. M., Kerp J., Dedes L., Haud U., 2014, Astrophysical Journal, 794, 90

Kasparova A. V., Katkov I. Y., Chilingarian I. V., Silchenko O. K., Moiseev A. V., Borisov S. B., 2016, Monthly Notices of the Royal Astronomical Society: Letters, 460, L89

Kasparova A. V., Katkov I. Y., Chilingarian I. V., 2020, Monthly Notices of the Royal Astronomical Society, 493, 5464

Kaviraj S., Peirani S., Khochfar S., Silk J., Kay S., 2009, Monthly Notices of the Royal Astronomical Society, 394, 1713

Kazantzidis S., Bullock J. S., Zentner A. R., Kravtsov A. V., Moustakas L. A., 2008, The Astrophysical Journal, 688, 254

Kazantzidis S., Zentner A. R., Kravtsov A. V., Bullock J. S., Debattista V. P., 2009, Astrophysical Journal, 700, 1896

Kelvin L. S., et al., 2014, Monthly Notices of the Royal Astronomical Society, 444, 1647

Kennicutt Jr. R. C., 1998, The Astrophysical Journal, 498, 541

Kereš D., Katz N., Weinberg D. H., Davé R., 2005, Monthly Notices of the Royal Astronomical Society, 363, 2

Kereš D., Katz N., Fardal M., Davé R., Weinberg D. H., 2009, Monthly Notices of the Royal Astronomical Society, 395, 160

Khachaturyants T., Beraldo e Silva L., Debattista V. P., 2021, Monthly Notices of the Royal Astronomical Society, 508, 2350

Khoperskov A., Bizyaev D., Tiurina N., Butenko M., 2010, Astronomische Nachrichten, Vol.331, Issue 7, p.731, 331, 731

Kim J. H., Peirani S., Kim S., Ann H. B., An S. H., Yoon S. J., 2014, Astrophysical Journal, 789, 90

Kim J.-h., et al., 2016, The Astrophysical Journal, 833, 202

Knapen J. H., 2005, Astronomy & Astrophysics, 429, 141

Knapen J. H., Shlosman I., Peletier R. F., 2000, The Astrophysical Journal, 529, 93

Kormendy J., Fisher D. B., 2008, ASPC, 396, 297

Kormendy J. 1993, IAUS, 153, 209

Kormendy J., Drory N., Bender R., Cornell M. E., 2010, Astrophysical Journal, 723, 54

Kowalski M., et al., 2008, ] 10.1086/589937, 686, 749

Kubryk M., Prantzos N., Athanassoula E., 2015, Astronomy and Astrophysics, 580, A126

Lacey C., Cole S., 1993, Monthly Notices of the Royal Astronomical Society, 262, 627

Laporte C. F. P., Gómez F. A., Besla G., Johnston K. V., Garavito-Camargo N., 2018, MNRAS, 473, 1218

Laporte C. F. P., Minchev I., Johnston K. V., Gómez F. A., 2019, Monthly Notices of the Royal Astronomical Society, 485, 3134

Laurikainen E., Salo H., Buta R., Knapen J. H., 2007, Monthly Notices of the Royal Astronomical Society, 381, 401

Le Fèvre O., et al., 2000, Monthly Notices of the Royal Astronomical Society, 311, 565

Lee K. G., Hennawi J. F., White M., Croft R. A., Ozbek M., 2014, Astrophysical Journal, 788, 49

Leroy A. K., Walter F., Brinks E., Bigiel F., De Blok W. J., Madore B., Thornley M. D., 2008, Astronomical Journal, 136, 2782

Leroy A. K., et al., 2013, Astronomical Journal, 146, 19

Levine E. S., Blitz L., Heiles C., 2006, The Astrophysical Journal, 643, 881

Liddle A. R., Lyth D. H., 1993, The cold dark matter density perturbation (arXiv:9303019v1), doi:10.1016/0370-1573(93)90114-S, https://arxiv.org/pdf/astro-ph/9303019.pdf

Lin L., et al., 2004, The Astrophysical Journal, 617, L9

Liu C., Tian H. J., Wan J. C., 2016, Proceedings of the International Astronomical Union, 11, 6

Loebman S. R., Roškar R., Debattista V. P., Ivezić , Quinn T. R., Wadsley J., 2011, Astrophysical Journal, 737

López-Corredoira M., Molgó J., 2014, Astronomy and Astrophysics, 567, 106

López-Corredoira M., Cabrera-Lavers A., Garzón F., Hammersley P. L., 2002, Astronomy and Astrophysics, 394, 883

López-Corredoira M., Prieto C. A., Garzón F., Wang H., Liu C., Deng L., 2018, Astronomy and Astrophysics, 612, L8

López-Sanjuan C., Balcells M., Pérez-Gonzlez P. G., Barro G., García-Dabó C. E., Gallego J., Zamorano J., 2010, The Astrophysical Journal, 710, 1170

Lotz J. M., Jonsson P., Cox T. J., Croton D., Primack J. R., Somerville R. S., Stewart K., 2011, The Astrophysical Journal, 742, 103

Lynden-Bell D., 1967, Monthly Notices of the Royal Astronomical Society, 136, 101

Lynden-Bell D., Kalnajs A. J., 1972, Monthly Notices of the Royal Astronomical Society, 157, 1

Mackereth J. T., et al., 2017, Monthly Notices of the Royal Astronomical Society, 471, 3057

Mackereth T. J., Crain R. A., Schiavon R. P., Schaye J., Theuns T., Schaller M., 2018, Monthly Notices of the Royal Astronomical Society, 477, 5072

Maller A. H., Dekel A., Somerville R., 2002, MNRAS, 329, 423

Maller A. H., Katz N., Kereš D., Dave R., Weinberg D. H., 2006, The Astrophysical Journal, 647, 763

Marinova I., Jogee S., 2007, The Astrophysical Journal, 659, 1176

Martig M., Bournaud F., Teyssier R., Dekel A., 2009, Astrophysical Journal, 707, 250

Martig M., Bournaud F., Croton D. J., Dekel A., Teyssier R., 2012, Astrophysical Journal, 756, 26

Martig M., Minchev I., Flynn C., 2014a, MNRAS, 442, 2474

Martig M., Minchev I., Flynn C., 2014b, Monthly Notices of the Royal Astronomical Society, 443, 2452

Martig M., Minchev I., Ness M., Fouesneau M., Rix H.-W., 2016, The Astrophysical Journal, 831, 139

Martin D. C., et al., 2005, The Astrophysical Journal, 619, L1

Martínez-Lombilla C., Knapen J. H., 2019, Astronomy and Astrophysics, 629, 12

Mateu C., Katherina Vivas A., 2018, Monthly Notices of the Royal Astronomical Society, 479, 211

McNamara B. R., Nulsen P. E., 2007, in Annual Review of Astronomy and Astrophysics. pp 117–175, doi:10.1146/annurev.astro.45.051806.110625, https://ui.adsabs.harvard.edu/abs/2007ARA&A..45..117M/abstract

Menendez-Delmestre K., Sheth K., Schinnerer E., Jarrett T. H., Scoville N. Z., 2007, The Astrophysical Journal, 657, 790

Metropolis N., Rosenbluth A. W., Rosenbluth M. N., Teller A. H., Teller E., 1953, The Journal of Chemical Physics, 21, 1087

Meza A., Navarro J. F., Abadi M. G., Steinmetz M., 2005, Monthly Notices of the Royal Astronomical Society, 359, 93

Minchev I., Famaey B., 2010, Astrophysical Journal, 722, 112

Minchev I., Quillen A. C., 2006, Monthly Notices of the Royal Astronomical Society, 368, 623

Minchev I., Famaey B., Quillen A. C., Di Matteo P., Combes F., Vlajić M., Erwin P., Bland-Hawthorn J., 2012a, Astronomy and Astrophysics, 548, A126

Minchev I., Famaey B., Quillen A. C., Dehnen W., Martig M., Siebert A., 2012b, Astronomy and Astrophysics, 548, A127

Minchev I., Chiappini C., Martig M., 2013, Astronomy and Astrophysics, 558, A9

Minchev I., Chiappini C., Martig M., 2014, Astronomy and Astrophysics, 572, A92

Minchev I., Martig M., Streich D., Scannapieco C., De Jong R. S., Steinmetz M., 2015, Astrophysical Journal Letters, 804, L9

Minchev I., Steinmetz M., Chiappini C., Martig M., Anders F., Matijevic G., Jong R. S. d., 2016, The Astrophysical Journal, 834, 27

Minchev I., et al., 2018, Monthly Notices of the Royal Astronomical Society, 481, 1645

Minchev I., et al., 2019, Monthly Notices of the Royal Astronomical Society, 487, 3946

Moetazedian R., Just A., 2016, Monthly Notices of the Royal Astronomical Society, 459, 2905

Mosenkov A., et al., 2020, Monthly Notices of the Royal Astronomical Society, 494, 1751

Mould J., 2005, The Astronomical Journal, 129, 698

Myeong G. C., Vasiliev E., Iorio G., Evans N. W., Belokurov V., 2019, Monthly Notices of the Royal Astronomical Society, 000, 1235

Narayan C. A., Jog C. J., 2002, Origin of radially increasing stellar scaleheight in a galactic disk, doi:10.1051/0004-6361:20020961, http://www.aanda.org/10.1051/0004-6361:20020961

Navarro J. F., Abadi M. G., Venn K. A., Freeman K. C., Anguiano B., 2011, Monthly Notices of the Royal Astronomical Society, 412, 1203

Navarro J. F., et al., 2018, Monthly Notices of the Royal Astronomical Society, 476, 3648

Nelson D., et al., 2019, Computational Astrophysics and Cosmology, 6, 2

Nemec J., Nemec A. F. L., 1991, Publications of the Astronomical Society of the Pacific, 103, 95

Nemec J. M., Nemec A. F. L., 1993, The Astronomical Journal, 105, 1455

Ness M., Hogg D. W., Rix H.-W., Martig M., Pinsonneault M. H., Ho A. Y. Q., 2016, The Astrophysical Journal, 823, 114

Newberg H. J., Willett B. A., Yanny B., Xu Y., 2010, Astrophysical Journal, 711, 32

Nissen P. E., Schuster W. J., 2010, Astronomy and Astrophysics, 511, 10

Norris J. E., 1999, Astrophysics and Space Science, 265, 213

Ocvirk P., Pichon C., Teyssier R., 2008, Monthly Notices of the Royal Astronomical Society, 390, 1326

Ortolani S., Renzini A., Gilmozzi R., Marconi G., Barbuy B., Bica E., Rich R. M., 1995, Nature 1995 377:6551, 377, 701

Ostriker E. C., Binney J. J., 1989, Monthly Notices of the Royal Astronomical Society, 237, 785

Park C., Choi Y., Vogeley M. S., Gott III J. R., Blanton M. R., 2007, The Astrophysical Journal, 658, 898

Park M. J., et al., 2020, arXiv: 2009.12373

Patel E., Besla G., Mandel K., Sohn S. T., 2018, The Astrophysical Journal, 857, 78

Peebles P. J. E., 1982, ] 10.1086/183911, 263, L1

Peletier R. F., et al., 2007, Monthly Notices of the Royal Astronomical Society, 379, 445

Percival W. J., Cole S., Eisenstein D. J., Nichol R. C., Peacock J. A., Pope A. C., Szalay A. S., 2007, ] 10.1111/j.1365-2966.2007.12268.x, 381, 1053

Peschken N., Athanassoula E., Rodionov S. A., 2017, Monthly Notices of the Royal Astronomical Society, 468, 994

Pfuhl O., et al., 2011, Astrophysical Journal, 741

Piffl T., et al., 2014, Monthly Notices of the Royal Astronomical Society, 445, 3133

Pinna F., Falcón-Barroso J., Martig M., Martínez-Valpuesta I., Méndez-Abreu J., van de Ven G., Leaman R., Lyubenova M., 2018, Monthly Notices of the Royal Astronomical Society, 475, 2697

Pinna F., et al., 2019a, Astronomy and Astrophysics, 623, A19

Pinna F., et al., 2019b, Astronomy and Astrophysics, 625, A95

Pinsonneault M. H., et al., 2015, Astrophysical Journal, Supplement Series, 215, 19

Poggio E., et al., 2018, Monthly Notices of the Royal Astronomical Society: Letters, 481, L21

Poggio E., Laporte C. F. P., Johnston K. V., D'Onghia E., Drimmel R., Filho D. G., 2020, MNRAS, 000, 1

Polido P., Jablonski F., Lépine J. R., 2013, Astrophysical Journal, 778, 32

Posti L., Helmi A., 2019, Astronomy & Astrophysics, 621, A56

Press W. H., Schechter P., 1974, ] 10.1086/152650, 187, 425

Prochaska J. X., Naumov S. O., Carney B. W., McWilliam A., Wolfe A. M., 2000, The Astronomical Journal, 120, 2513

Qu Y., Di Matteo P., Lehnert M. D., Van Driel W., 2011, Astronomy and Astrophysics, 530, A10

Quinn P. J., Hernquist L., Fullagar D. P., 1993, The Astrophysical Journal, 403, 74

Rahman N., et al., 2012, Astrophysical Journal, 745, 183

Ravindranath S., et al., 2004, The Astrophysical Journal, 604, L9

Read J. I., Lake G., Agertz O., Debattista V. P., 2008, Monthly Notices of the Royal Astronomical Society, 389, 1041

Recio-Blanco A., et al., 2016, A&A, 585, 93

Reddy B. E., Tomkin J., Lambert D. L., Prieto C. A., 2003, Monthly Notices of the Royal Astronomical Society, 340, 304

Rees M. J., Ostriker J. P., 1977, ] 10.1093/mnras/179.4.541, 179, 541

Reese A. S., Williams T. B., Sellwood J. A., Barnes E. I., Powell B. A., 2007, AJ, 133, 2846

Reshetnikov V., Combes F., 1998, Astronomy and Astrophysics, 337, 9

Reshetnikov V. P., Mosenkov A. V., Moiseev A. V., Kotov S. S., Savchenko S. S., 2016, Monthly Notices of the Royal Astronomical Society, 461, 4233

Revaz Y., Pfenniger D., 2004, Astronomy & Astrophysics, 425, 67

Reylé C., Marshall D. J., Robin A. C., Schultheis M., 2009, Astronomy and Astrophysics, 495, 819

Rich R. M., et al., 2019, Monthly Notices of the Royal Astronomical Society, 490, 1539

Riess A. G., et al., 1998, The Astronomical Journal, 116, 1009

Rix H. W., Bovy J., 2013, The Milky Way's stellar disk: Mapping and modeling the Galactic disk, doi:10.1007/s00159-013-0061-8, `https://ui.adsabs.harvard.edu/abs/2013A%26ARv..21...61R/abstract`

Roberts M. S., Haynes M. P., 1994, Annual Review of Astronomy and Astrophysics, 32, 115

Robin A. C., Reylé C., Fliri J., Czekaj M., Robert C. P., Martins A. M., 2014, Astronomy and Astrophysics, 569, A13

Robotham A. S., et al., 2012, Monthly Notices of the Royal Astronomical Society, 424, 1448

Rodionov S. A., Athanassoula E., Peschken N., 2017, Astronomy & Astrophysics, 600, A25

Romero-Gómez M., Mateu C., Aguilar L., Figueras F., Castro-Ginard A., 2019, A&A, 627, 150

Roškar R., Debattista V. P., Quinn T. R., Stinson G. S., Wadsley J., 2008, The Astrophysical Journal, 684, L79

Roškar R., Debattista V. P., Brooks A. M., Quinn T. R., Brook C. B., Governato F., Dalcanton J. J., Wadsley J., 2010, Monthly Notices of the Royal Astronomical Society, 408, 783

Roškar R., Debattista V. P., Loebman S. R., 2013, Monthly Notices of the Royal Astronomical Society, 433, 976

Rozo E., et al., 2010, ] 10.1088/0004-637X/708/1/645, 708, 645

Rubin K. H., Prochaska J. X., Koo D. C., Phillips A. C., Martin C. L., Winstrom L. O., 2014, Astrophysical Journal, 794, 156

Ruiz-Lara T., et al., 2017, J. Bland-Hawthorn, 604, 20

Ruiz-Lara T., Gallart C., Bernard E. J., Cassisi S., 2020, Nature Astronomy, 4, 965

Saha K., Jog C. J., 2006, Astronomy and Astrophysics, 446, 897

Sakamoto K., Okumura S. K., Ishizuki S., Scoville N. Z., 1999, The Astrophysical Journal, 525, 691

Sánchez-Saavedra M. L., Battaner E., Guijarro A., López-Corredoira M., Castro-Rodríguez N., 2003, Astronomy and Astrophysics, 399, 457

Sánchez A. G., Crocce M., Cabré A., Baugh C. M., Gaztañaga E., 2009, ] 10.1111/j.1365-2966.2009.15572.x, 400, 1643

Sancisi R., 1976, Astronomy and Astrophysics, Vol. 53, 159

Sarkar S., Jog C. J., 2019, Astronomy & Astrophysics, 628, A58

Scannapieco C., White S. D., Springel V., Tissera P. B., 2009, Monthly Notices of the Royal Astronomical Society, 396, 696

Schaye J., et al., 2015, Monthly Notices of the Royal Astronomical Society, 446, 521

Schönrich R., Binney J., 2009, Monthly Notices of the Royal Astronomical Society, 399, 1145

Schwarzkopf U., Dettmar R. J., 2001, Astronomy and Astrophysics, 373, 402

Seigar M., Carollo C. M., Stiavelli M., de Zeeuw P. T., Dejonghe H., 2002, The Astronomical Journal, 123, 184

Sellwood J. A., 2013, in , Planets, Stars and Stellar Systems: Volume 5: Galactic Structure and Stellar Populations. pp 923–983, doi:10.1007/978-94-007-5612-0_18

Sellwood J. A., 2021, Monthly Notices of the Royal Astronomical Society, 506, 3018

Sellwood J. A., Binney J. J., 2002, Monthly Notices of the Royal Astronomical Society, 336, 785

Sellwood J. A., Nelson R. W., Tremaine S., 1998, THE ASTROPHYSICAL JOURNAL, 506, 590

Semczuk M., Lokas E. L., D'Onghia E., Athanassoula E., Debattista V. P., Hernquist L., 2020, Monthly Notices of the Royal Astronomical Society, 498, 3535

Seth A. C., Dalcanton J. J., de Jong R. S., 2005, The Astronomical Journal, 130, 1574

Shapley A. E., Steidel C. C., Pettini M., Adelberger K. L., 2003, The Astrophysical Journal, 588, 65

Sharma S., 2017, Annual Review of Astronomy and Astrophysics, 55, 1

Shen J., Sellwood J. A., 2006, Monthly Notices of the Royal Astronomical Society, 370, 2

Shen J., et al., 2021

Sheth K., Vogel S. N., Regan M. W., Thornley M. D., Teuben P. J., 2005, The Astrophysical Journal, 632, 217

Silk J., Rees M. J., 1998, Astronomy and Astrophysics, 331, 6

Silk J., Silk J. 1977, ApJ, 211, 638

Smith M. C., et al., 2007, Monthly Notices of the Royal Astronomical Society, 379, 755

Soderblom D. R., 2010, Annual Review of Astronomy and Astrophysics, 48, 581

Solway M., Sellwood J. A., Schönrich R., 2012, Monthly Notices of the Royal Astronomical Society, 422, 1363

Somerville R. S., Davé R., 2014

Soubiran C., Bienaymé O., Mishenina V., Kovtyukh V., 2008, Astronomy & Astrophysics, 480, 91

Sparke L. S., Casertano S., 1988, Monthly Notices of the Royal Astronomical Society, 234, 873

Sparre M., Springel V., 2017, Monthly Notices of the Royal Astronomical Society, 470, 3946

Spitzer Lyman J., Schwarzschild M., Spitzer Lyman J., Schwarzschild M., 1951, ApJ, 114, 385

Springel V., Frenk C. S., White S. D. M., 2006, ] 10.1038/nature04805, 440, 1137

Springel V., et al., 2008, Monthly Notices of the Royal Astronomical Society, 391, 1685

Stewart K. R., Bullock J. S., Wechsler R. H., Maller A. H., Zentner A. R., 2008, The Astrophysical Journal, 683, 597

Streich D., De Jong R. S., Bailin J., Bell E. F., Holwerda B. W., Minchev I., Monachesi A., Radburn-Smith D. J., 2016, Astronomy and Astrophysics, 585

Taranu D. S., Dubinski J., Yee H. K., 2013, The Astrophysical Journal, 778, 61

Teyssier R., 2002, Astronomy and Astrophysics, 385, 337

Thomas G. F., et al., 2018, Monthly Notices of the Royal Astronomical Society, 481, 5223

Toomre A., 1977, Evolution of Galaxies and Stellar Populations, pp 401–

Toomre A., Toomre J., 1972, The Astrophysical Journal, 178, 623

Toth G., Ostriker J. P., 1992, Astrophysical Journal v.389, p.5, 389, 5

Trujillo I., Pohlen M., 2005, The Astrophysical Journal, 630, L17

Trujillo I., et al., 2006, The Astrophysical Journal, 650, 18

Tsikoudi V., 1979, The Astrophysical Journal, 234, 842

Van Der Kruit P. C., 2007, Astronomy and Astrophysics, 466, 883

Van Dokkum P. G., et al., 2013, The Astrophysical Journal Letters, 771, L35

Van Starkenburg L., Van Der Werf P. P., Franx M., Labbé I., Rudnick G., Wuyts S., 2008, Astronomy & Astrophysics, 488, 99

Velázquez H., White S. D., 1999, Monthly Notices of the Royal Astronomical Society, 304, 254

Vera-Ciro C., D'Onghia E., Navarro J., Abadi M., 2014, Astrophysical Journal, 794

Vikhlinin A., et al., 2009, ] 10.1088/0004-637X/692/2/1060, 692, 1060

Villalobos A., Helmi A., 2008, Monthly Notices of the Royal Astronomical Society, 391, 1806

Virtanen P., et al., 2019, Technical report, SciPy 1.0-Fundamental Algorithms for Scientific Computing in Python

Vitvitska M., Klypin A. A., Kravtsov A. V., Wechsler R. H., Primack J. R., Bullock J. S., 2002, Astrophysical Journal, 581, 799

Wang W., Han J., Cooper A. P., Cole S., Frenk C., Lowing B., 2015, Monthly Notices of the Royal Astronomical Society, 453, 377

Weinberg M. D., 1998, Monthly Notices of the Royal Astronomical Society, 299, 499

Weiner B. J., et al., 2009, Astrophysical Journal, 692, 187

Weinzirl T., Jogee S., Khochfar S., Burkert A., Kormendy J., 2009, Astrophysical Journal, 696, 411

White S. D. M., 1984, Astrophysical Journal, 286, 38

White S. D. M., Frenk C. S., 1991, ] 10.1086/170483, 379, 52

White S. D. M., Rees M. J., 1978a, Monthly Notices of the Royal Astronomical Society, 183, 341

White S. D. M., Rees M. J., 1978b, Monthly Notices of the Royal Astronomical Society, 183, 341

Widrow L. M., Barber J., Chequers M. H., Cheng E., 2014, Monthly Notices of the Royal Astronomical Society, 440, 1971

Xiang M., et al., 2017, The Astrophysical Journal Supplement Series, 232, 2

Yoachim P., Dalcanton J. J., 2006, The Astronomical Journal, 131, 226

Yoachim P., Dalcanton J. J., 2008, The Astrophysical Journal, 683, 707

Yoshida N., Omukai K., Hernquist L., 2008, Science, 321, 669

Yu Y., et al., 2021, Technical report, The Flare and Warp of the Young Stellar Disk traced with LAMOST DR5 OB-type stars

Zheng Z., Flynn C., Gould A., Bahcall J. N., Salim S., 2001, The Astrophysical Journal, 555, 393

van de Voort F., Schaye J., Booth C. M., Haas M. R., Dalla Vecchia C., 2011, Monthly Notices of the Royal Astronomical Society, 414, 2458

van den Bosch F. C., Ogiya G., Hahn O., Burkert A., 2018, Monthly Notices of the Royal Astronomical Society, 474, 3043

van der Kruit P., Freeman K., 2011, Annual Review of Astronomy and Astrophysics, 49, 301

van der Kruit P., Searle L., 1981, Astronomy & astrophysics, 95, 105